NASA Technical Paper 1863

Static and Yawed-Rolling Mechanical Properties of Two Type VII Aircraft Tires

John A. Tanner, Sandy M. Stubbs,
and John L. McCarty

MAY 1981

NASA

NASA Technical Paper 1863

Static and Yawed-Rolling Mechanical Properties of Two Type VII Aircraft Tires

John A. Tanner, Sandy M. Stubbs,
and John L. McCarty
Langley Research Center
Hampton, Virginia

National Aeronautics
and Space Administration

**Scientific and Technical
Information Branch**

1981

CONTENTS

INTRODUCTION

Designers of tires and landing-gear systems must have knowledge of tire mechanical properties in order to solve problems associated with aircraft take-off, landing, and taxi operations. For example, tire mechanical stiffness properties are fundamental to computation of landing-gear shimmy characteristics and to design of antiskid braking systems. Among the publications which deal with the many mechanical properties of the pneumatic aircraft tire, references 1 and 2 are noteworthy. Reference 1 collected and summarized the knowledge of tire mechanical properties as it existed in 1950; and reference 2, relying on experimental and theoretical studies conducted prior to 1958, established empirical expressions to describe most tire mechanical properties. Reference 2 is generally recognized as the basis of current knowledge of tire mechanical properties; however, it is limited to static and low-speed conditions.

During the past 20 years, many new aircraft tires have been introduced into the world's fleet of commercial and military aircraft, and there have been a number of isolated tire studies. These studies, however, have been limited in scope. The University of Michigan, for example, has centered its research of tire mechanical properties primarily around the development and use of scale model tires to predict full-scale tire behavior (refs. 3, 4, and 5). References 6 and 7 are typical of NASA studies to obtain steady-state yawed-rolling data on new tire concepts, and references 8 and 9 present results from studies limited to braked-rolling and static fore-and-aft tire properties.

In view of the concern that new tires may not exhibit characteristics or trends observed for earlier designs, the Society of Automotive Engineers, Inc. (Committee A-5 on Aerospace Landing Gear Systems) requested NASA to participate in a joint experimental program with the U.S. Air Force and the University of Michigan to evaluate mechanical properties of two sizes of aircraft tires currently in wide use. The purpose of this paper is to contribute to that request and present in detail results from the test program at NASA to measure static and dynamic mechanical properties of 18 × 5.5 and 49 × 17 type VII aircraft tires. During this program, tires were subjected to pure vertical load and to combined vertical and lateral loads under both static and dynamic (rolling) conditions. Test parameters for the static tests consisted of tire load in the vertical and lateral directions, and test parameters for the dynamic tests included tire vertical load, yaw angle, and ground speed. Effects of each of these parameters on the measured tire characteristics are discussed; and, where possible, comparisons are made with previous work. An appendix is included which defines terms and expressions used in studying these tire characteristics and symbols used in presenting results of the study.

APPARATUS AND TEST PROCEDURE

Static tests and yawed rolling tests were conducted on two sizes of high-pressure, high-speed, bias-ply aircraft tires in this experimental investiga-

tion: size 18 × 5.5 with a 14-ply rating and size 49 × 17 with a 26-ply rating. Characteristics of the two tire designs are presented in table I. Several tires of each size were furnished by the U.S. Air Force, and each size was procured from the same manufacturer with closely spaced serial numbers and dates of manufacture. Prior to testing, all tires were broken in at rated pressure and load for three taxi runs of 3.2 km (2 miles) each on a road wheel (drum) dynamometer) at the Landing Gear Development Facility, Wright-Patterson Air Force Base.

Tire vertical load consisted of 50, 75, 100, and 125 percent of the rated load, and for the static tests, these loads were each applied at four equally spaced peripheral positions around the tire. For all tests, the inflation pressure was limited to the rated pressure, which was set prior to loading.

Both the static and the rolling tests were conducted with the tires installed on test carriages at the Langley Landing Loads Track. The 48 000-kg (106 000-lb) test carriage shown in figure 1 and described in reference 9 was employed in tests of the 49 × 17 tire, and the 29 500-kg (65 000-lb) carriage shown in figure 2 and described in reference 10 was used in tests of the 18 × 5.5 tire. On both carriages, the test tire was mounted within an instrumented dynamometer (described in the appendix) to measure drag, vertical, and lateral tire forces. The dynamometer used to support the 49 × 17 tire on the large carriage is shown in figure 3.

Static Vertical-Loading Tests

Static vertical-loading tests were performed to measure the geometric properties of the tire footprint and to determine vertical load-deflection relationships for the tires over the range of test vertical load. Footprint data were obtained by coating the tire tread with chalk, applying the desired vertical load to the tire on a sheet of paper covering a flat surface, and measuring the geometric characteristics of the resulting "chalked" footprint with a scale and a planimeter. Vertical load-deflection curves were established according to the procedure recommended in reference 11 by continuously monitoring the vertical load on the tire, which was hydraulically applied, and the corresponding deflection between the wheel flange and the flat bearing surface. The vertical load was measured with strain-gage beams in the dynamometer, and the tire deflection was obtained from a linear motion transducer. The load was increased beginning when the tire came in contact with the flat bearing surface until the desired load (50, 75, 100, and 125 percent of the rated load) was reached. The load was then reduced to zero. The resulting load-deflection curve, or loop, is indicative of the tire vertical-loading behavior and provides information which defines the tire vertical spring rate and hysteresis loss. Both the footprint and the load-deflection tests were conducted at four peripheral positions around the tire.

Static, Combined Vertical- and Lateral-Loading Tests

Static tests with combined vertical and lateral loadings were performed to determine tire lateral load-deflection relationships which include lateral

spring rate and hysteresis loss, lateral center-of-pressure shift, and static relaxation length. The spring rate and hysteresis loss were determined from lateral load-deflection curves which were obtained by again following the procedures recommended in reference 11. The process involved applying the desired vertical load to the tire followed by displacing the frictionless bearing plate, against which the tire rested, in a direction perpendicular to the wheel plane. The lateral displacement, imposed in the presence of the vertical load, was increased until the lateral load was approximately 30 percent of the vertical load as recommended in reference 11. The lateral load was then reduced to zero, increased in the opposite direction to 30 percent of the vertical load, and finally reduced to zero again. One such hysteresis loop was generated for each load and at each peripheral position for the 49 × 17 tire, two such loops were generated for the 18 × 5.5 tire. During the loading cycles, both the lateral load and the lateral displacement of the bearing plate were continuously monitored. The lateral load was measured by a load cell located between a hydraulic piston and a backstop, and lateral displacements of the bearing plate were measured by a linear motion transducer. The vertical load, hydraulically applied to the tire, was measured by load cells under the bearing plate.

The lateral shift in the center of pressure (centroid of vertical forces in the tire footprint) was obtained during the lateral-loading tests from data provided by multiple load cells which supported the bearing plate and from lateral displacement measurements of the plate. Static relaxation lengths were computed from measurements of the deformation in the tire free-tread periphery due to the combined vertical and lateral loads. These deformation measurements were taken from linear motion transducers and dial displacement gages located along the tire centerline at known peripheral positions.

Yawed-Rolling Vertical-Loading Tests

Yawed-rolling tests were performed to measure the rolling relaxation length of the tires and to establish tire steady-state characteristics over a range of ground speed. The relaxation lengths for several yaw angles at each vertical load were determined from a procedure which involved first yawing the wheel assembly, then lowering the tire onto the pavement and applying the desired vertical load, and subsequently rolling the tire straight ahead at the constant yaw angle while monitoring the distance traveled and the buildup of lateral force. Steady-state yawed data were obtained by either propelling or towing the carriage over a dry concrete runway at a preselected ground speed, releasing the fixture which supported the wheel assembly to apply the desired vertical load to the tire, and monitoring the output from the instrumented dynamometer. The dynamometer and its output are described in the appendix. The yaw angle of the wheel assembly was held constant for each test run and consisted of 1°, 3°, 6°, and 9° for each vertical load and ground speed. Nominal ground speeds for these tests were 5, 50, 75, and 100 knots. For a speed of 5 knots, the test carriage was towed by a ground vehicle; for higher speeds, the carriage was propelled by the hydraulic water jet catapult. During each test on the 49 × 17 tire, a discrete vertical load was applied to the tire to yield steady-state data; on the 18 × 5.5 tire, the vertical load was gradually increased to approximately 125 percent of the tire rated load, and the quasi-steady-state characteristics were measured as the load reached selected values. Early tests performed dur-

ing this program had confirmed that characteristics measured at a particular vertical load during the course of a variable loading (quasi-steady-state condition) agreed with those measured during tests conducted with that load held constant.

RESULTS AND DISCUSSION

Static Vertical Loading

This section of the paper discusses the results from static (nonrotating) vertical-loading tests conducted on the two tire sizes. For all tests the tires, inflated to their rated pressure, were loaded to 50, 75, 100, and 125 percent of their rated load (see table I). The results include geometric properties of the tire footprint and relationships between the vertical load and the corresponding tire vertical deflection.

Footprint Geometric Properties

Footprint length.- The length of the footprint area L_f is presented as a function of tire vertical deflection δ in figure 4 where both parameters have been nondimensionalized by the tire outside diameter d. The data from the two tire sizes can be faired in a least squares manner by a single-valued, nonlinear curve described by the expression,

$$L_f/d = 1.66\sqrt{(\delta/d) - (\delta/d)^2} \tag{1}$$

The numerical constant in this expression is slightly lower than the value (1.70) presented in reference 2 for other type VII tires. Also included in figure 4 is the curve for the expression that defines the relationship between footprint length and vertical deflection if the tire were not distorted by the vertical load. Without distortion, the length of the footprint equals the length of the geometric chord formed by the intersection with the ground plane of a circle having a diameter equal to that of the tire, and the numerical constant is 2.0. Thus, for both tire sizes the experimental footprint length is approximately 83 percent of the geometric-chord length.

Footprint width.- The variation of footprint width W_f with tire vertical deflection is presented in figure 5 where both parameters have been made dimensionless by w, the maximum width of the undeflected tire. The data are faired by two single-valued, nonlinear curves, one for each tire size, that differ only by a multiplication factor. The width of the footprint for the 18 × 5.5 tire is closely approximated by the expression,

$$W_f/w = 2\sqrt{(\delta/w) - (\delta/w)^2} \tag{2}$$

which defines the length of the geometric chord generated at the ground plane by an undeformed circle of diameter w. It is similar to the expression in

reference 2 for other larger type VII tires. For the 49 × 17 tire of this program, the measured widths are roughly 86 percent of the length of such a chord and hence are somewhat lower than those presented in reference 2.

Gross footprint area.- Gross footprint area A_G is defined as the overall area of contact between the tire and the pavement including spaces created by the tread pattern. If the footprint is assumed to be elliptical, then

$$A_G = \frac{\pi}{4} L_f W_f \tag{3a}$$

Substituting the expressions which fair the experimental data for L_f and W_f in figures 4 and 5, respectively, results in the following area equation in terms of tire deflection and geometry:

$$A_G = \pi\left(k_L\sqrt{d\delta - \delta^2}\right)\left(k_W\sqrt{w\delta - \delta^2}\right) \tag{3b}$$

where k_L is the constant associated with the footprint length and determined experimentally to equal 0.83 for both tire sizes, and k_W is the constant for footprint width found to equal 1.0 for the 18 × 5.5 tire and 0.86 for the 49 × 17 tire.

In equation (3b), the area can be nondimensionalized and expressed in terms of dimensionless tire deflection to obtain the gross-footprint-area parameter:

$$A_G/w\sqrt{dw} = k_L k_W \pi (\delta/w)\sqrt{1 - (\delta/d) - (\delta/w) + (\delta^2/dw)} \tag{4}$$

If the fractions under the radical are neglected, equation (4) simplifies to a linear equation:

$$A_G/w\sqrt{dw} = k_L k_W \pi (\delta/w) \tag{5}$$

Measured gross footprint areas from the 16 tests conducted on each tire size (4 loadings at 4 peripheral tire positions) were nondimensionalized as in equation (5) and plotted as a function of dimensionless tire deflection in figure 6. The data are faired by expressions which take the form of equation (5) where the product of $k_L k_W \pi$ is 2.5 for the 18 × 5.5 tire and 2.1 for the 49 × 17 tire. These values are slightly lower than the values of 2.61 and 2.24 computed from constants k_L and k_W based on footprint length and width measurements (see discussion of eq. (3b)). These differences can be attributed perhaps to the footprint not being truly elliptical. The curves which describe the data for the two tire sizes of this test program encompass the data of reference 2 for other type VII aircraft tires.

Net footprint area.- Net footprint area A_N of a tire is defined as the area of actual rubber contact between tire and pavement, that is, excluding the spaces created by the tread pattern. The ratio of this net area to gross area for each tire size under all loading conditions is presented as a function of dimensionless tire deflection in figure 7. Experimental data for both tire sizes are faired by lines which indicate that the area ratio increases slightly with increasing tire deflection. Over the load range of this program, this area ratio for the 18 × 5.5 tire varies between approximately 0.66 and 0.75, values that agree with data presented in reference 2. Higher values, extending from 0.81 to 0.88, are noted in figure 7 for the 49 × 17 tire.

Bearing pressure.- Gross and net tire bearing pressures were calculated for both tire sizes and are presented as a function of vertical load in figure 8. Also shown in the figure is the tire inflation pressure which was set at the rated value for each tire prior to loading and was estimated to increase with the applied load according to equation (17) of reference 2. The bearing pressure based on net area should equal the tire inflation pressure if no carcass or tread stiffness is available. In that situation the load is entirely supported by the air spring. It is apparent from figure 8 that the carcass and/or tread provides some structural support, since the net bearing pressure for both tires exceeds the inflation pressure.

Vertical Load-Deflection Relationships

This section discusses characteristics of curves which relate the tire vertical load to the corresponding tire deflection. A typical load-deflection curve is presented in figure 9, which illustrates how the tire vertical spring rate is defined and depicts the hysteretic nature of the relationship. The curve of figure 9 is one of 16 collected for the 18 × 5.5 tire; curves for the 49 × 17 tire show identical trends. Both tire sizes show a hardening spring (increasing slope) during the initial loading phase which becomes, and remains, constant (linear curve) with further increases in vertical load up to the maximum test value. The slope of the curve is steeper during initial load relaxation than during the loading phase, thereby suggesting an even stiffer spring. With a further load reduction, this spring appears to soften gradually and continues to do so until the load returns to zero. Hysteresis loss during the cycle is shown by the area enclosed within the loading and unloading curves.

In the past, vertical load-deflection data have been presented in dimensionless form to condense the data from a variety of tire sizes to a single curve. The empirical equation developed in reference 2 to accomplish this condensation takes the form

$$\frac{F_Z}{(p + 0.08p_r)w\sqrt{dw}} = \text{Function of } (\delta/w) \tag{6}$$

where F_Z is the tire vertical load, p is the tire inflation pressure, and p_r is the rated inflation pressure. The pressure term $(p + 0.08p_r)$ is intended

to account for both the air spring and the tire carcass stiffness. In keeping with these earlier approaches, the data from the vertical-loading tests are presented in figure 10 in terms of the vertical-load parameter (left side of eq. (6)). Since the data were acquired during the linear portion of the loading (prior to any load relaxation), the data are faired by straight lines. The equation of the line which fairs the data from the 49 × 17 tire is identical to equation (23) of reference 2; however, the equation which fairs the data from the 18 × 5.5 tire has different coefficients. Thus, the term $0.08p_r$ does not completely describe the carcass stiffness effects for this smaller size tire. This observation is in keeping with reference 1 which presupposes that the carcass of smaller tires plays a greater structural role than does the carcass of larger tires.

Spring rate.- Various methods exist for computing the vertical spring rate of a tire based on load-deflection curves such as that of figure 9. For example, some investigators (see ref. 2) base the spring rate on the linear portion of the load-application phase, and others (ref. 5, for example) take the slope of a line which connects the maximum load to some intermediate value that splits the hysteresis loop. The method chosen to define the spring rates from the tests in this program is described with the aid of figure 9, and results are plotted in figure 11. In figure 11, curves for two spring rates are presented as a function of tire deflection in both dimensional and dimensionless form for each of the two tire sizes. One curve describes the slope of the load-deflection curves during load application, and the other fairs the measured slopes of those curves during initial load relaxation. The curve corresponding to load application generally represents the lower bound on tire vertical stiffness, and the curve for initial load relief essentially defines an upper bound on tire vertical stiffness. The data are presented in this fashion to cover the range of spring rates which the tire would experience as the result of vertical perturbations during aircraft take-off, landing, and taxiing.

The linear portion of the load-deflection curves for both tire sizes commences when the tire deflection reaches approximately 10 percent of the maximum width of the undeflected tire. The slope of the linear portion, representing the maximum spring rate during load application, is approximately 1050 kN/m (600 lb/in.) for the 18 × 5.5 tire and 2220 kN/m (12 700 lb/in.) for the 49 × 17 tire. The spring rates associated with initial load relief appear to be a function of vertical load and, hence, tire deflection, since higher spring rates result from higher loads. The scatter in the data is due to the difficulty in reading the slope of these short line segments. Figure 11 shows that the initial load relief spring rates for the 49 × 17 tire are roughly twice those for the 18 × 5.5 tire at corresponding values of vertical deflection and, as such, are approximately in the same proportion as the load-application spring rates for the two tire sizes.

Hysteresis loss.- The area enclosed within the load-deflection cycle, such as that depicted in figure 9, represents hysteresis loss, that is, energy dissipated by the tire during that loading and unloading period. A knowledge of hysteresis loss under various vertical-loading conditions is important because the extent of this loss is an indication of the energy dissipation mechanism active during tire deformation. The area enclosed within the load-deflection curves generated during the 16 vertical-loading tests conducted on each of the

tire sizes was measured with a planimeter, and the results are presented in figure 12 where vertical hysteresis loss is plotted on a logarithmic scale as a function of applied vertical load on a linear scale. Straight lines fair the data for each tire and equations for these lines are shown. The significance of the hysteresis losses under vertical loads is suggested by expressing the ratio of the energy loss to the total energy input to the tire during the loading cycle. This ratio, referred to as the vertical hysteresis ratio, was computed from planimeter measurements and plotted as a function of vertical load in figure 13. Approximately 11 percent of the input energy was lost to hysteresis during vertical tire loadings for the 18 × 5.5 tire, and approximately 9 percent was lost for the 49 × 17 tire. This ratio is insensitive to vertical load with the exception of the highest load on the smaller tire where the ratio slightly increases.

Supplemental load-deflection tests.- To better understand tire vertical spring rates and hysteresis losses, load-deflection tests were conducted subsequent to this program on an available 32 × 8.8, type VII aircraft tire. The specific objective of these additional tests was to examine effects on the overall load-deflection curve of partial, multiple loading cycles in an attempt to duplicate the tire vertical-load environment during aircraft ground operations. Results of these tests are shown in figure 14. The load-deflection curve labeled (a) is the single-cycle relationship. Curves labeled (b) and (c) resulted from reapplications of the vertical load during the unloading phase. In (b) the load was reapplied only once (at the point labeled 1) and the cycle repeated; in (c) the load was reapplied four times in succession, each time starting from a lower initial value (points 1 through 4) and each time returning to near the maximum vertical load. The loading phase was interrupted in the curve labeled (d) and the sequence of events was as follows: at point 1 the load was relaxed to the load denoted by 0, then reapplied to point 2, again relaxed to point 0, reapplied to point 3, relaxed to point 0, and recycled to the maximum load at point 4 before returning to zero. These curves confirm the earlier observation that spring rates defined by the loading portion of the load-deflection curve and those associated with the initial unloading from the maximum load bound all spring rates generated during intermediate loading cycles. It is also apparent from the data of figure 14 that the single-cycle curve based on the maximum load envelops all hysteresis loops generated during muliple loading cycles of lesser magnitude.

Static, Combined Vertical and Lateral Loading

This section of the paper discusses results from static (nonrolling) tests conducted on the two tire sizes where the tires were first loaded vertically to 50, 75, 100, and 125 percent of their rated loads and then subjected to a lateral load perpendicular to the wheel plane. The lateral load was limited to roughly 30 percent of the vertical load and was applied cyclically in both directions by moving the bearing plate. The acquired data consist of lateral load-deflection relationships which include tire spring rates, hysteresis losses, and lateral shifts in the vertical-load center of pressure; also static relaxation lengths were obtained from tire lateral deformations.

Lateral Load-Deflection Relationships

A typical lateral load-deflection curve is presented in figure 15. After the initial portion of the loading, these curves are characterized by a nearly constant spring (linear curve) throughout the loading phase (in both directions), an immediate hardening of the spring when the load is first relaxed (from either extreme), and a gradual softening of the spring during load release until the slope of the curve reaches that associated with the load-application phase. As with the vertical load-deflection curves, the area enclosed within the loop formed by the loading and unloading cycles is a measure of dissipated energy, or hysteresis loss.

Spring rate.- As pointed out in reference 2, the load-deflection curve should be taken through a complete cycle to obtain a reliable measure of tire spring rate in the lateral direction. Once a cycle has been experimentally established, there are several ways of defining spring rate. For example, the spring rate was obtained in reference 5 by measuring the slope of the line joining end points of the load-deflection loop, and in reference 2 the slope of the nearly linear response in the loading phase was considered the spring rate. For purposes of this program, two lateral spring rates, defined by the slope of lines AA and BB in figure 15, were calculated for each test condition. Line AA corresponds to the linear portion of the load-deflection curve during load application, and line BB approximates the slope of the curve at initial load relief. These two sets of spring rates were selected because they appear to be upper and lower bounds for each loading condition. Note that the slopes of both lines AA and BB are repeated in the other loading quadrant.

Spring rates calculated from lateral load-deflection tests conducted at the four tire peripheral positions at each of the four loading conditions are summarized in figure 16 where each data point is the average of rates from loadings in both directions. Scatter is more pronounced in the spring rates for initial load relief because of early onset of nonlinearity associated with the softening spring. Data for both tire sizes are faired by straight lines, and figure 16 shows that the load-application spring rates decrease with increasing vertical load. This trend is consistent with that noted in reference 2. Spring rates associated with initial load relief are essentially insensitive to vertical load.

To compare results from these tests with results from other type VII tires presented in reference 2, the spring rates associated with load application were made dimensionless by use of ratio $K_y/(p + 0.24p_r)w$ which in reference 2 is referred to as the lateral-stiffness parameter. This parameter was computed for both tires and is presented as a function of dimensionless vertical deflection in figure 17. Two separate and distinct curves, one for each tire size, are required to fair the data; however, the data for both tires fall within the lower edge of the scatter band of the data presented in figure 20(c) of reference 2. Also presented in figure 17 is the curve representing empirical equation (33) of reference 2 which attempts to fair the stiffness parameter data of that reference. All three curves show similar trends in that lateral-

stiffness parameter decreases with increasing tire vertical deflection, although the decrease associated with the present tests appears to be more pronounced than that of reference 2.

Hysteresis loss.- The static lateral hysteresis loss can be obtained from load-deflection curves, such as that in figure 15, by measuring the area enclosed within the lateral loading and unloading cycle. Losses measured from the curves for the two tire sizes are summarized in figure 18. These losses were computed from the areas of complete hysteresis loops formed by repeated loading cycles and are plotted on a logarithmic scale in the figure as a function of the average of the extreme lateral loads applied in both directions. Recall that these extreme loads were limited to approximately 30 percent of the vertical load. Data for both tire sizes are faired by straight lines, and equations for these exponential curves are included in figure 18.

The extent of the hysteresis loss is illustrated in figure 19 where lateral hysteresis ratio is plotted as a function of lateral load. The lateral hysteresis ratio, the ratio of hysteresis loss to total energy input to the tire, is obtained by dividing the area within the hysteresis loop by the area under the load-deflection curve including the hysteresis loop (see appendix). The data of figure 19 indicate that the input energy lost to hysteresis during lateral loadings is roughly twice that lost during pure vertical loadings and is a function of the applied load. Since the lateral load applied to the tires was limited to 30 percent of the vertical load, trends in the hysteresis ratio noted in figure 19 could be attributed to either the vertical or the lateral load, or to both.

To isolate the effect of lateral load, additional tests were conducted on the 49 × 17 tire: hysteresis loops were generated by various lateral loads while the vertical load was held essentially constant. Results from these tests are presented in figure 20 for several vertical loads. Increasing lateral load increases the input energy lost to hysteresis, and the influence of vertical load is inconsequential. Figures 21(a) and 21(b) are reproductions of hysteresis loops which provided a portion of the data for figure 20. These load-deflection curves together with those of figure 21(c) are included to aid understanding of tire static lateral response. In figure 21(a) the hysteresis loops were decreased in size with each successive cycle; in figure 21(b) the size of the loops was sequentially increased; and in figure 21(c) the cycles were randomly varied. In all three figures the loading steps are sequentially numbered. A study of these figures reveals that for a given vertical load, the lateral spring rates as defined in this paper are essentially independent of lateral load. It is apparent, however, that spring rates defined by the slope of the line connecting the end points of the load-deflection loop (see ref. 5) would show a distinct increase with decreasing lateral load. The spring rates associated with this latter definition would fall between the two curves of figure 16 which bound the spring rate data at each loading condition.

Center-of-pressure shift.- When a lateral load is applied to a standing tire, the footprint is displaced laterally, and the center of the vertical-load reaction (center of pressure) is also displaced in the same direction. The

shift in the center of pressure is less than the displacement of the footprint, and reference 2 considered the ratio of these two distances C_λ to be a tire constant with a value of 0.7 for type VII tires. Values of C_λ, referred to as the center-of-pressure coefficient, are plotted in figure 22 as a function of dimensionless vertical deflection. For the 49 × 17 tire, C_λ is essentially independent of vertical deflection, and hence loading, and has a mean value of about 0.69 which is compatible with the results presented in reference 2. For the 18 × 5.5 tire, however, C_λ is sensitive to vertical deflection over the test range and is considerably lower than the 0.7 predicted by reference 2. It is apparent, therefore, that one value of C_λ is not valid for all type VII tires.

Static Relaxation Length

Another parameter available from static, combined vertical and lateral tire loading is the static relaxation length which is obtained from displacements of the tire equator at various angular positions around the circumference. Such measurements taken on the two tire sizes under four vertical-loading conditions are presented in figure 23 where lateral deflection of the tire equator λ is plotted as a function of tire peripheral angle θ measured from the footprint centerline. The angular positions of the footprint leading edge are identified in figure 23. The lateral displacement of the free-tread periphery of the tire near the leading edge of the footprint varies exponentially with circumferential angular position and, as pointed out in reference 2, can be expressed in the following form:

$$\lambda = Ae^{-s/L_s} \tag{7}$$

where A is a constant, s is the circumferential distance from the footprint leading edge, and L_s is called the tire static relaxation length. Relaxation lengths were computed from the data of figure 23, nondimensionalized by the tire width w, and plotted as a function of dimensionless vertical deflection in figure 24. Data from the two tire sizes are faired by separate linear curves both showing a decrease in relaxation length with increasing tire deflection. Static relaxation lengths for the 49 × 17 tire are consistent with data presented in figures 24 and 25 of reference 2 for other type VII tires. Static relaxation lengths for the 18 × 5.5 tire, however, are higher than those predicted by reference 2.

Yawed Rolling Under Vertical Loading

This section of the paper discusses results from tests conducted on the two sizes of tires to define the yawed-rolling relaxation lengths and the steady-state characteristics of the tires under various combinations of vertical load, yaw angle, and ground speed. All tests were conducted on dry concrete.

Yawed-Rolling Relaxation Length

When a wheel and tire are positioned at a yaw angle and then rolled straight ahead while maintaining that angle, the lateral force F_y perpendicular to the direction of motion builds up exponentially with distance rolled x to a steady-state value $F_{y,e}$. For a tire that is initially undistorted, the increase in lateral force can be expressed by an equation of the following form:

$$F_y = F_{y,e}\left(1 - e^{-x/L_y}\right) \tag{8}$$

where L_y is called the yawed-rolling relaxation length. Values of L_y were calculated from low-speed yawed-rolling tests conducted on the two tire sizes under various combinations of vertical load and yaw angle. These values, in dimensionless form, are plotted as a function of dimensionless vertical deflection in figure 25 where the yaw angle for each test is identified. Also included in figure 25 for comparison are linear curves which faired the static-relaxation-length data of figure 24. The yawed-rolling data from both tires exhibit substantial scatter because irregularities in the side force required a certain amount of fairing judgment, and all attempts to establish trends associated with variations in vertical deflection and yaw angle proved unsuccessful. The mean value of L_y/w for the 18 × 5.5 tire is 0.75 with a standard deviation of 0.40. This value is considerably below values computed from the static data. For the 49 × 17 tire the mean value of L_y/w is 1.30 with a standard deviation of 0.32. In figure 25(b), the curve which fairs the static-relaxation-length data falls within the scatter of the dynamic data for this tire.

Steady-State Characteristics

All steady-state data from the yawed-rolling tests conducted on the two tire sizes are presented, together with the corresponding test conditions, in tables II and III. For purposes of discussion, these data are also presented in figures 26 to 31. The tests examined the effects of three parameters - tire vertical load, yaw angle, and ground speed - on the steady-state characteristics of side force, self-aligning and overturning torques, friction-force moment arm, and lateral center-of-pressure shift. To simplify the presentation of results, analysis-of-variance studies were performed on the characteristics, and it was found that all but the lateral center-of-pressure shift were strongly affected by the tire vertical load and yaw angle and insensitive to ground speed over the range of speed examined in this program. Therefore, for those characteristics, the data are presented in the form of carpet plots to illustrate functional relationships between the characteristics and the test parameters. In the carpet plots, the steady-state characteristic is presented as a function of both vertical load and yaw angle, and the ground speed is identified by test-point symbols. Lines of constant load and constant yaw angle were then fitted to the data in a least squares fashion to serve as an interpolation aid. The dashed lines are extrapolations of the data to zero vertical load or to zero yaw angle. The intersections of the faired lines represent the desired test conditions; the data points represent the actual test conditions. The actual vertical load some-

times differed significantly from the desired load, but the desired and actual yaw angles always agreed because of the control maintained over that parameter.

The following paragraphs discuss in detail the effects of tire vertical load, yaw angle, and ground speed on the steady-state characteristics determined from yawed-rolling tests.

Side force.- The effect of the test parameters on the developed side force F_S is presented in figure 26 where the side force is measured normal to the wheel plane (as opposed to cornering force which is measured normal to the direction of motion). When yaw angle is held constant, side force increases with increasing vertical load and reaches a maximum at vertical loads between 75 and 100 percent of the rated vertical load for the 18 × 5.5 tire and between 100 and 125 percent of the rated load for the 49 × 17 tire. Figure 26 further shows that the effect on side force due to changes in vertical load becomes more pronounced as yaw angle is increased. As expected, increasing yaw angle while holding vertical load constant increases side force, regardless of the vertical load. No discernible trends are evident with variations in ground speed. Since side-force data are generally presented in dimensionless form, they were divided by the respective vertical load on the tire. This process yielded, by definition, side-force friction coefficients μ_S, which are presented in the carpet plot of figure 27. Historically, it has been believed that side-force friction coefficient is insensitive to variations in vertical load; however the data of figure 27 indicate a distinct vertical-load effect. For fixed yaw angles, there is a decrease in μ_S with increasing vertical load, and this trend becomes more pronounced as yaw angle is increased. These observations may have important implications for simulations of aircraft ground-handling problems. The figure also shows that for fixed vertical loads, μ_S increases with increasing yaw angle and the rate of increase decreases with increasing yaw angle. Thus a peak friction coefficient is associated with each vertical load at some higher yaw angle. Again, no trends due to variations in ground speed are evident.

Aligning torque.- Aligning torque M_Z is defined as the torque developed about the steering axis of a yawed tire. When positive, M_Z is self-aligning, that is, it tends to reduce yaw angle. Aligning torques from tests with the two tire sizes are presented in carpet plot form in figure 28. When yaw angle is held constant, aligning torque increases with increasing vertical load, and the rate of change of torque with vertical load is greater at higher yaw angles. The figure also shows that when vertical load is held constant and yaw angle is increased from zero, aligning torque increases rapidly, reaches a maximum, and then decreases with further increases in yaw. For several conditions, specifically when the tires were lightly loaded and at a high yaw angle, the torque is negative, that is, no longer self-aligning. In general, the aligning torque appears to reach a maximum value at yaw angles between 3° and 6°. These trends, including the insensitivity of aligning torque to ground speed, are consistent with data from reference 6.

Overturning torque.- The torque which tends to tilt the wheel plane away from the vertical is referred to as overturning torque M_X. The carpet plots of figure 29 for the two tire sizes show the effects that vertical load, yaw

angle, and ground speed have on this characteristic. At small yaw angles, overturning torque is generally insensitive to variations in vertical load; however, as the yaw angle increases, the torque becomes more sensitive to load (torque increases with increasing load). Figure 29 also shows that, as expected, an increase in yaw angle at a fixed vertical load increases overturning torque and that the rate of increase generally increases as vertical load becomes larger. As in the case of the other characteristics, no discernible trends are attributed to ground speed variations.

Friction-force moment arm.- The friction-force moment arm q is the distance from the friction-force resultant vector to the steering axis and is considered positive when the friction force acts along a line behind the steering axis. This moment arm is akin to pneumatic caster, but unlike that parameter, it includes the drag force in the resultant vector. The friction-force resultant vector and the moment arm represent a force system which is statically equivalent to the actual forces and moments in the footprint. Friction-force moment arms computed from the data of these tests are plotted in figure 30 to show the effect of the various test parameters. Linear curves were used to fair the data. The moment arm for both tire sizes increases with increasing vertical load on the tire and decreases with increasing yaw angle. Again, no identifiable trends are associated with variations in ground speed. Values of q are negative at light loads and high yaw angles, as expected, since the aligning torque (fig. 28) is negative at these test conditions.

Center-of-pressure shift.- Little information is available in the literature on lateral movement of the center of pressure in the tire footprint under yawed-rolling conditions because of the severe instrumentation demands to acquire that parameter. Analysis-of-variance studies indicated that the effects on the lateral center-of-pressure shift y_c due to tire vertical load and yaw angle could not be isolated by using a carpet plot. The analysis further indicated that the y_c data were not sensitive to speed variations. Consequently, the center-of-pressure shift is plotted in figure 31 as a function of yaw angle only, and vertical-load ranges are denoted by test-point symbols. For the 18 × 5.5 tire (fig. 31(a)), y_c generally increases with yaw angle but exhibits no consistent trend for variations in vertical load. For the 49 × 17 tire (fig. 31(b)), no trends in y_c can be established for variations in either vertical load or yaw angle.

CONCLUDING REMARKS

An experimental program was conducted to evaluate selected mechanical properties of two sizes of type VII aircraft tires currently in widespread use. Data were obtained under static loading conditions and under yawed-rolling conditions at ground speeds up to 100 knots. Results of the yawed-rolling tests indicate that dynamic tire characteristics under investigation were generally insensitive to speed variations and therefore support the conclusion that many of these characteristics can be obtained from static and low-speed rolling tests. Furthermore, many tire mechanical properties presented here are in good agreement with empirical predictions based on earlier research performed on aircraft tires of various types and sizes. Among these properties are tire footprint geometry characteristics, vertical and lateral load-deflection relationships, and tire

yawed-rolling properties of side force and aligning torque. Sufficient differences do exist in some properties, however, to warrant additional research before extending the current empirical prediction procedures to include all new tire designs.

Langley Research Center
National Aeronautics and Space Administration
Hampton, VA 23665
April 7, 1981

APPENDIX

GLOSSARY OF TERMS AND SYMBOLS

The purpose of this appendix is to define terms, expressions, and symbols used in the study of tire mechanical properties. Many of these terms are associated with the forces and moments developed in the footprint plane, the wheel plane, and the vertical plane perpendicular to the wheel plane. Other terms are defined by various normalizing functions.

Forces and Moment in Footprint Plane

The forces and moment developed in the footprint plane are shown in sketch A, in which the tire is rolling at a yaw angle ψ. Identified in the sketch are the friction-force moment arm q and the steering axis of the

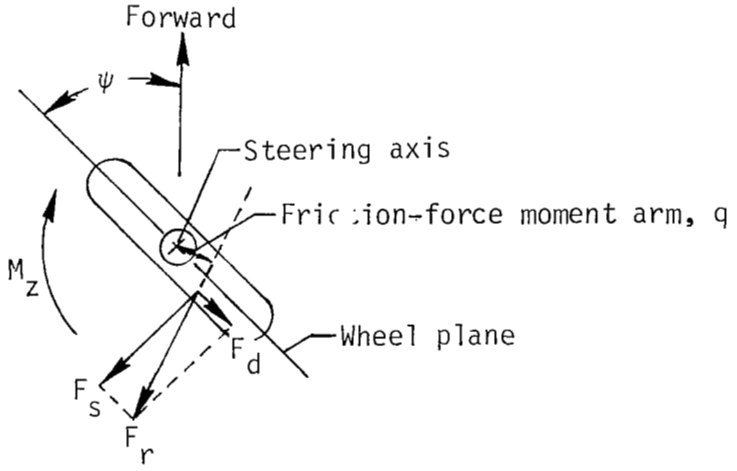

Sketch A

wheel. The forces developed within the tire footprint include the braking force F_d parallel to the wheel plane, the side force F_s perpendicular to the wheel plane, and the resultant friction force F_r which is the vector sum of F_d and F_s. The moment M_z developed by the tire in the footprint plane is usually referred to as the aligning torque and is positive when the moment acts to realign the wheel plane with the direction of motion. The aligning torque can be expressed in terms of the friction force according to the following equation:

$$M_z = F_r q \tag{A1}$$

Aligning torque is an important tire property critical to shimmy analyses.

APPENDIX

A schematic of the instrumented NASA dynamometer used to measure the tire forces and moments during this research program is presented in sketch B. Five

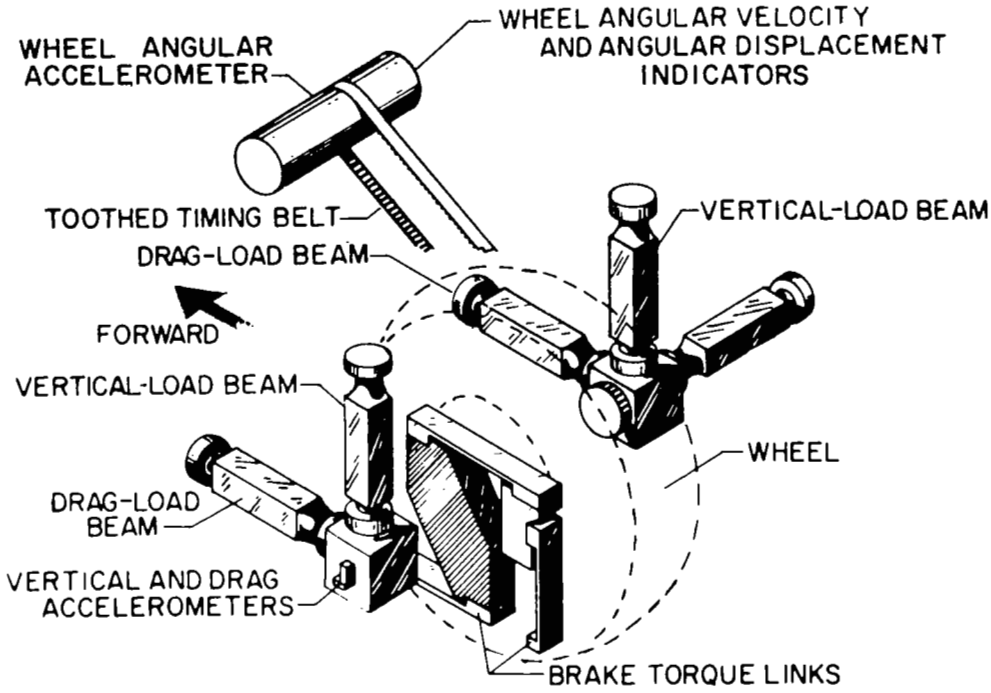

Sketch B

strain gage beams measure the various axle loads and accelerometers are mounted on the axle centerline to make inertial corrections to the axle loads, thereby converting them to ground reaction forces. A measurement of the aligning torque is obtained from the load transfer between the two drag-load beams.

Forces and Moment in Vertical Plane Perpendicular to Wheel Plane

The forces developed within the vertical plane perpendicular to the wheel plane (see sketch C) are the side force F_S perpendicular to the wheel plane and the vertical force F_Z. The moment M_X developed by the tire in this plane is called the overturning torque, and since it affects the load distribution between the two wheel flanges, it is an important consideration in wheel design. The overturning torque can be expressed in terms of the two forces F_S and F_Z as follows:

$$M_X = F_S h + F_Z y_C \tag{A2}$$

where h is the axle height above the runway and y_c is the lateral center-of-pressure shift due to the applied side force.

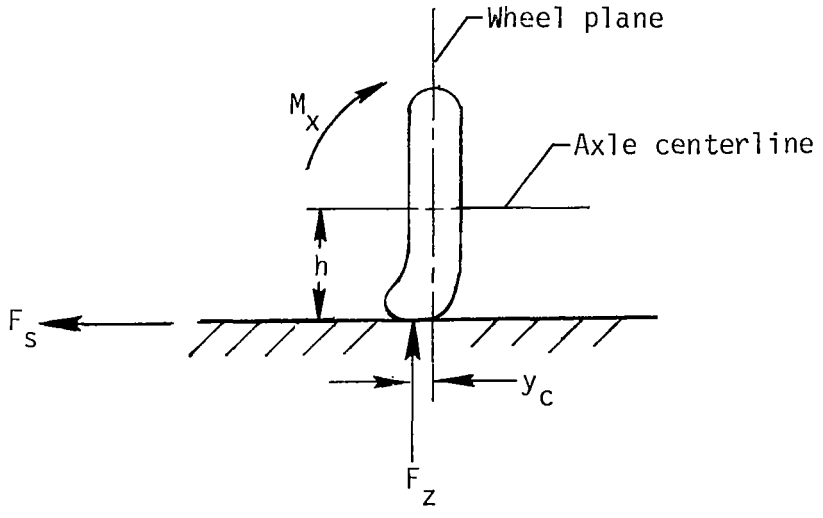

Sketch C

For the tests of this program the output from the appropriate load beams of the instrumented dynamometer shown in sketch B provide F_s and F_z, and the load transfer between the two vertical-load beams provides the overturning torque. A linear potentiometer is used to determine axle height h. With these data, the tire lateral center-of-pressure shift during yawed rolling can be solved from equation (A2) in terms of known quantities:

$$y_c = (M_x - F_s h)/F_z \tag{A3}$$

A second method for measuring the tire lateral center-of-pressure shift from a static loading on a frictionless bearing plate is illustrated in sketch D. From the geometry depicted in the sketch, the lateral center-of-pressure shift is defined as

$$y_c = (y_1' - y_1) - (y_2' - y_2) \tag{A4}$$

where $(y_1' - y_1)$ defines the displacement of the frictionless bearing plate relative to the wheel plane due to the applied side force F_s, and $(y_2' - y_2)$ is the center-of-pressure shift relative to the plate and determined from the load transfer measured by the load cells.

APPENDIX

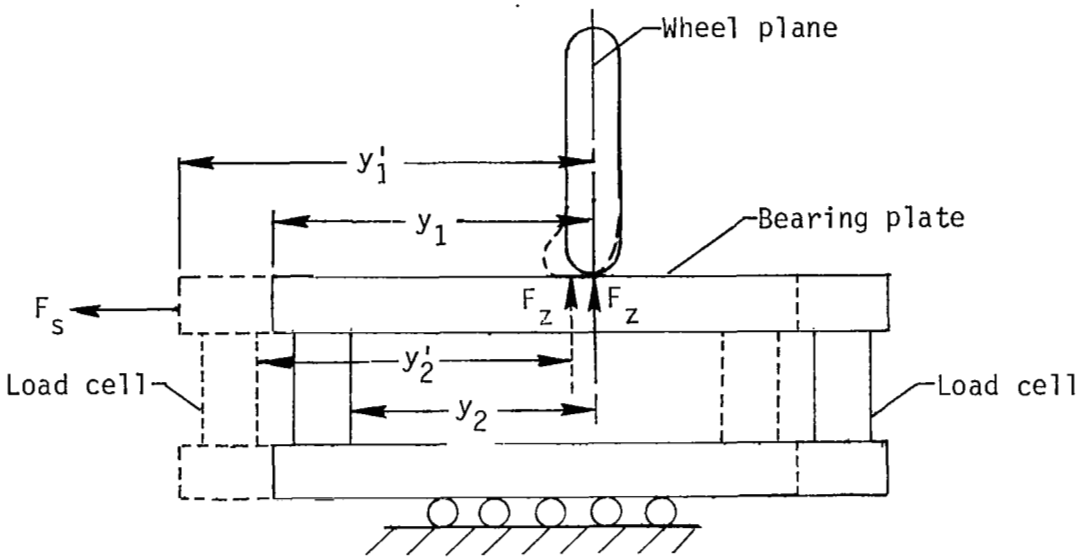

Sketch D

Forces and Moment in Wheel Plane

The forces and moment developed in the wheel plane are shown in sketch E. Also noted in the sketch are the polar moment of inertia I of the wheel, tire,

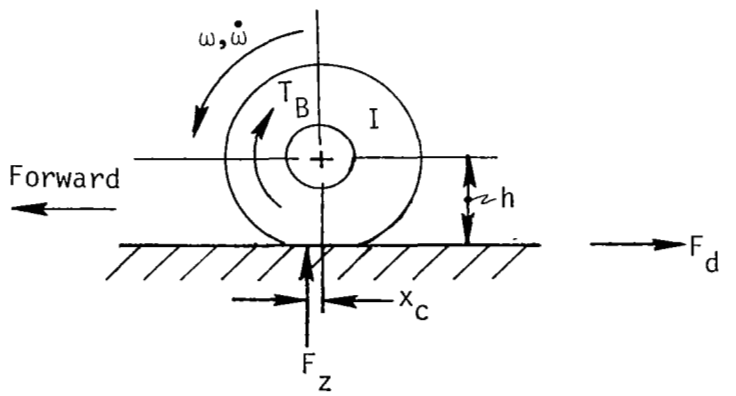

Sketch E

and rotating parts of the brake assembly, the wheel angular velocity ω, and acceleration $\dot{\omega}$, the axle height above the runway h, and the fore-and-aft

center-of-pressure-shift of the tire x_c. The moment developed about the axle T_B is called brake torque and is defined to be positive when it opposes wheel rotation. The brake torque can be expressed in terms of the angular acceleration of the wheel and the forces in the wheel plane in the following manner:

$$T_B = I\dot{\omega} + F_d h - F_z x_c \tag{A5}$$

The brake torque links in the NASA dynamometer (sketch B) are used to obtain a measure of the brake torque independent of the braking force.

For a tire freely rolling (unbraked) at a constant angular velocity, both the brake torque T_B and the wheel angular acceleration $\dot{\omega}$ equal zero, and equation (A5) reduces to

$$F_d h = F_z x_c \tag{A6}$$

In the freely rolling case, F_d is a measure of rolling resistance, and for aircraft tires the value of the fore-and-aft center-of-pressure shift is usually between 2 and 5 percent of the axle height.

Miscellaneous Terms

The following paragraphs describe several additional terms associated with the study of tire mechanical properties.

Free-tread periphery.- That portion of the tread not in contact with the pavement is frequently called the free-tread periphery.

Gross-footprint-area parameter ($A_G/w\sqrt{wd}$).- The gross-footprint area is normalized by the maximum tire width times the square root of the product of the maximum tire width and the maximum tire diameter. This gross-footprint-area parameter is a measure of the flotation capability of the tire.

Hysteresis loss ratio.- The ratio of energy lost during a loading-unloading cycle to the total energy input is called the hysteresis loss ratio. A typical example of a tire load-deflection hysteresis loop in the lateral direction is shown in sketch F. The area cdbfc enclosed by the hysteresis loop represents the total energy loss associated with a complete loading-unloading cycle in both lateral directions. The total energy input to the tire is the sum of the two triangular areas acda and ebfe. Similar loops are generated in the vertical and fore-and-aft directions. The hysteresis loss ratio is an indicator of the damping characteristics of a tire and is an important factor in the tire landing impact capability, shimmy performance, and braking and rolling resistance characteristics.

APPENDIX

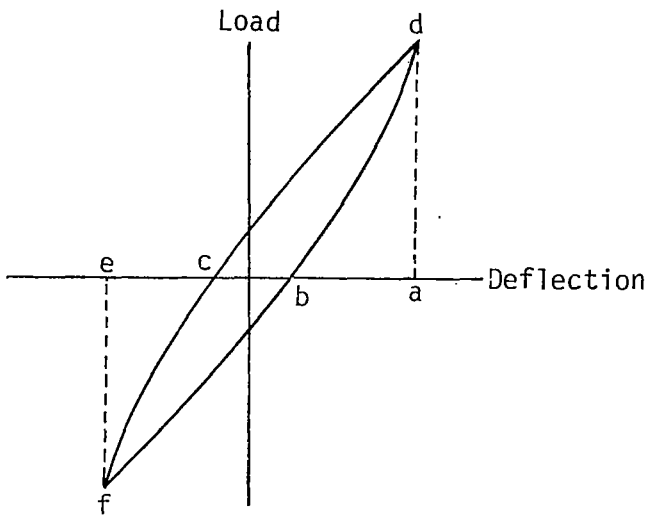

Sketch F

Lateral-stiffness parameter $(K_y/(p + 0.24p_r)w)$.- The spring constant associated with the linear portion of the static lateral load-deflection curve of a tire is normalized by the product of the maximum width of the tire and a pressure function which includes the effects of inflation pressure and carcass stiffness. This lateral-stiffness parameter is an indicator of the cornering capability and shimmy behavior of a tire.

Relaxation length.- The exponential character of tire deformation is described by a coefficient called relaxation length. For the static case the following relationship holds in the free-tread periphery:

$$\lambda = \lambda_o e^{-s/L_s} \tag{A7}$$

where

λ tire deformation in the free-tread periphery

λ_o tire deformation at the leading edge of the footprint

s curvilinear coordinate measuring circumferential distance from the footprint leading edge

L_s static lateral relaxation length

At the circumferential position on the free-tread periphery where $s = L_s$, the value of λ has been relaxed to a value of 37 percent of λ_o.

APPENDIX

The initial buildup in side force under yawed rolling follows a similar exponential law:

$$F_y = F_{y,e}\left(1 - e^{-x/L_y}\right) \tag{A8}$$

where

x distance rolled

F_y instantaneous cornering force perpendicular to the direction of motion

$F_{y,e}$ steady-state cornering force

L_y yawed-rolling relaxation length

Equation (A8) states that F_y reaches approximately 63 percent of the steady-state value when the tire rolls a distance $x = L_y$. The relaxation length is an important tire characteristic which influences tire shimmy behavior.

Spring rate.- The nonlinear stiffness of a tire in its various operational modes is measured by spring rate. It is defined in this paper as the instantaneous slope of the tire load-deflection curve. The spring rate of a tire affects its landing impact capability, shimmy characteristics, and response to braking and steering inputs.

Vertical-force parameter $(F_z/(p + 0.08p_r)w\sqrt{wd})$.- Tire vertical load is normalized by the product of a pressure function, which includes the effects of inflation pressure and carcass stiffness, and a footprint-area function.

Symbols

Values are given in both SI and U.S. Customary Units. The measurements and calculations were made in U.S. Customary Units. Factors relating the two systems are presented in reference 12.

A constant

A_G gross footprint area

A_N net footprint area

C_λ ratio of lateral shift in center of pressure to tire footprint displacement

d outside diameter of unloaded tire

F_d drag force parallel to wheel plane

APPENDIX

F_s	side force perpendicular to wheel plane
F_y	lateral or cornering force perpendicular to direction of motion
$F_{y,e}$	steady-state lateral force perpendicular to direction of motion
F_z	tire vertical loading
k_L	constant associated with footprint length
k_W	constant associated with footprint width
K_y	tire lateral spring rate
K_z	tire vertical spring rate
L_f	length of tire-ground contact area (footprint)
L_s	tire static relaxation length
L_y	tire yawed-rolling relaxation length
M_x	overturning torque, moment about horizontal axis in wheel plane through wheel center
M_z	aligning torque, moment about vertical axis through wheel center
P_ℓ	tire lateral-stiffness parameter
P_v	tire vertical-force parameter
p	tire inflation pressure
p_r	tire rated inflation pressure
q	friction-force moment arm
s	peripheral distance around tire
V	ground speed
W_f	width of tire-ground contact area (footprint)
w	maximum width of undeflected tire
x	displacement in direction of motion
y_c	lateral center-of-pressure shift
λ	lateral deflection of tire equator
δ	vertical tire deflection

APPENDIX

ψ	tire yaw angle
θ	tire peripheral angle
μ_s	side-force friction coefficient

REFERENCES

1. Hadekel, R.: The Mechanical Characteristics of Pneumatic Tyres - A Digest of Present Knowledge. S & T Memo. No. 10/52, TPA 3/TIB, British Min. Supply, Nov. 1952. (Supersedes S & T Memo. No. 5/50.)

2. Smiley, Robert F.; and Horne, Walter B.: Mechanical Properties of Pneumatic Tires With Special Reference to Modern Aircraft Tires. NASA TR R-64, 1960. (Supersedes NACA TN 4110.)

3. Nybakken, G. H.; Dodge, R. N.; and Clark, S. K.: A Study of Dynamic Tire Properties Over a Range of Tire Constructions. NASA CR-2219, 1973.

4. Clark, S. K.; Dodge, R. N.; Lackey, J. I.; and Nybakken, G. H.: Structural Modeling of Aircraft Tires. NASA CR-2220, 1973.

5. Dodge, R. N.; Larson, R. B.; Clark, S. K.; and Nybakken, G. H.: Testing Techniques for Determining Static Mechanical Properties of Pneumatic Tires. NASA CR-2412, 1974.

6. Tanner, John A.; and Dreher, Robert C.: Cornering Characteristics of a 40 × 14-16 Type VII Aircraft Tire and a Comparison With Characteristics of a C40 × 14-21 Cantilever Aircraft Tire. NASA TN D-7351, 1973.

7. Dreher, Robert C.; and Tanner John A.: Experimental Investigation of the Cornering Characteristics of 18 × 5.5, Type VII, Aircraft Tires With Different Tread Patterns. NASA TN D-7815, 1974.

8. Tanner, John A.; McCarty, John L.; and Batterson, Sidney A.: The Elastic Response of Bias-Ply Aircraft Tires to Braking Forces. NASA TN D-6426, 1971.

9. Tanner, John A.: Fore-and-Aft Elastic Response Characteristics of 34 × 9.9, Type VII, 14 Ply-Rating Aircraft Tires of Bias-Ply, Bias-Belted, and Radial-Belted Design. NASA TN D-7449, 1974.

10. Dreher, Robert C.; and Yager, Thomas J.: Friction Characteristics of 20 × 4.4, Type VII, Aircraft Tires Constructed With Different Tread Rubber Compounds. NASA TN D-8252, 1976.

11. Recommended Practice for Measurement of Static Mechanical Stiffness Properties of Aircraft Tires. AIR 1380, Soc. Automot. Eng., Aug. 1975.

12. Standard for Metric Practice. E 380-79, American Soc. Testing & Mater., c.1980.

TABLE I.- CHARACTERISTICS OF TWO TIRE SIZES

	18 × 5.5	49 × 17
Type	VII	VII
Ply rating	14	26
Type of ply	Bias	Bias
Rated vertical load F_z, kN (lb)	27.6 (6200)	176 (39 600)
Rated inflation pressure, p_r, kPa (psi)	1482 (215)	1172 (170)
Outside diameter of unloaded tire, d, cm (in.)	44.7 (17.6)	122.49 (48.225)
Maximum width of unloaded tire, w, cm (in.)	14.03 (5.525)	42.74 (16.825)
Tread description (no. of circumferential grooves) . . .	3	4

TABLE II.- SUMMARY OF TEST CONDITIONS AND STEADY-STATE RESULTS FROM YAWED-ROLLING TESTS OF 18 × 5.5 TIRE

V	ψ	F_z		F_s		F_d		M_z		M_x		y_c		q	
knots	deg	kN	lbf	kN	lbf	kN	lbf	N-m	in-lbf	N-m	in-lbf	cm	in.	cm	in.
5	1	13.12	2950	2.14	481	.55	123	61.7	547	135.7	1201	-2.29	-.90	2.79	1.10
		20.33	4570	2.52	567	.74	167	77.3	684	257.9	2283	-1.19	-.47	2.95	1.16
		27.46	6173	2.44	549	1.18	266	115.7	1024	239.6	2121	-.81	-.32	4.27	1.68
		33.79	7595	2.44	549	1.44	323	140.4	1243	242.4	2146	-.61	-.24	4.95	1.95
5	3	13.20	2967	5.14	1156	.31	69	116.6	1032	723.8	6406	-2.29	-.90	2.26	.89
		20.08	4515	5.95	1338	.66	148	162.8	1441	968.6	8573	-.91	-.36	2.72	1.07
		27.13	6100	5.95	1338	.79	177	245.0	2168	991.2	8773	-.41	-.16	4.09	1.61
		34.00	7644	5.44	1222	1.20	269	327.9	2902	942.5	8342	-.10	-.04	5.89	2.32
5	6	13.60	3056	7.57	1701	.05	10	34.7	307	1404.6	12432	-.84	-.33	.46	.18
		20.88	4695	9.21	2071	.66	149	134.8	1193	1835.4	16245	.30	.12	1.45	.57
		27.56	6195	10.16	2285	.61	136	236.9	2096	2112.0	18692	.84	.33	2.34	.92
		34.25	7701	9.65	2170	1.17	264	363.9	3221	1990.4	17616	.86	.34	3.73	1.47
5	6	13.86	3115	7.79	1751	.35	80	32.5	287	1315.9	11647	-1.73	-.68	.41	.16
		20.65	4643	9.22	2073	.52	117	113.0	1000	1746.9	15461	-.13	-.05	1.22	.48
		27.58	6201	9.99	2246	.78	175	235.7	2086	1910.7	16911	.23	.09	2.36	.93
		32.51	7309	9.92	2229	.79	178	335.5	2970	1956.8	17319	.48	.19	3.38	1.33
5	9	13.84	3112	9.99	2246	.28	62	-2.8	-25	2498.9	22117	3.78	1.49	-.03	-.01
		20.46	4600	12.19	2741	.55	123	89.1	789	3096.4	27406	3.81	1.50	.74	.29
		27.30	6137	13.26	2981	1.03	231	216.5	1916	3486.0	30854	3.96	1.56	1.63	.64
		28.94	6506	13.15	2956	1.05	235	287.9	2548	3512.5	31089	3.99	1.57	2.18	.86
5	9	13.59	3055	9.40	2114	.24	55	9.1	80	2293.8	20302	3.12	1.23	.10	.04
		20.78	4671	11.46	2576	.65	146	98.2	870	2888.4	25564	3.38	1.33	.86	.34
		27.83	6257	12.41	2791	.89	201	252.5	2235	3255.6	28815	3.58	1.41	2.03	.80
		28.53	6415	12.56	2824	1.05	236	283.0	2504	3297.6	29186	3.58	1.41	2.24	.88
5	9	14.55	3270	9.31	2094	.27	61	48.2	426	2347.3	20775	3.35	1.32	.51	.20
		21.46	4824	11.42	2568	.64	143	165.2	1462	2933.8	25966	3.48	1.37	1.45	.57
		28.53	6414	12.22	2748	.97	218	305.8	2706	3199.3	28316	3.33	1.31	2.49	.98
		29.91	6724	12.37	2781	1.14	257	276.5	2447	3238.2	28660	3.20	1.26	2.24	.88
50	1	13.12	2949	2.36	530	.52	116	57.6	510	215.3	1906	-1.98	-.78	2.39	.94
		20.43	4593	2.58	581	1.07	242	60.2	533	308.4	2730	-.99	-.39	2.16	.85
		27.26	6129	2.74	615	1.26	284	129.5	1146	324.9	2875	-.74	-.29	4.29	1.69
		34.80	7823	2.66	598	1.92	431	146.5	1297	334.6	2962	-.46	-.18	4.47	1.76
50	3	13.56	3049	5.14	1156	.50	113	68.6	607	1095.6	9697	.33	.13	1.32	.52
		19.30	4339	5.80	1305	.46	103	165.8	1467	1176.9	10416	.18	.07	2.84	1.12
		25.74	5786	5.66	1272	1.15	258	173.0	1531	1302.7	11530	.94	.37	3.00	1.18
		32.55	7317	5.29	1189	1.14	256	282.6	2501	1173.2	10384	.61	.24	5.23	2.06
50	6	12.52	2815	7.24	1627	.23	51	13.9	123	1418.2	12553	-.64	-.25	.20	.08
		20.73	4659	9.80	2202	.43	97	126.5	1119	2155.3	19076	1.07	.42	1.30	.51
		27.00	6070	10.24	2301	.81	182	197.1	1744	2245.7	19876	1.02	.40	1.93	.76
		34.52	7760	9.21	2071	1.30	293	339.2	3002	2147.7	19009	1.37	.54	3.66	1.44
50	9	13.39	3010	8.46	1902	.14	31	-41.1	-364	2168.6	19194	3.18	1.25	-.48	-.19
		20.70	4654	11.46	2576	.57	129	11.0	97	2960.2	26200	3.25	1.28	.10	.04
		26.83	6031	12.51	2811	.91	204	116.5	1031	3283.2	29058	3.25	1.28	.94	.37
		30.10	6767	13.03	2929	1.01	226	289.2	2560	3387.5	29982	3.15	1.24	2.21	.87

TABLE II.- Concluded

V	ψ	F_z		F_s		F_d		M_z		M_x		y_c		q	
knots	deg	kN	lbf	kN	lbf	kN	lbf	N-m	in-lbf	N-m	in-lbf	cm	in.	cm	in.
75	1	13.20	2966	2.08	468	.58	131	46.6	412	153.4	1358	-2.06	-.81	2.16	.85
		20.06	4510	2.55	572	.92	208	56.8	502	364.2	3223	-.74	-.29	2.11	.83
		26.68	5997	2.62	590	1.42	320	83.8	742	363.3	3215	-.56	-.22	2.82	1.11
		33.61	7555	2.78	624	1.40	316	156.7	1387	315.3	2790	-.61	-.24	5.03	1.98
75	3	13.82	3108	5.55	1248	.46	103	132.0	1168	1188.8	10522	.48	.19	2.36	.93
		20.56	4621	6.13	1377	.85	192	170.7	1511	1432.5	12679	1.09	.43	2.77	1.09
		28.02	6298	5.95	1337	1.17	263	267.4	2366	1515.8	13416	1.40	.55	4.42	1.74
		34.27	7704	5.19	1167	1.51	340	326.4	2889	1403.5	12422	1.32	.52	6.05	2.38
75	6	13.45	3024	7.45	1676	.58	130	-27.9	-247	1623.6	14370	.71	.28	-.38	-.15
		20.30	4563	10.33	2323	.35	80	128.1	1134	2219.9	19648	.84	.33	1.24	.49
		27.76	6241	11.22	2522	1.24	279	139.7	1236	2476.2	21917	1.19	.47	1.24	.49
		34.59	7776	10.63	2389	1.49	336	334.1	2957	2482.8	21974	1.55	.61	3.12	1.23
75	9	12.91	2903	8.46	1902	.05	12	-26.8	-238	2050.3	18146	2.44	.96	-.30	-.12
		19.29	4336	11.25	2530	.50	113	-14.4	-128	2816.8	24931	3.05	1.20	-.13	-.05
		27.52	6186	13.19	2965	.94	211	224.7	1989	3303.2	29236	2.97	1.17	1.70	.67
		29.89	6720	12.89	2898	1.14	256	275.9	2442	3339.6	29558	3.25	1.28	2.13	.84
100	1	12.28	2760	2.07	466	.63	143	40.7	361	263.5	2332	-1.37	-.54	1.88	.74
		20.36	4577	2.30	518	.96	216	96.9	858	454.8	4025	-.08	-.03	3.89	1.53
		26.68	5999	2.46	552	.96	215	178.6	1581	407.0	3602	-.30	-.12	6.78	2.67
		33.90	7621	2.46	552	1.89	425	140.8	1246	426.6	3776	-.13	-.05	4.55	1.79
100	3	13.23	2973	5.30	1191	.54	122	26.9	238	1192.9	10558	.76	.30	.51	.20
		21.01	4723	6.54	1471	.30	68	162.3	1437	1561.6	13821	1.14	.45	2.49	.98
		28.16	6331	6.70	1506	1.08	242	217.5	1925	1510.8	13372	.69	.27	3.20	1.26
		34.95	7857	6.39	1436	1.77	398	225.7	1997	1258.2	11136	.15	.06	3.40	1.34
100	6	12.14	2729	7.06	1588	.42	94	-59.1	-523	1745.1	15445	2.21	.87	-.84	-.33
		19.93	4480	9.17	2063	.46	104	29.1	258	2282.8	20204	2.16	.85	.30	.12
		27.16	6106	10.15	2282	1.39	312	114.3	1011	2601.9	23029	2.34	.92	1.12	.44
		33.75	7587	9.58	2154	.91	204	408.7	3617	2666.2	23598	2.57	1.01	4.24	1.67
100	9	14.12	3173	8.79	1977	.24	54	-148.1	-1310	2367.2	20952	3.91	1.54	-1.68	-.66
		20.48	4605	12.67	2848	-.74	-167	-50.7	-449	2970.8	26294	2.34	.92	-.41	-.16
		27.56	6195	13.34	2999	-.37	-84	107.6	952	3125.5	27663	2.24	.88	.81	.32
		30.41	6836	13.19	2965	.11	25	207.9	1840	3184.2	28183	2.49	.98	1.57	.62

TABLE III.- SUMMARY OF TEST CONDITIONS AND STEADY-STATE RESULTS FROM YAWED-ROLLING TESTS OF 49 × 17 TIRE

V	ψ	F_z		F_s		F_d		M_z		M_x		y_c		q	
knots	deg	kN	lbf	kN	lbf	kN	lbf	N-m	in-lbf	N-m	in-lbf	cm	in.	cm	in.
50	1	73.53	16531	15.92	3580	.73	163	676.2	5984	7689.5	68058	-2.41	-.95	4.24	1.67
		126.21	28374	16.82	3781	1.78	399	1622.1	14356	9304.9	82355	-.13	-.05	9.60	3.78
		157.88	35493	14.42	3241	3.61	812	2201.8	19487	14945.8	132282	4.47	1.76	14.81	5.83
		208.62	46900	12.96	2915	3.61	810	2389.8	21152	9554.0	84560	1.19	.47	17.75	6.99
50	3	95.73	21520	37.97	8536	1.51	339	1845.2	16331	20802.7	184120	-1.70	-.67	4.85	1.91
		126.02	28331	33.88	7617	1.51	339	3118.5	27601	25616.6	226726	5.05	1.99	9.19	3.62
		179.51	40354	42.14	9473	4.36	980	5221.0	46209	23027.4	203810	****N/A****		12.32	4.85
		204.36	45942	34.98	7864	4.18	939	5964.4	52790	21323.9	188733	1.24	.49	16.94	6.67
50	6	88.34	19859	59.97	13481	-.77	-173	769.7	6812	31947.9	282763	****N/A****		1.30	.51
		128.37	28859	67.46	15166	1.48	333	2564.6	22699	38526.8	340991	.03	.01	3.81	1.50
		184.25	41421	69.02	15515	2.05	460	6150.2	54434	40242.2	356173	1.50	.59	8.92	3.51
		203.43	45734	68.01	15289	3.77	846	7750.9	68601	40037.7	354363	1.73	.68	11.38	4.48
50	9	92.43	20780	63.47	14268	-1.26	-284	-796.7	-7051	36102.8	319537	-1.32	-.52	-1.24	-.49
		133.82	30083	83.12	18686	1.54	347	463.4	4101	48068.5	425442	.66	.26	.56	.22
		188.35	42343	90.17	20272	3.51	789	3767.2	33343	56234.3	497716	4.29	1.69	4.17	1.64
		204.92	46069	92.71	20842	4.89	1099	6321.0	55945	58521.0	517955	5.03	1.98	6.81	2.68
75	1	81.43	18307	13.75	3092	1.56	351	653.6	5785	9844.1	87127	2.01	.79	4.72	1.86
		128.28	28838	14.70	3304	2.19	491	1641.2	14526	10095.5	89352	1.24	.49	11.05	4.35
		181.48	40798	16.50	3709	3.26	732	2332.2	20642	8659.2	76641	-.20	-.08	13.87	5.46
		194.44	43711	15.62	3511	3.32	746	2477.0	21923	9408.8	83275	.53	.21	15.52	6.11
75	3	88.83	19969	31.23	7022	.09	21	1135.0	10045	19731.4	174637	1.09	.43	3.63	1.43
		127.03	28557	34.48	7752	.27	60	2939.8	26020	23491.2	207915	****N/A****		8.53	3.36
		158.40	35610	39.98	8988	2.48	558	5318.8	47075	29415.2	260346	4.42	1.74	13.28	5.23
		203.37	45719	37.18	8359	3.72	836	6169.5	54604	23713.2	209879	1.63	.64	16.51	6.50
75	6	89.97	20226	53.05	11925	-.53	-120	984.0	8709	30326.7	268414	-1.30	-.51	1.85	.73
		125.15	28136	67.23	15115	.65	147	2233.7	19770	39359.1	348357	.46	.18	3.33	1.31
		205.82	46270	69.77	15685	4.03	907	7878.8	69733	39360.6	348371	.91	.36	11.28	4.44
75	9	90.63	20374	61.96	13930	.52	117	-939.7	-8317	34868.3	308610	-2.24	-.88	-1.52	-.60
		136.14	30605	79.46	17863	.28	63	634.9	5619	46041.2	407499	.48	.19	.79	.31
		181.27	40752	90.63	20374	1.92	431	3411.2	30191	56607.9	501022	3.86	1.52	3.76	1.48
		212.19	47703	90.95	20447	3.42	770	6197.0	54848	56113.5	496646	3.51	1.38	6.81	2.68
100	1	91.77	20630	11.90	2675	.95	213	887.5	7855	7827.1	69275	****N/A****		7.44	2.93
		127.65	28698	12.39	2786	2.08	468	1314.0	11630	7176.9	63521	****N/A****		10.46	4.12
		170.79	38395	12.49	2809	2.41	541	2029.7	17964	8096.2	71657	.69	.27	15.95	6.28
		197.27	44347	11.31	2543	1.12	251	2613.0	23127	6774.7	59961	.28	.11	22.99	9.05
100	3	84.03	18890	34.26	7701	-.00	-0	1471.2	13021	20603.2	182354	-.13	-.05	4.29	1.69
		133.50	30013	39.71	8927	1.75	393	3105.3	27484	24489.7	216752	****N/A****		7.82	3.08
		176.65	39713	39.66	8916	1.79	402	4899.3	43362	24579.0	217542	1.09	.43	12.34	4.86
		192.05	43175	38.98	8763	4.17	937	5261.8	46571	24055.4	212908	1.37	.54	13.41	5.28
100	6	80.21	18031	48.47	10897	-.84	-189	81.6	722	28050.1	248264	-1.75	-.69	.18	.07
		127.53	28670	63.98	14383	.07	15	2480.0	21950	36968.3	327197	****N/A****		3.89	1.53
		185.18	41630	66.46	14942	2.04	458	6885.4	60941	38722.6	342724	1.12	.44	10.36	4.08
		191.57	43067	65.49	14723	2.59	583	7844.7	69432	39750.5	351821	1.88	.74	11.96	4.71
100	9	89.49	20119	60.93	13698	.08	18	-816.3	-7225	35903.0	317769	-1.30	-.51	-1.35	-.53
		126.04	28335	73.96	16627	1.22	275	-259.0	-2292	44826.9	396751	1.24	.49	-.36	-.14
		185.28	41652	88.16	19815	2.33	525	2902.2	25687	52063.4	460800	1.57	.62	3.30	1.30
		189.82	42673	90.45	20334	2.66	599	4503.3	39858	56884.5	503470	4.19	1.65	4.98	1.96

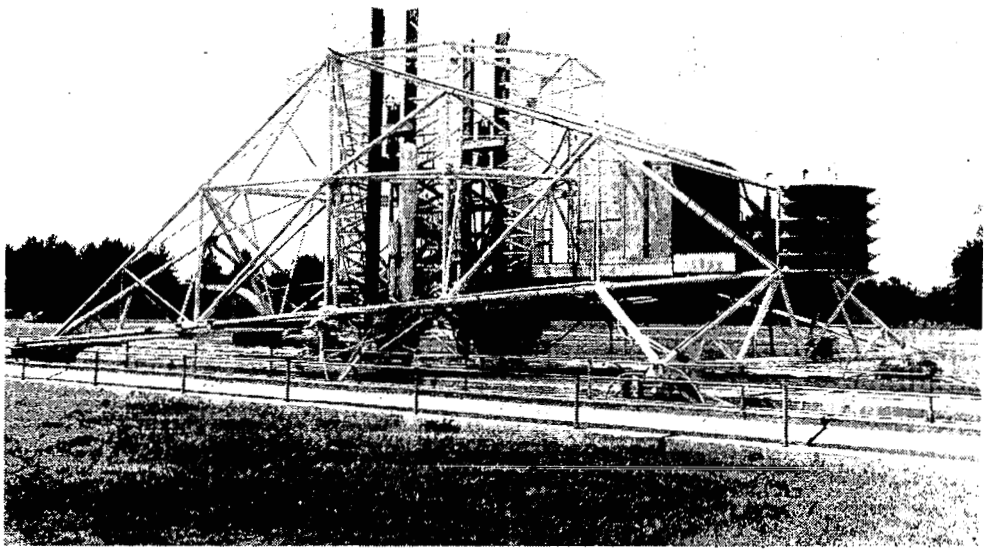

L-69-5858

Figure 1.- Carriage used in testing the 49 × 17 tire.

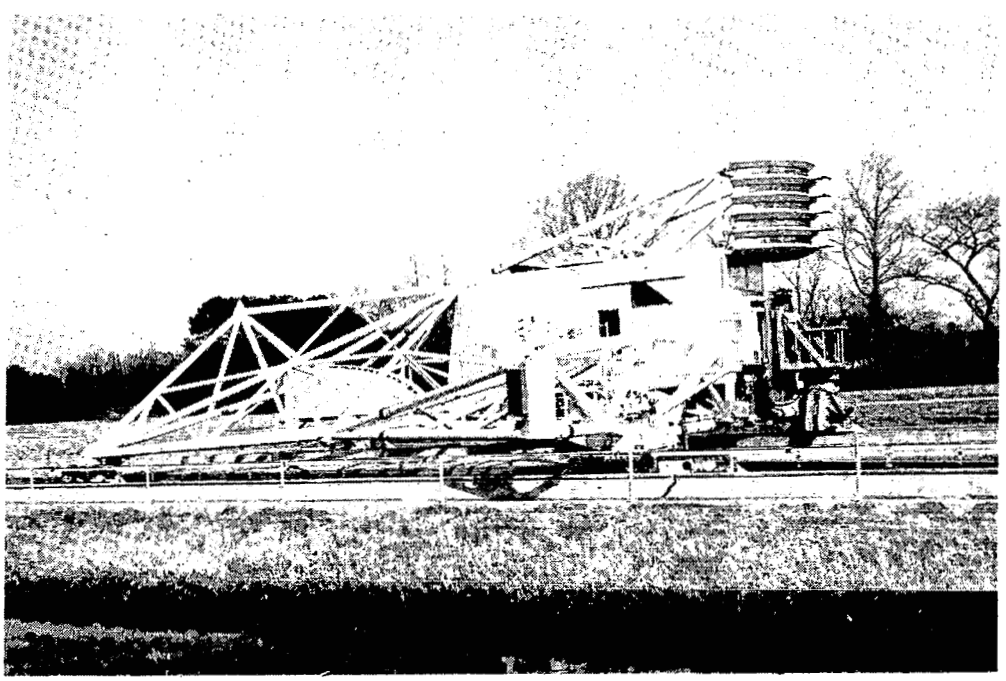

L-79-1761

Figure 2.- Carriage used in testing the 18 × 5.5 tire.

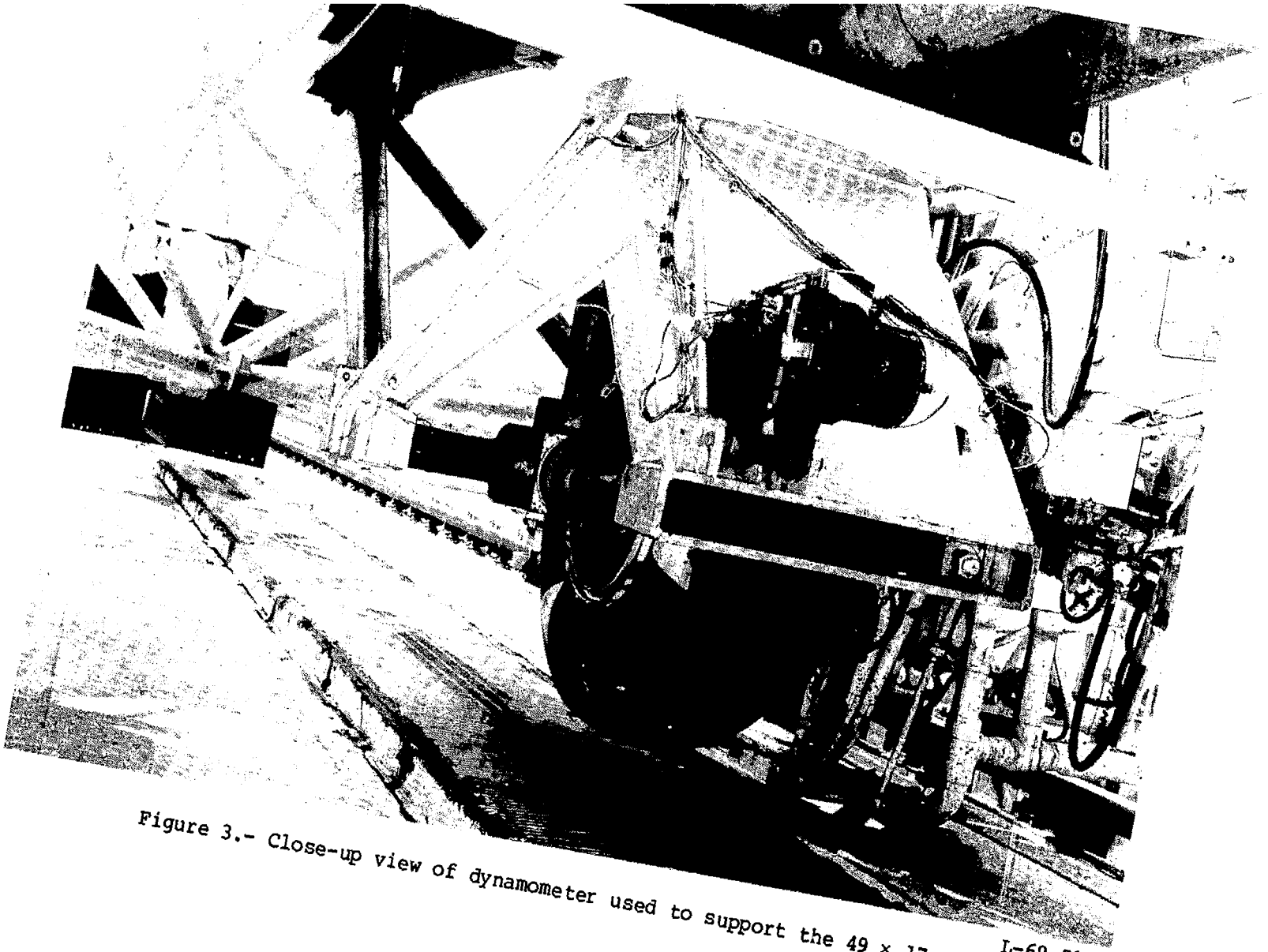

Figure 3.- Close-up view of dynamometer used to support the 49 × 17 tire. L-69-5862

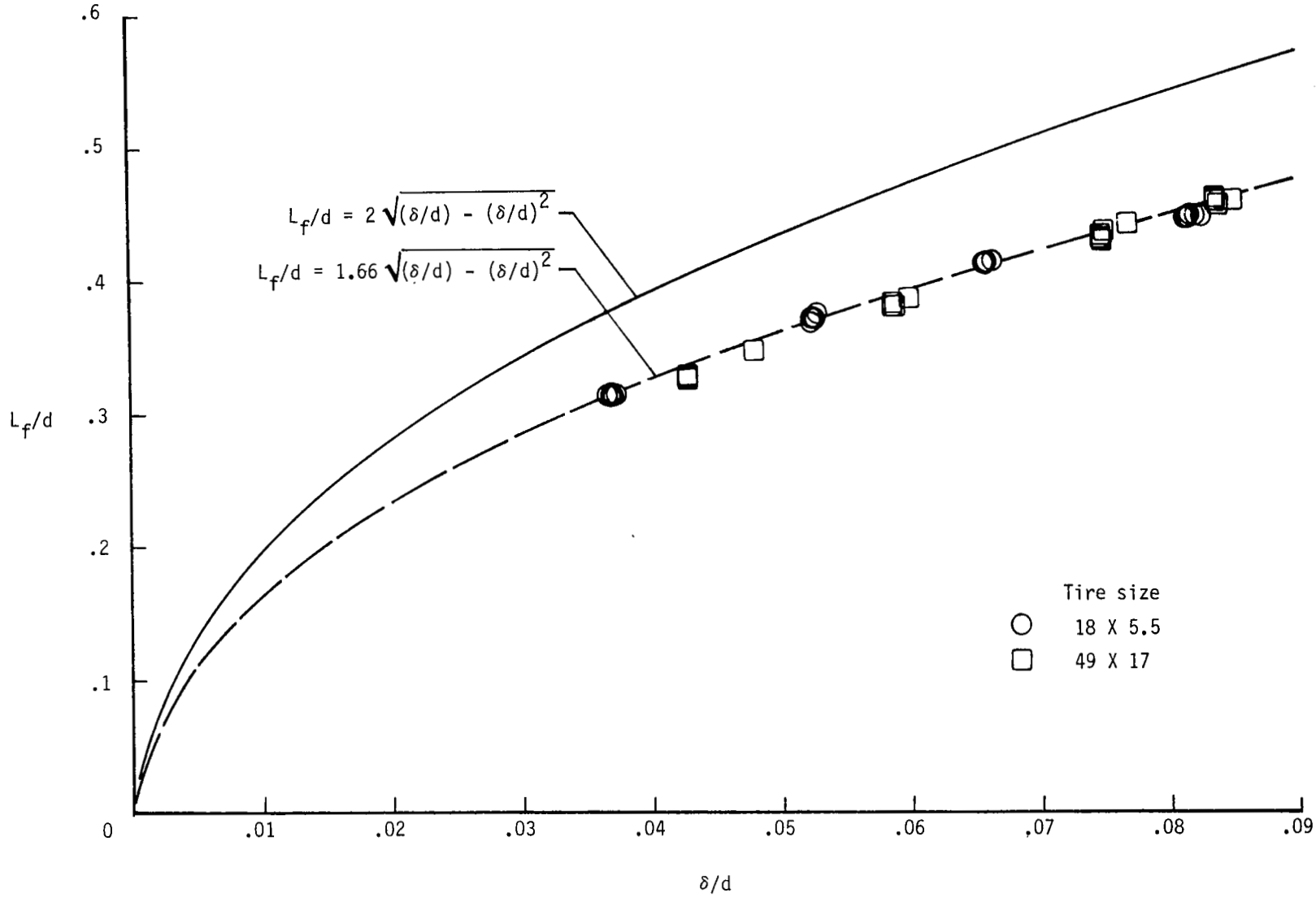

Figure 4.- Variation of tire footprint length with vertical deflection.

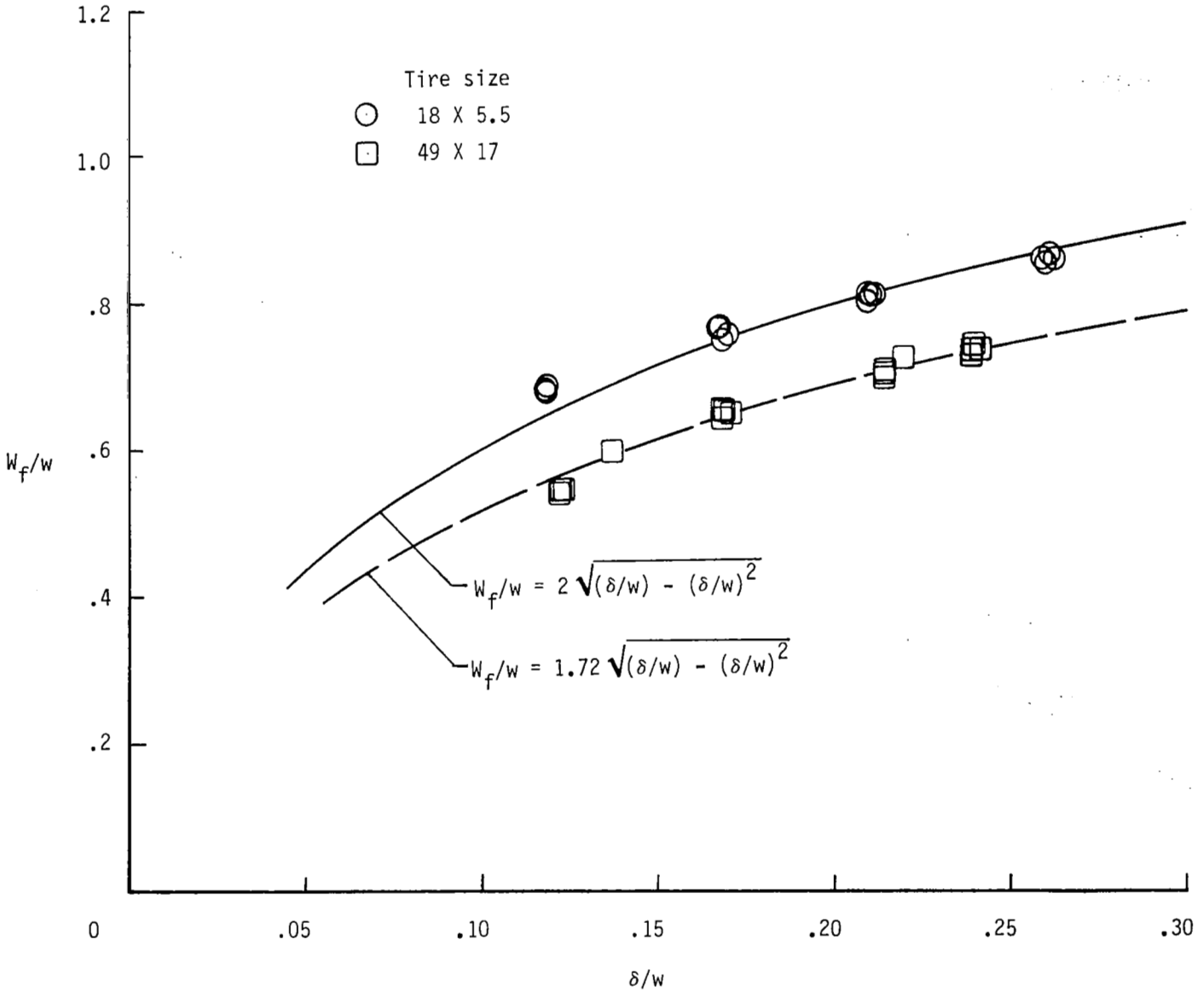

Figure 5.- Variation of tire footprint width with vertical deflection.

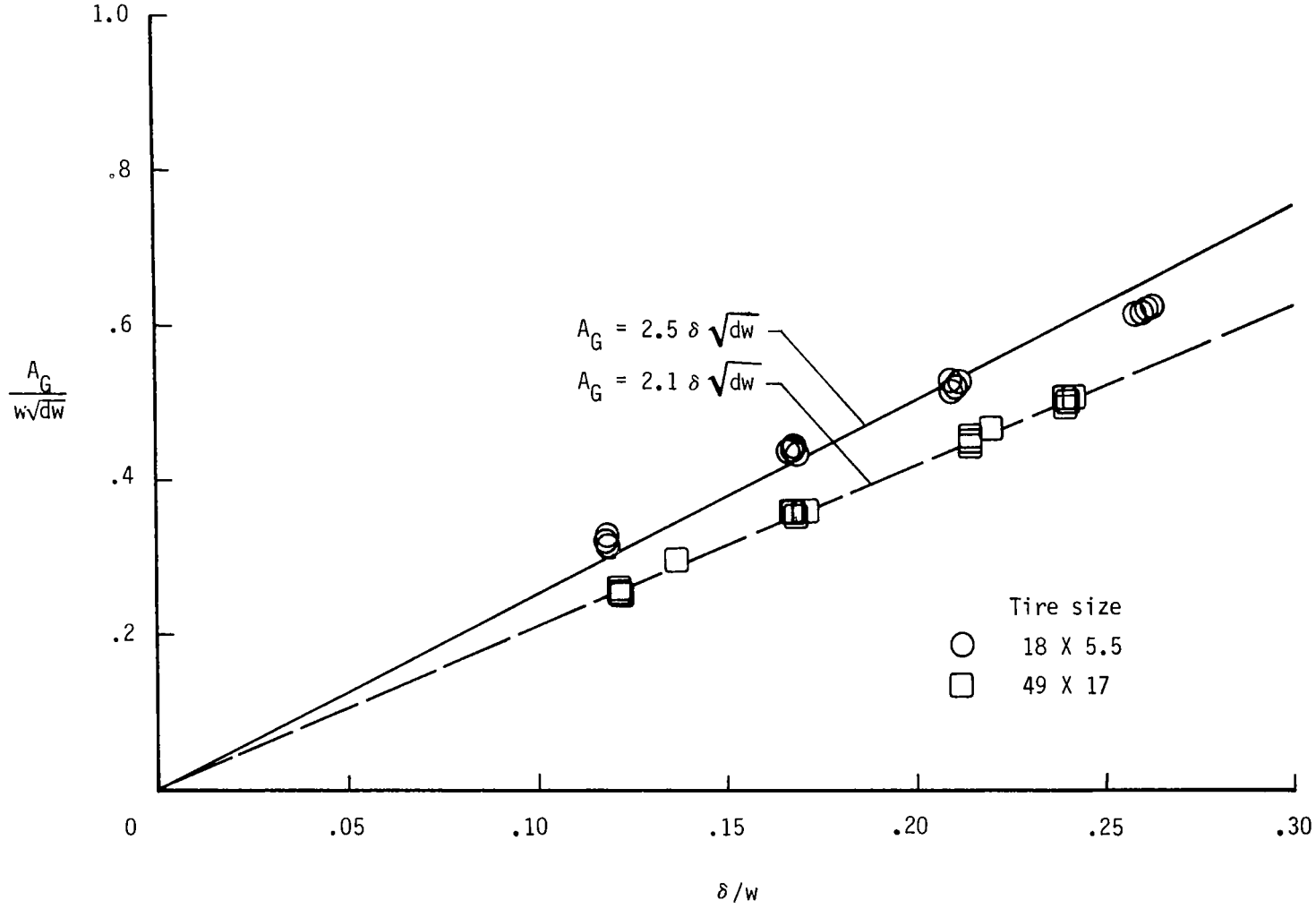

Figure 6.- Variation of tire gross-footprint-area parameter with vertical deflection.

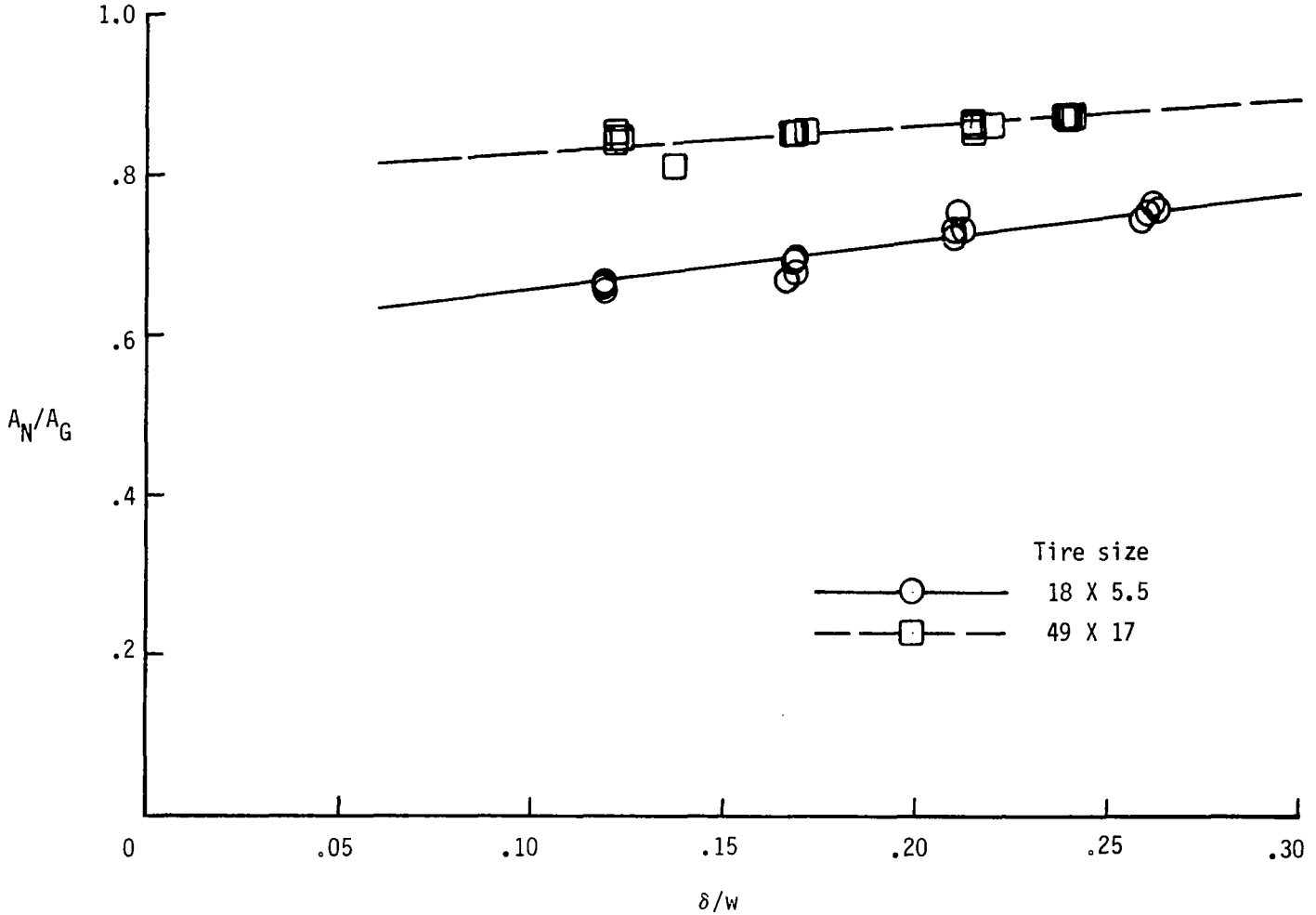

Figure 7.- Ratio of tire net footprint area to gross-footprint area as a function vertical deflection.

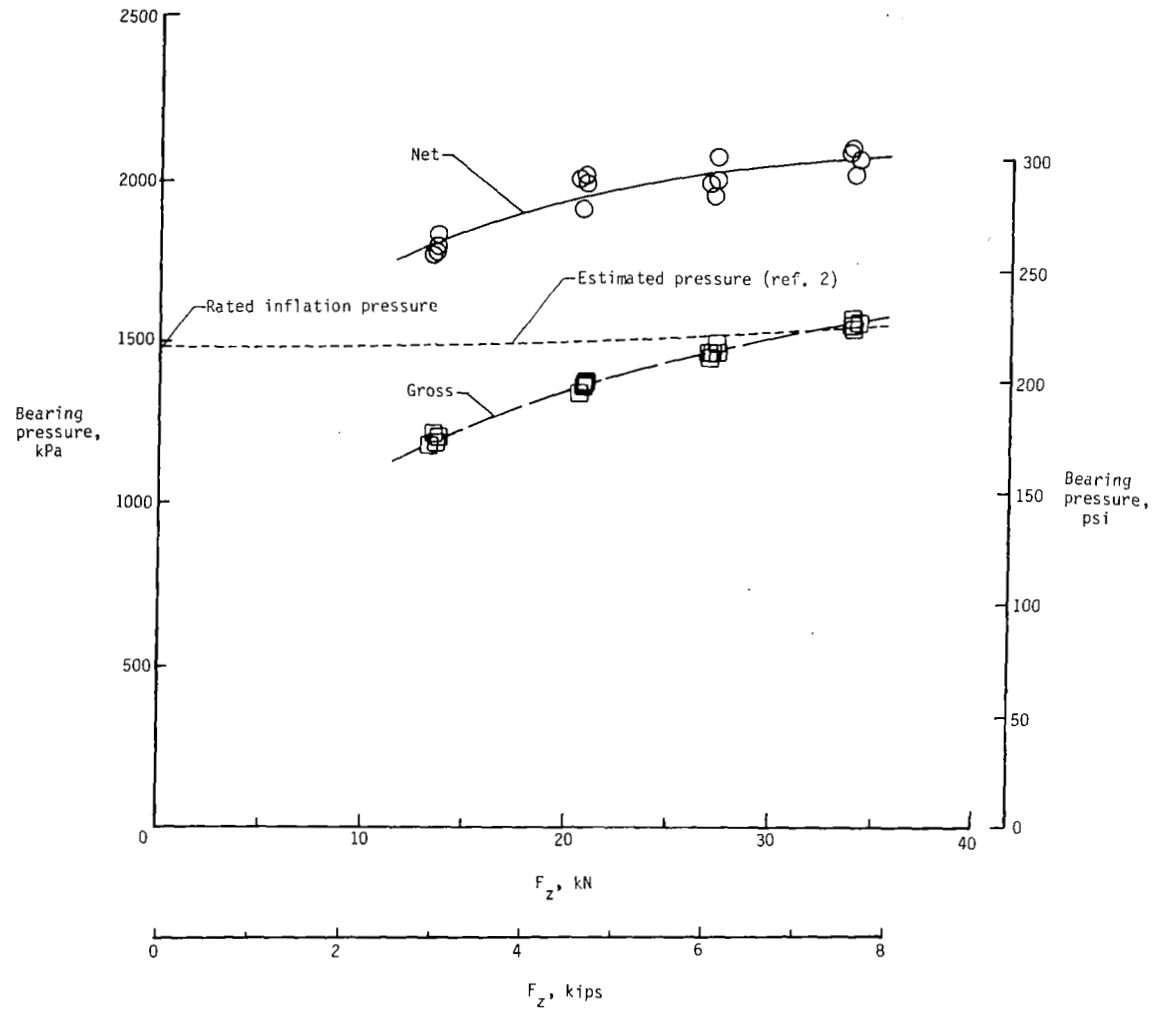

(a) 18 × 5.5 tire.

Figure 8.- Variation of tire net and gross bearing pressures with vertical load.

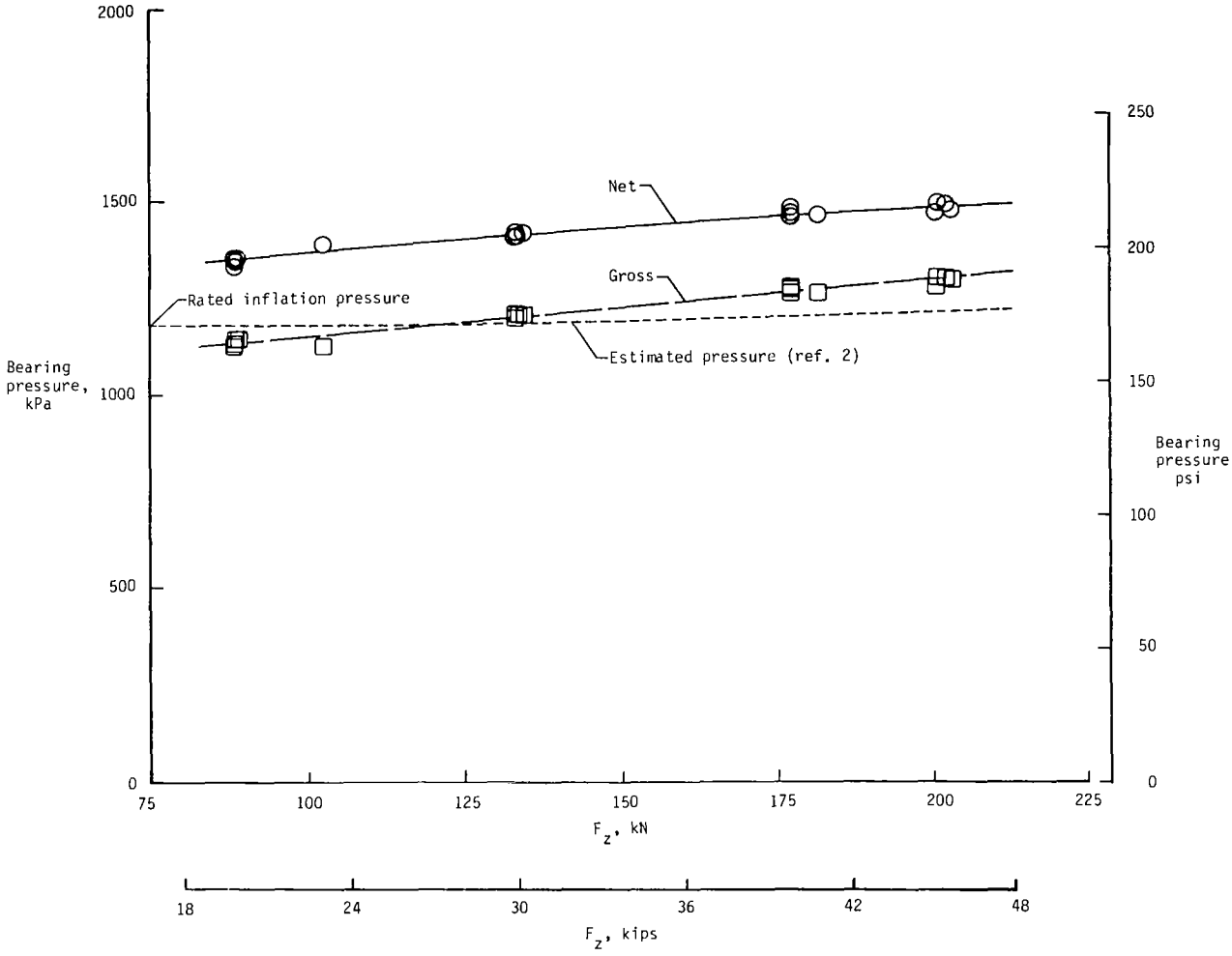

(b) 49 × 17 tire.

Figure 8.- Concluded.

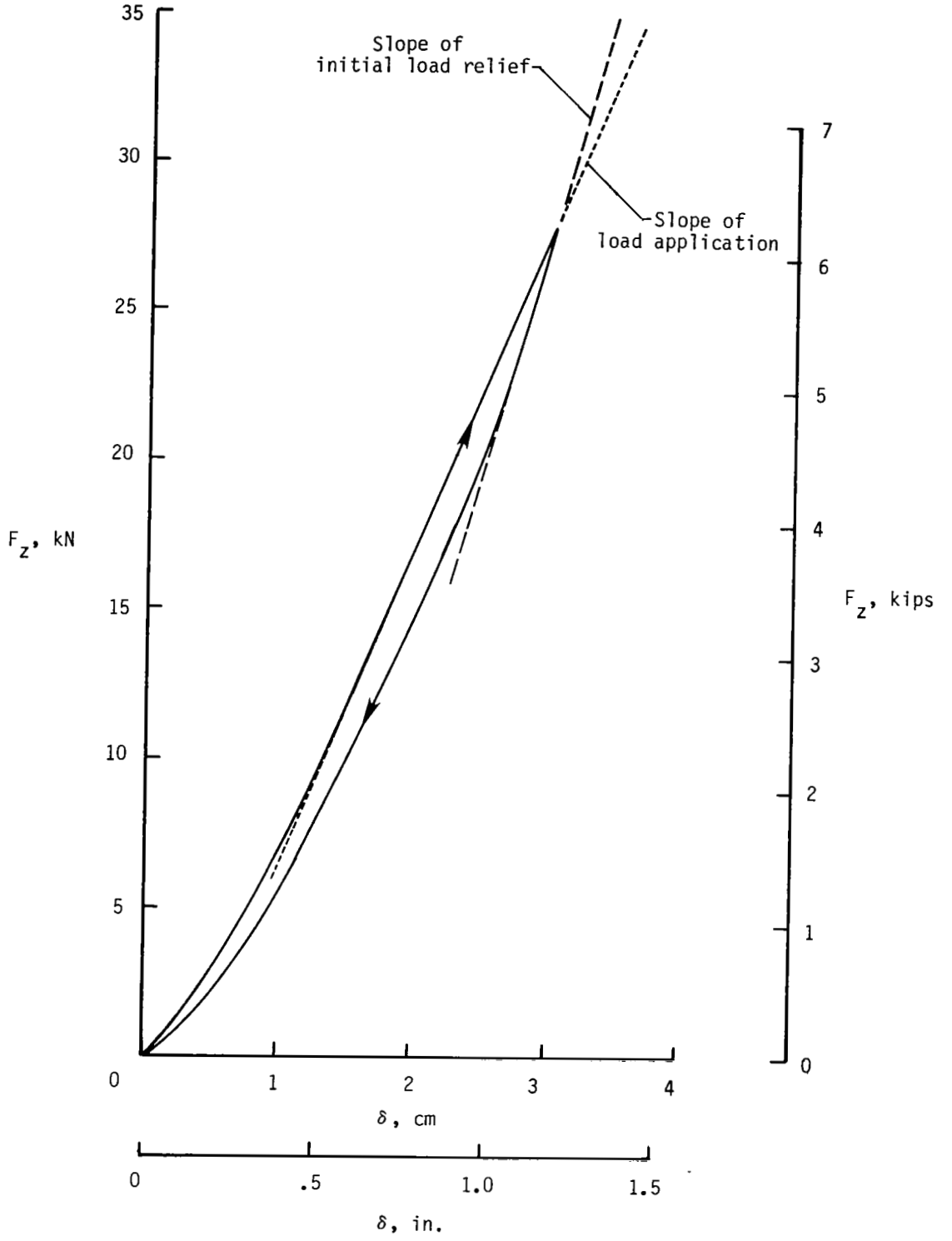

Figure 9.- Typical tire vertical load-deflection curve showing how vertical spring rates were acquired (18 × 5.5 tire).

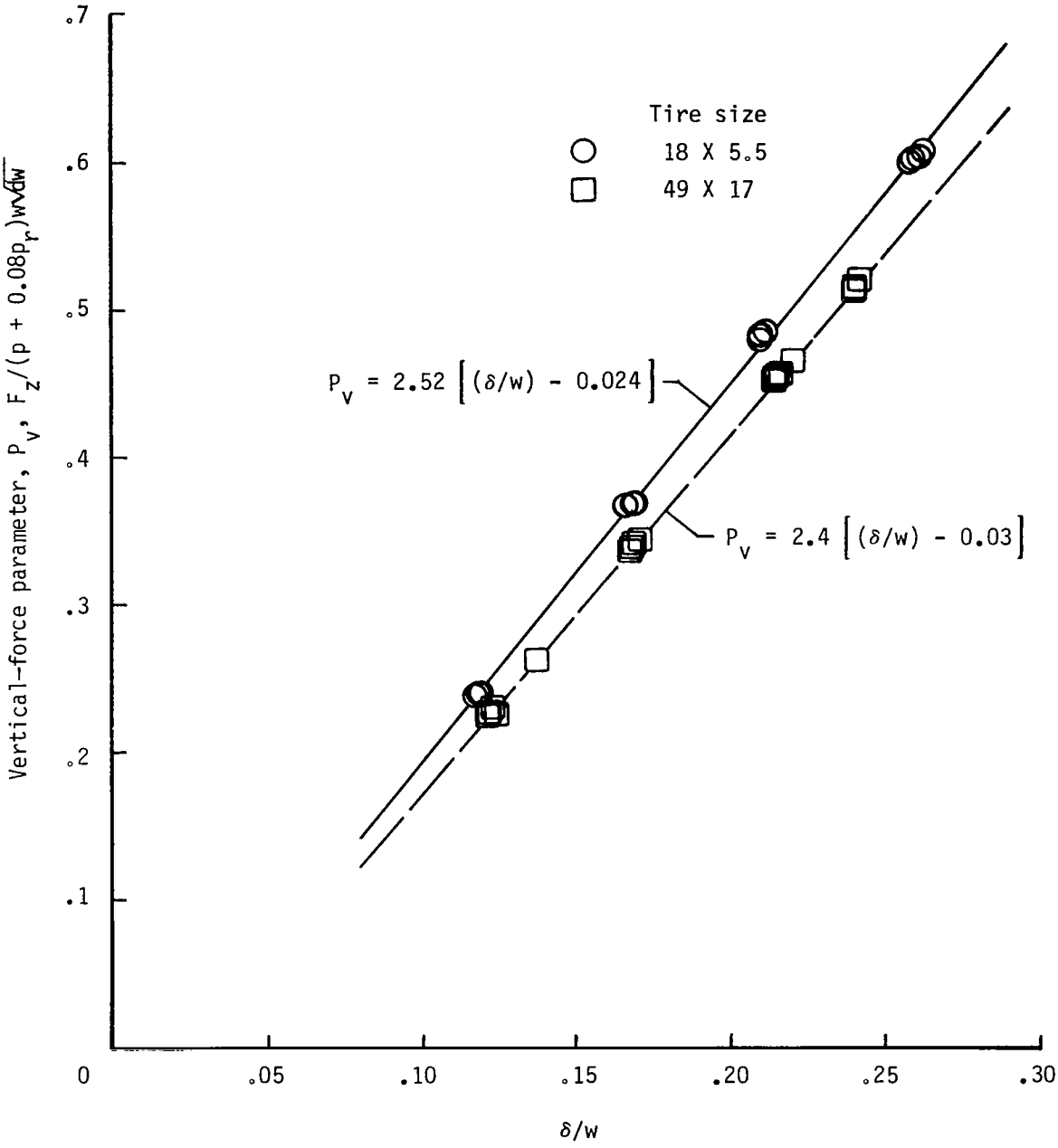

Figure 10.- Variation of tire vertical-force parameter with vertical deflection.

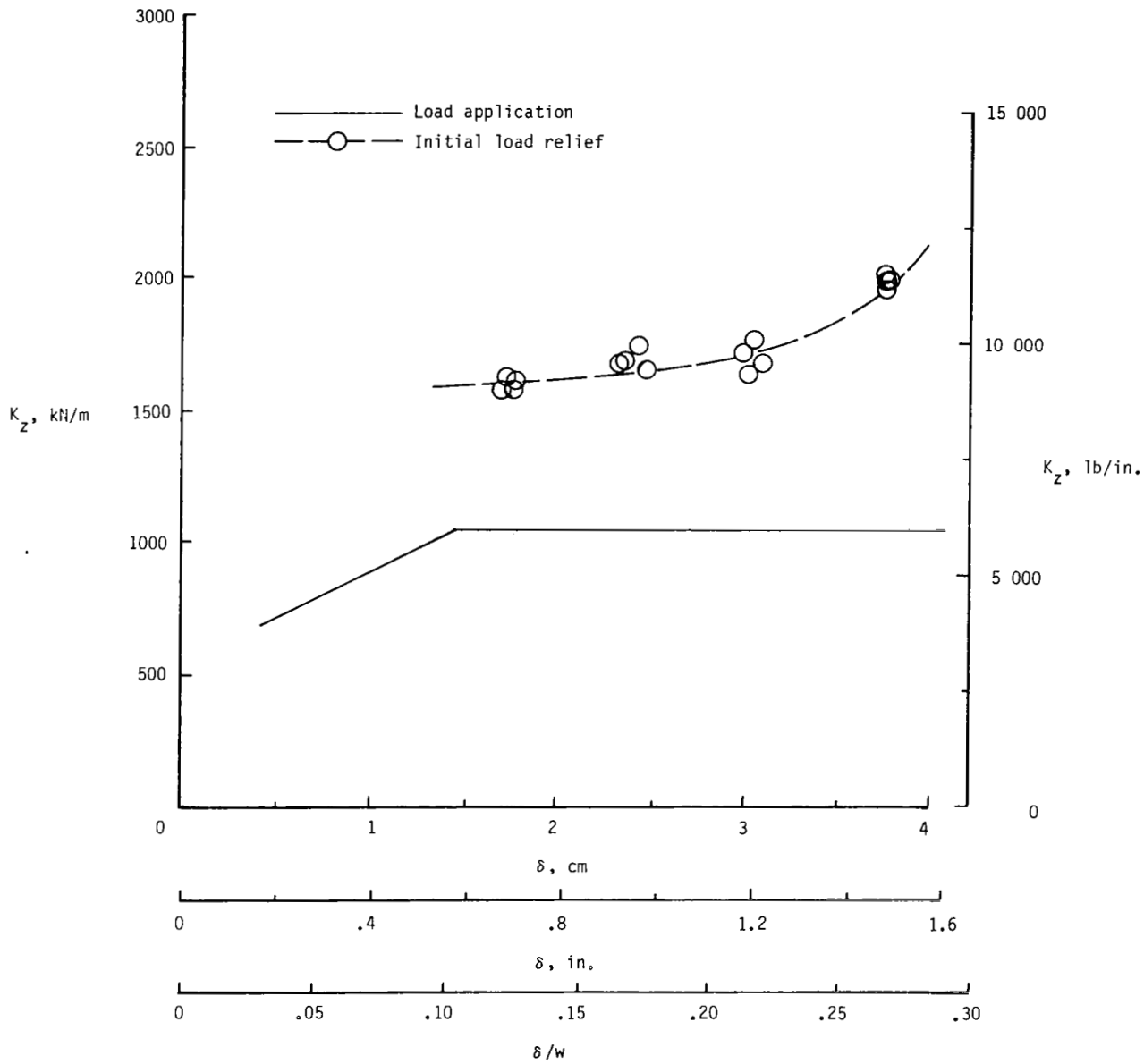

(a) 18 × 5.5 tire.

Figure 11.- Variation of tire vertical spring rates with vertical deflection.

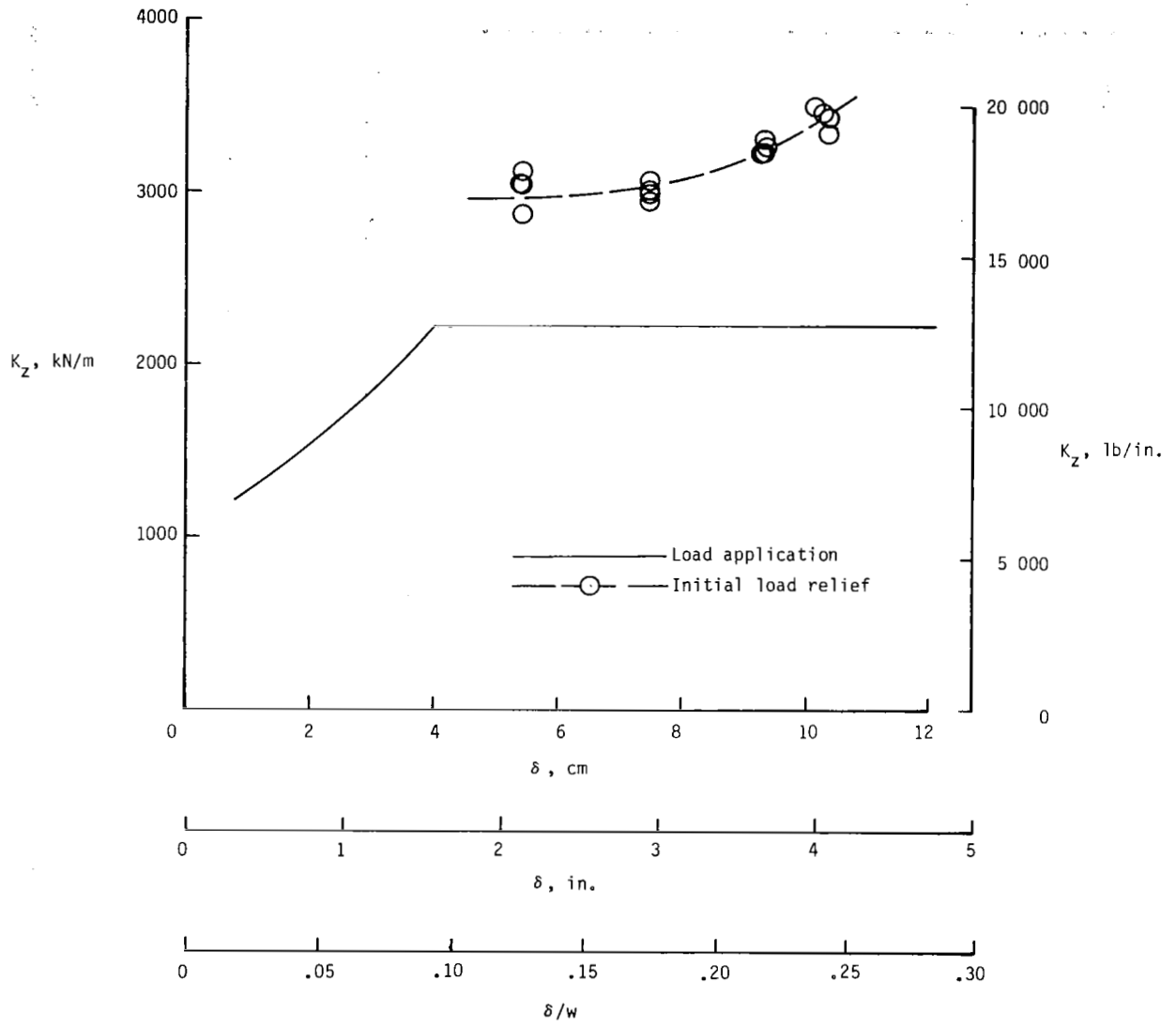

(b) 49 × 17 tire.

Figure 11.- Concluded.

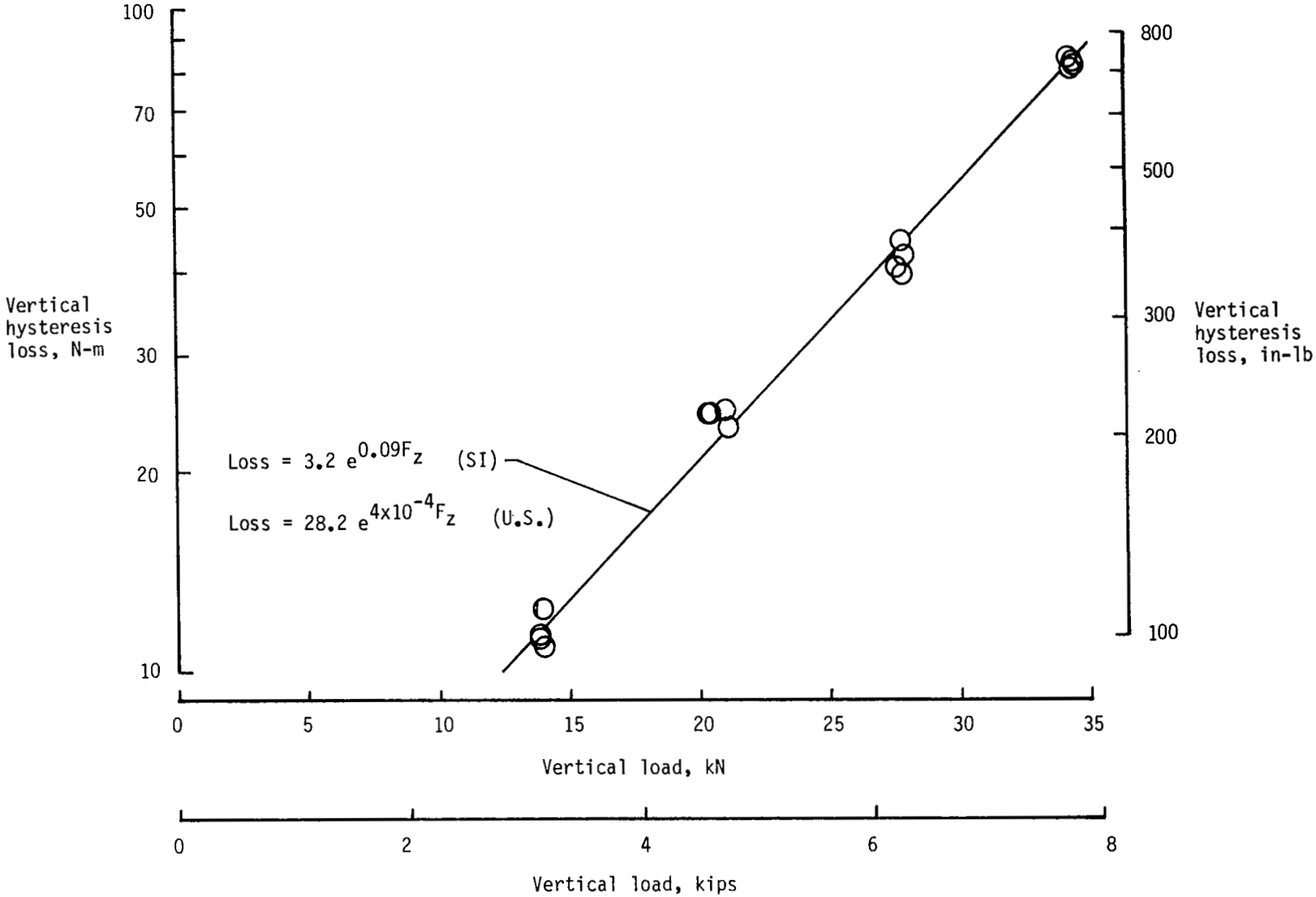

(a) 18 × 5.5 tire.

Figure 12.- Variation of tire vertical hysteresis loss with vertical loading.

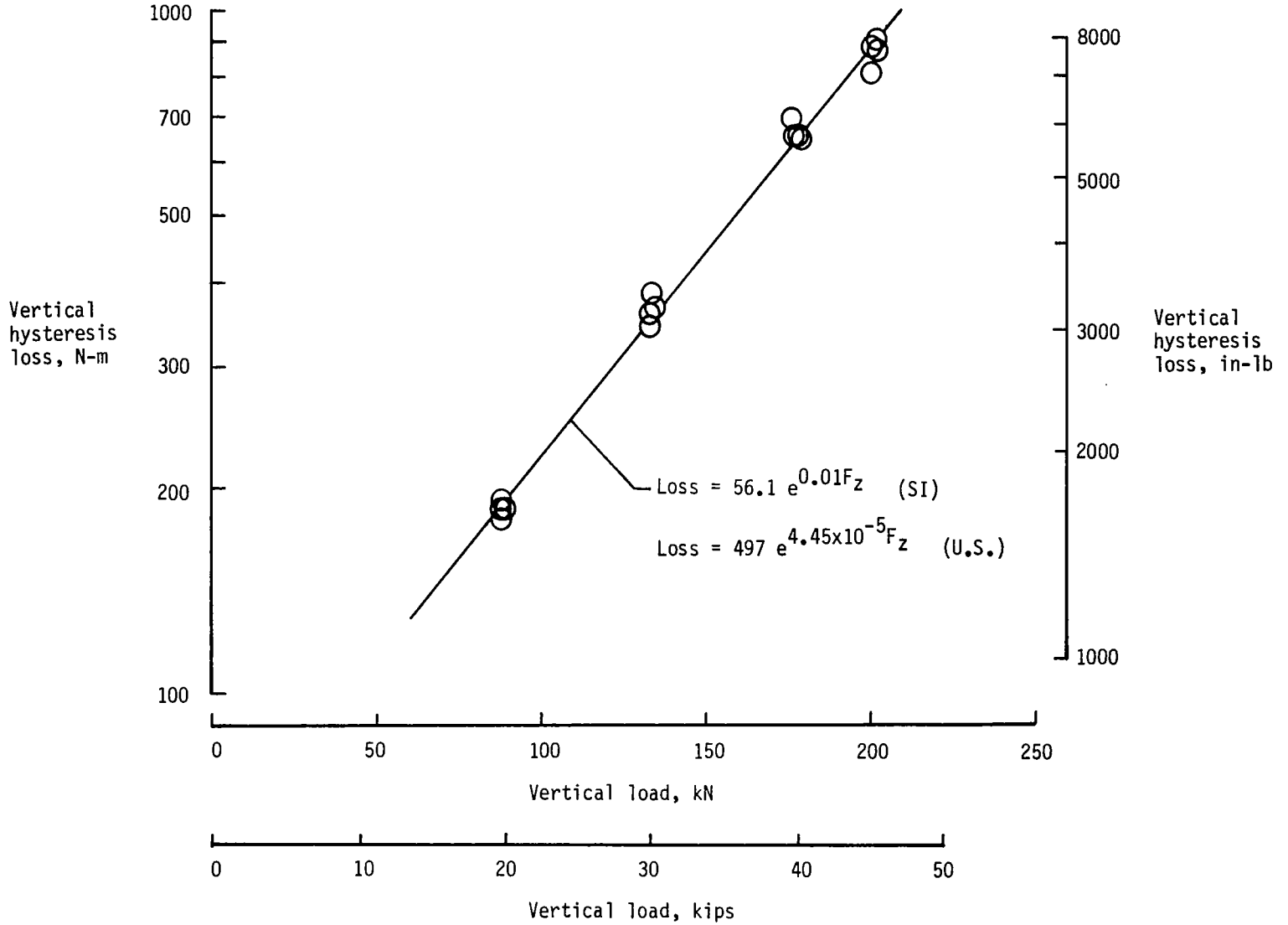

(b) 49 × 17 tire.

Figure 12.- Concluded.

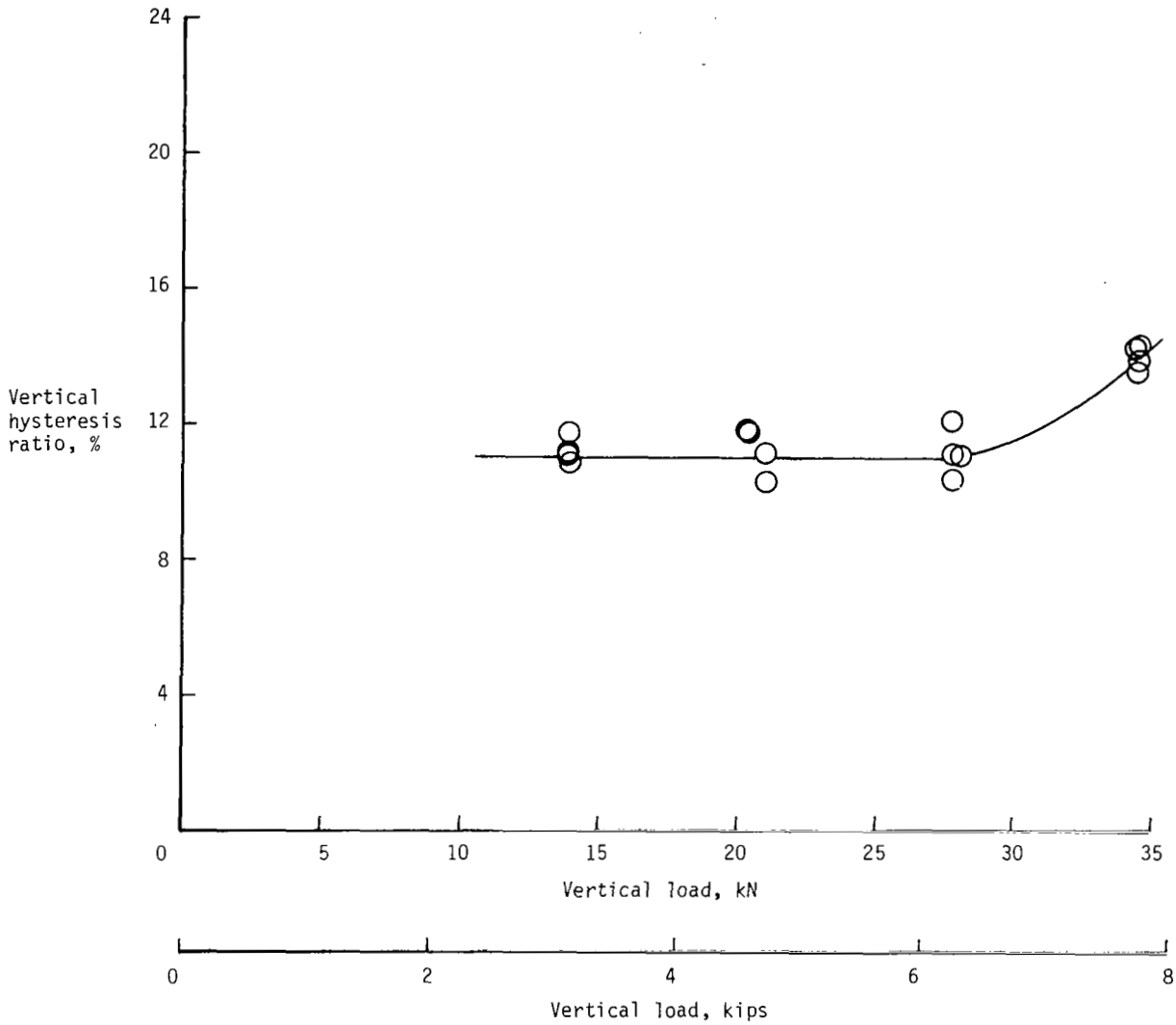

(a) 18 × 5.5 tire.

Figure 13.- Variation of tire vertical hysteresis ratio with vertical loading.

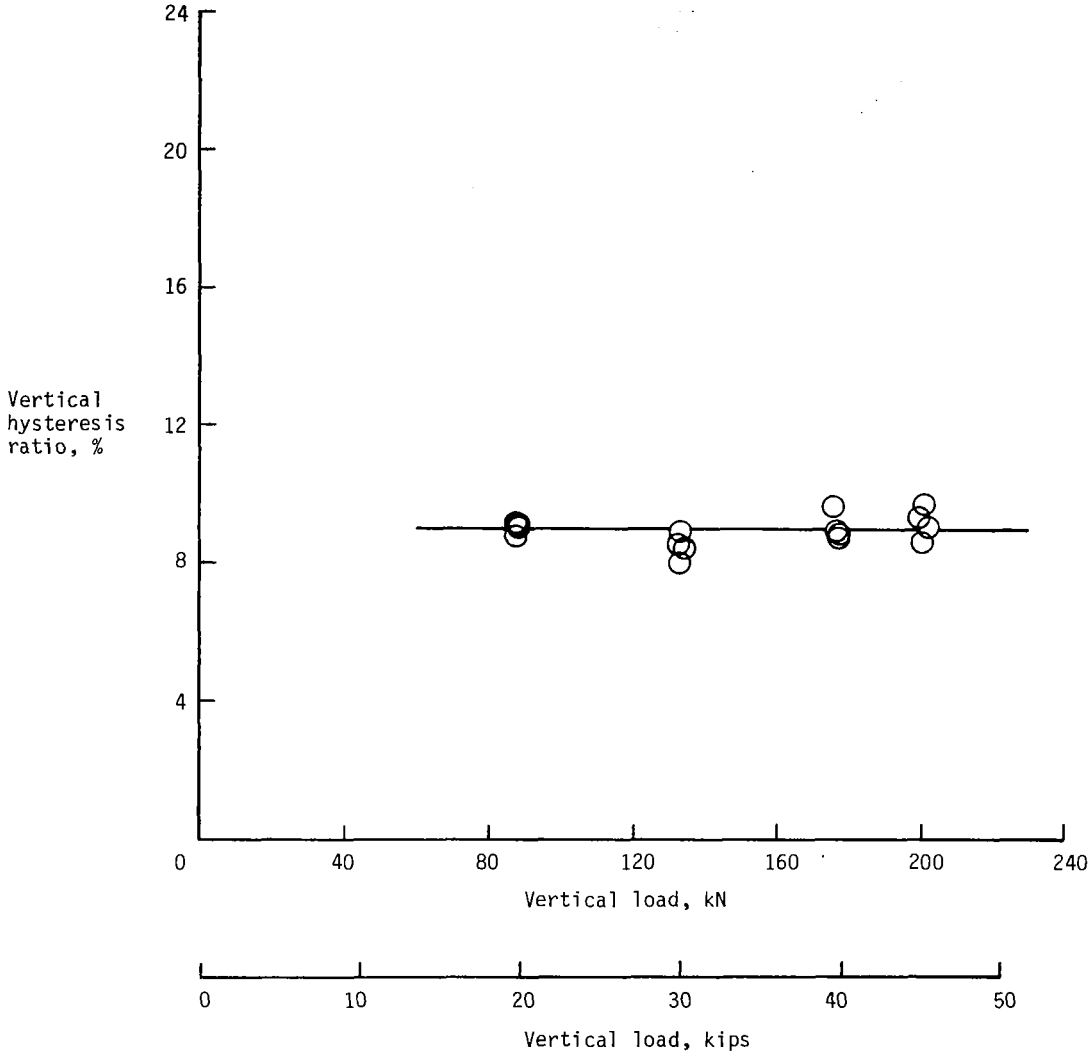

(b) 49 × 17 tire.

Figure 13.- Concluded.

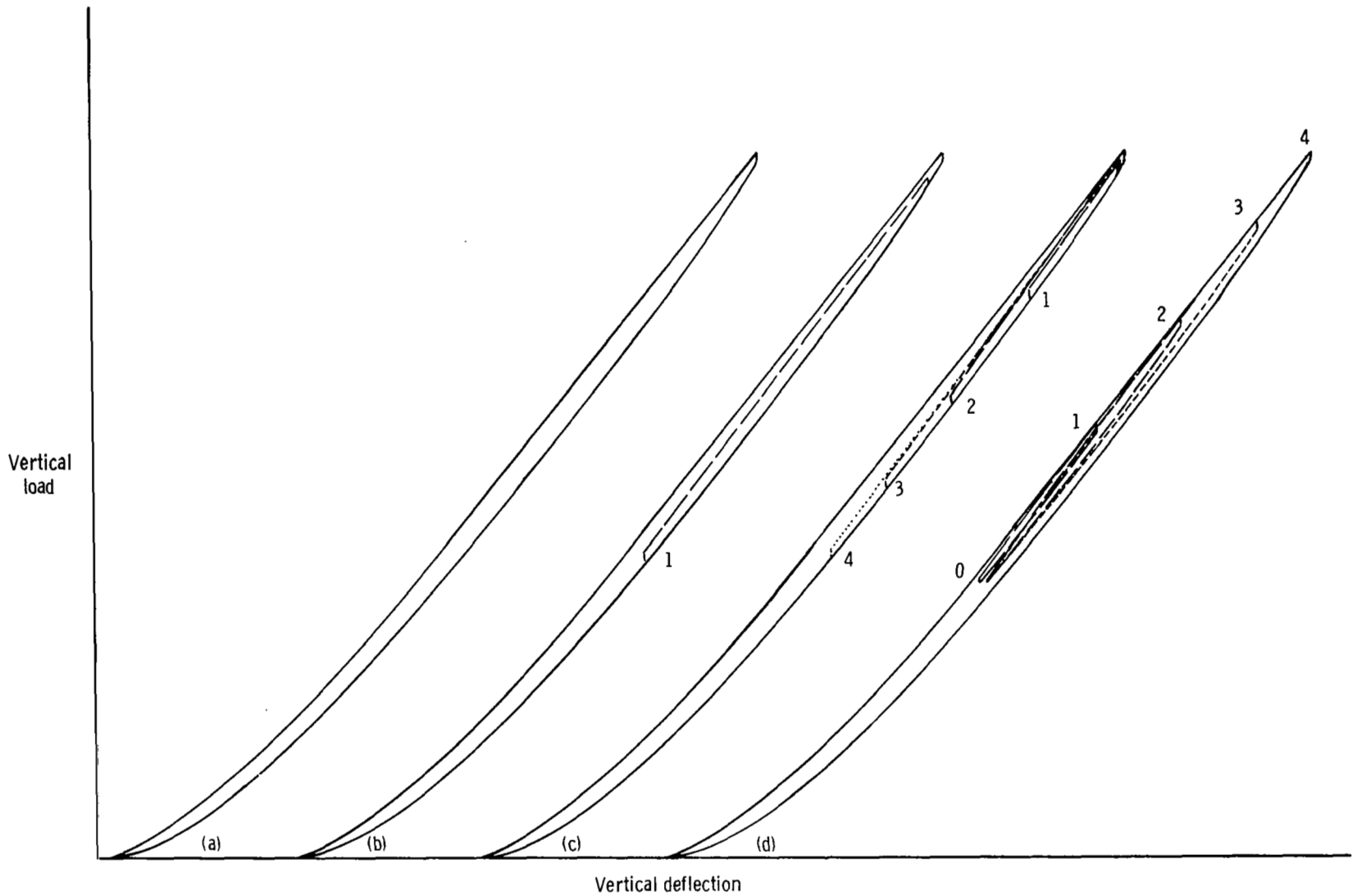

Figure 14.- Vertical load-deflection curves developed during various cyclic loading conditions.

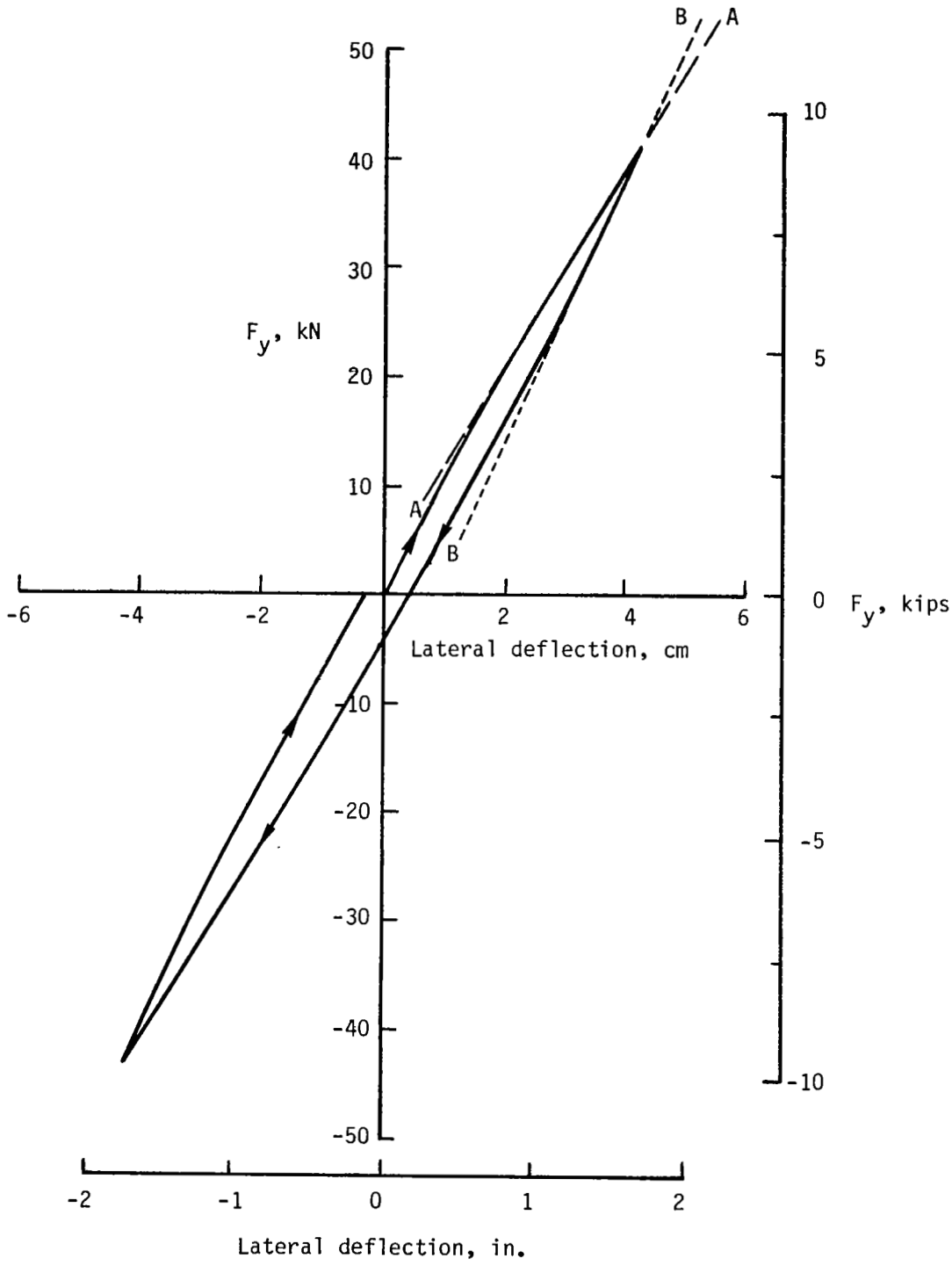

Figure 15.- Typical tire lateral load-deflection curve showing how lateral spring rates are acquired (49 × 17 tire).

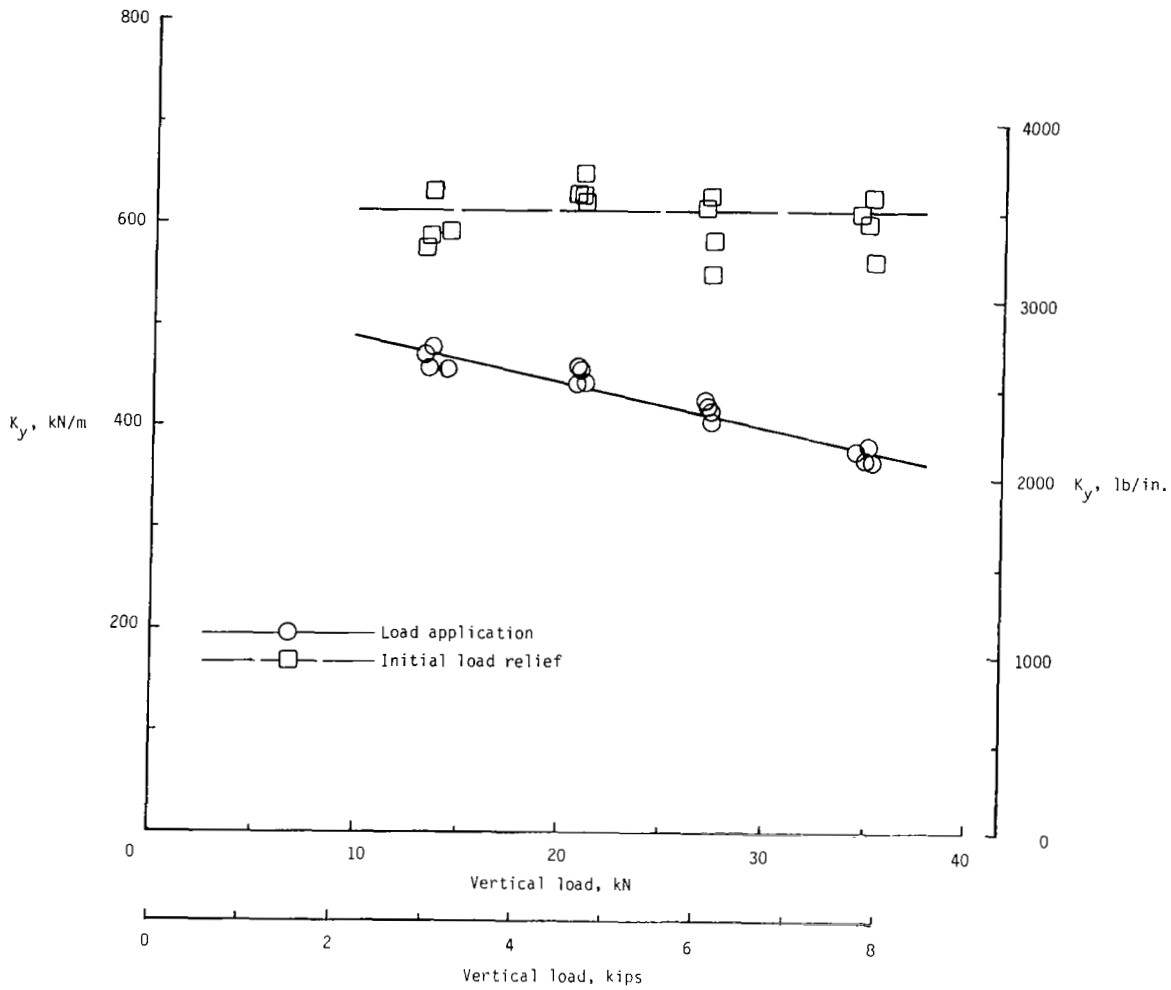

(a) 18 × 5.5 tire.

Figure 16.- Variation of tire lateral spring rates with vertical loading. Maximum lateral load ≈ 30% F_Z.

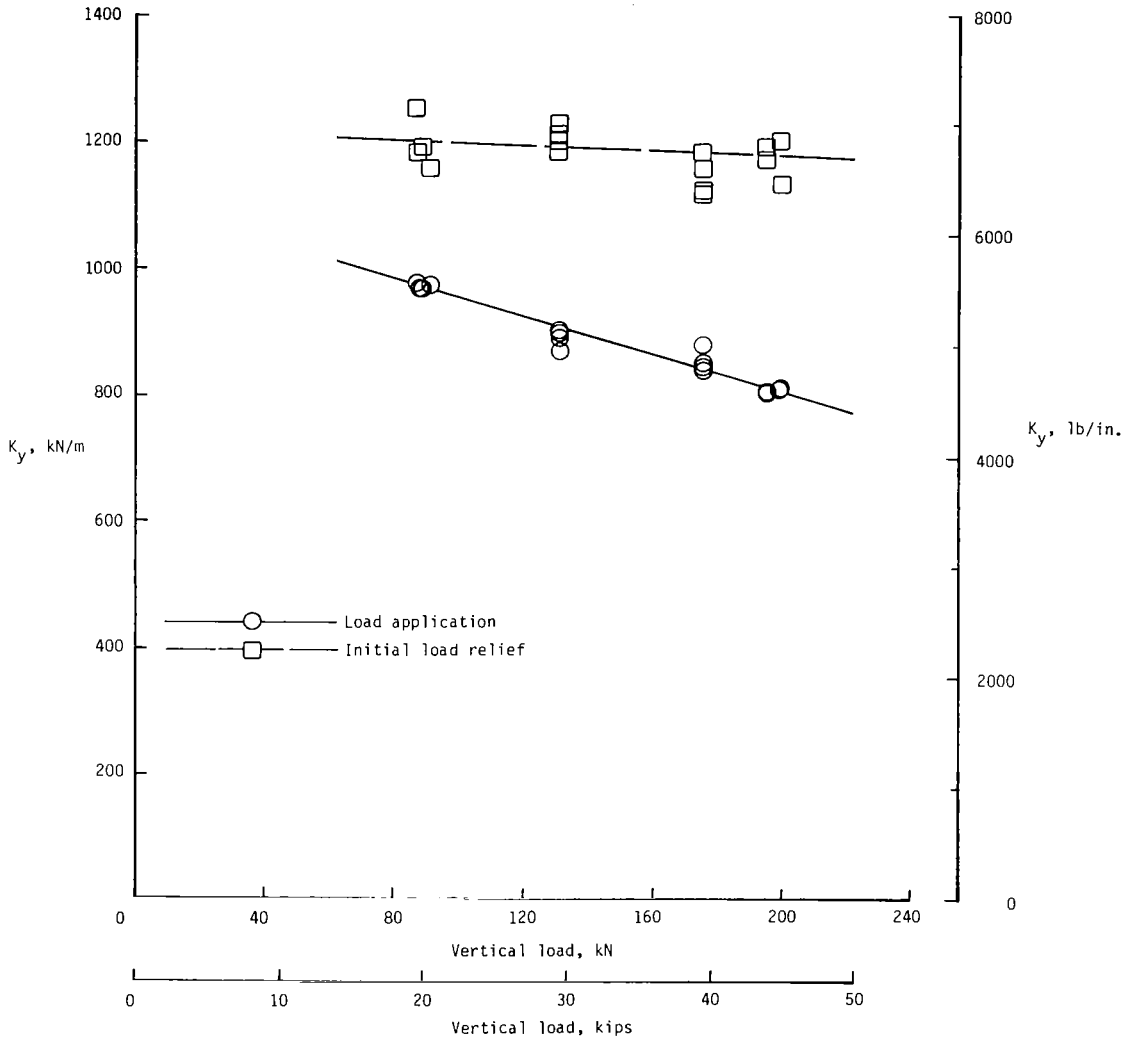

(b) 49 × 17 tire.

Figure 16.- Concluded.

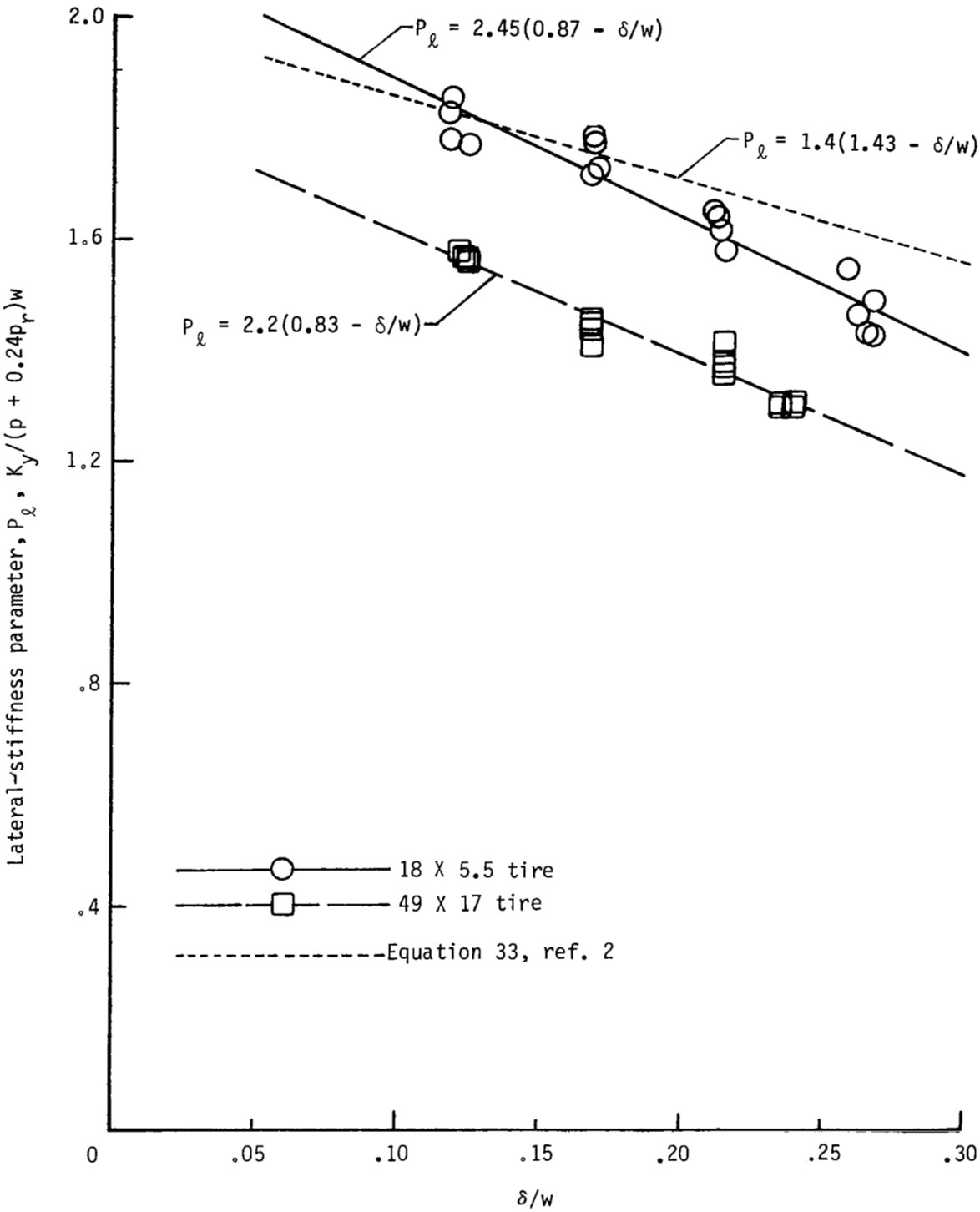

Figure 17.- Variation of tire lateral-stiffness parameter with vertical deflection.

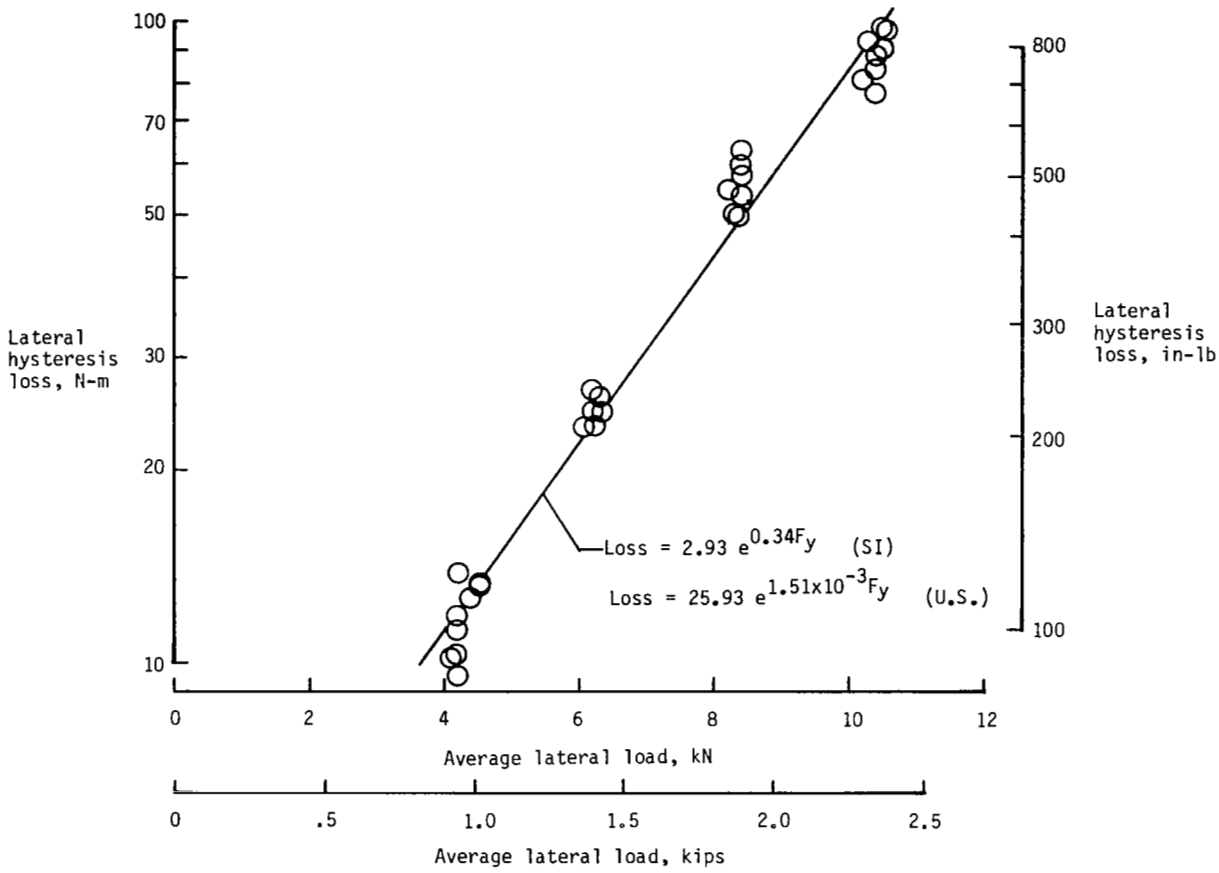

(a) 18 × 5.5 tire.

Figure 18.- Variation of tire lateral hysteresis loss with lateral load. Lateral load ≈ 30% F_z.

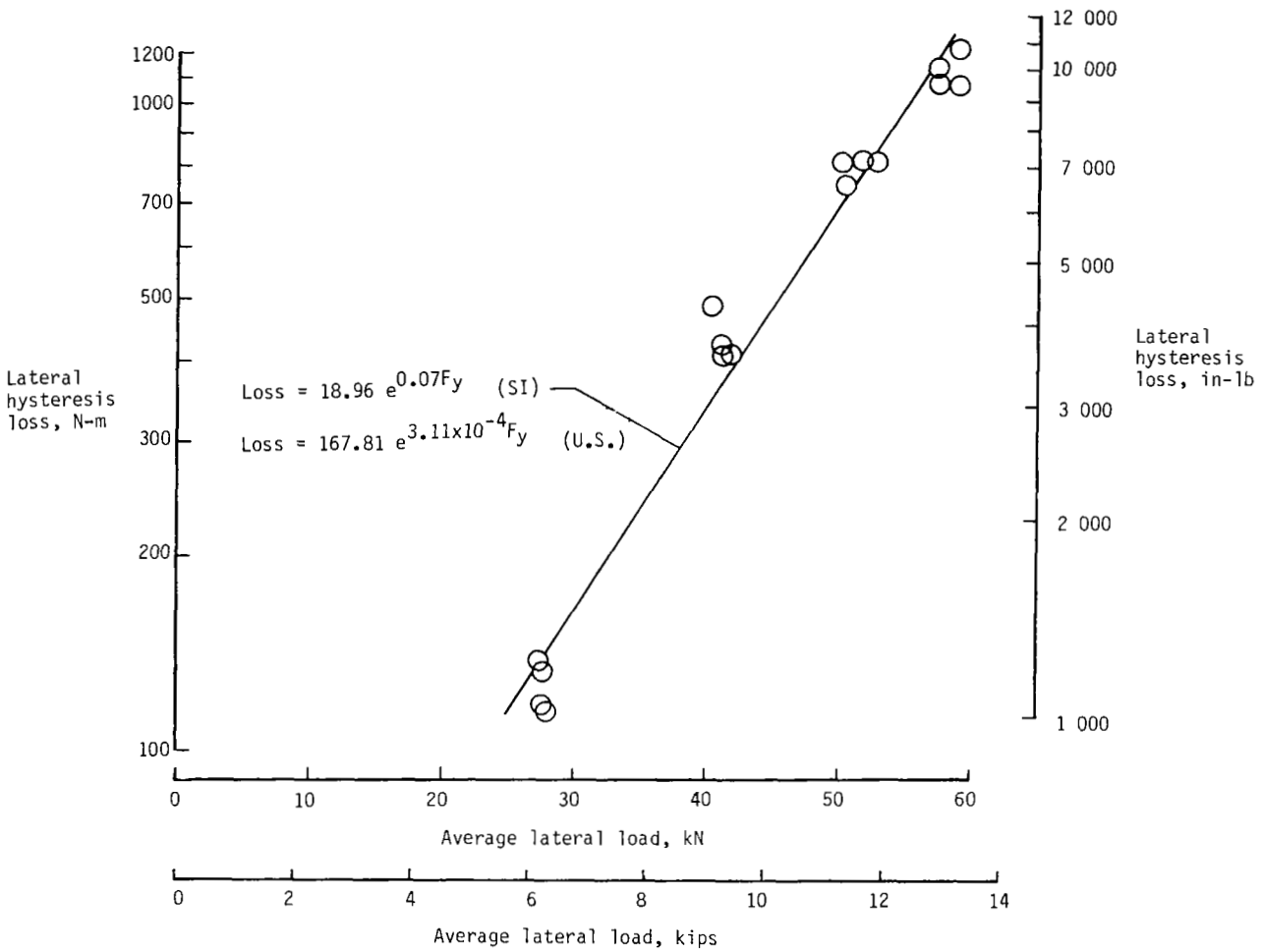

(b) 49 × 17 tire.

Figure 18.- Concluded.

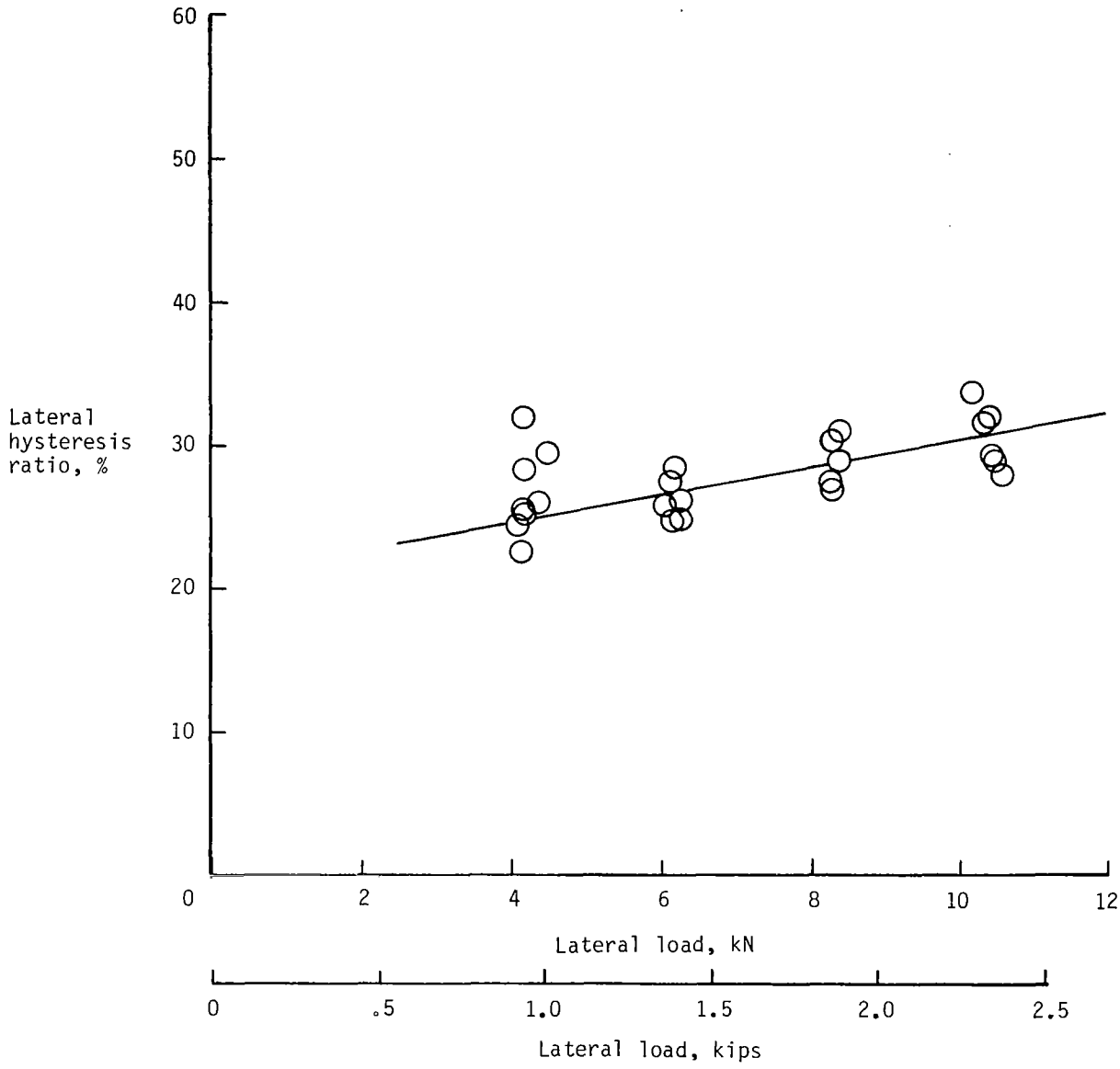

(a) 18 × 5.5 tire.

Figure 19.- Variation of tire lateral hysteresis ratio with lateral load. Lateral load ≈ 30% F_z.

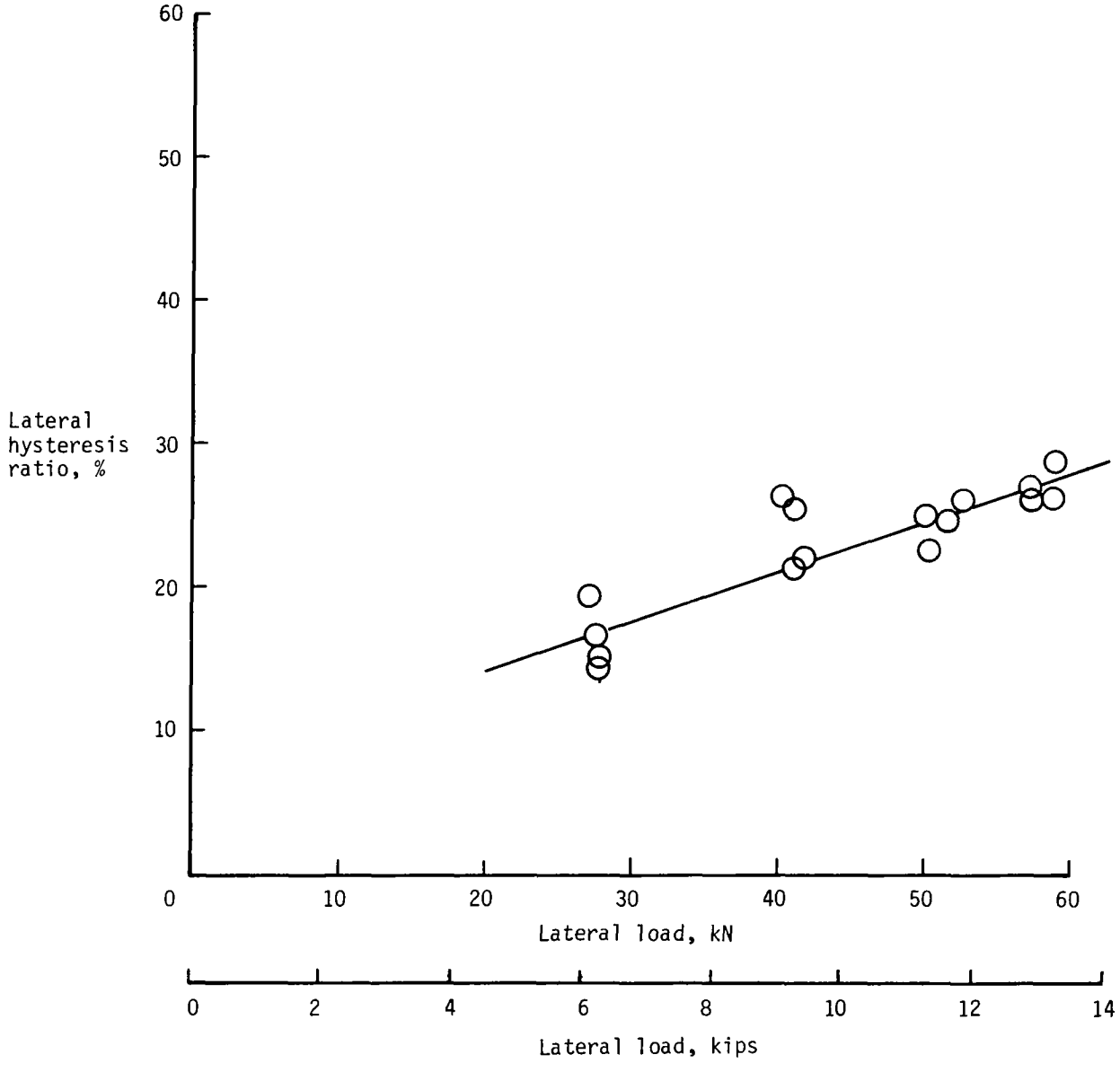

(b) 49 × 17 tire.

Figure 19.- Concluded.

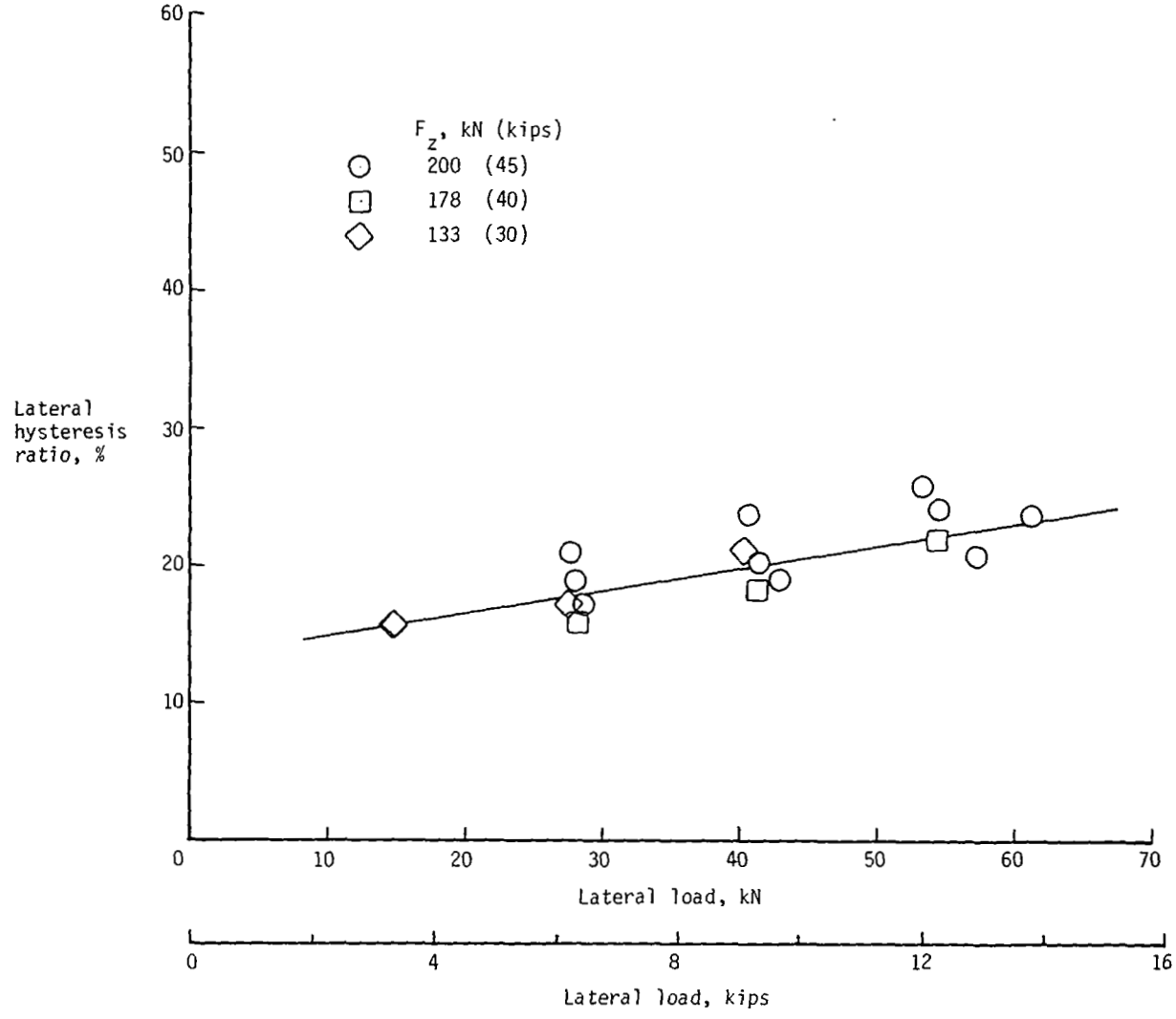

Figure 20.- Effect of tire lateral load on lateral hysteresis ratio at various vertical loadings (49 × 17 tire).

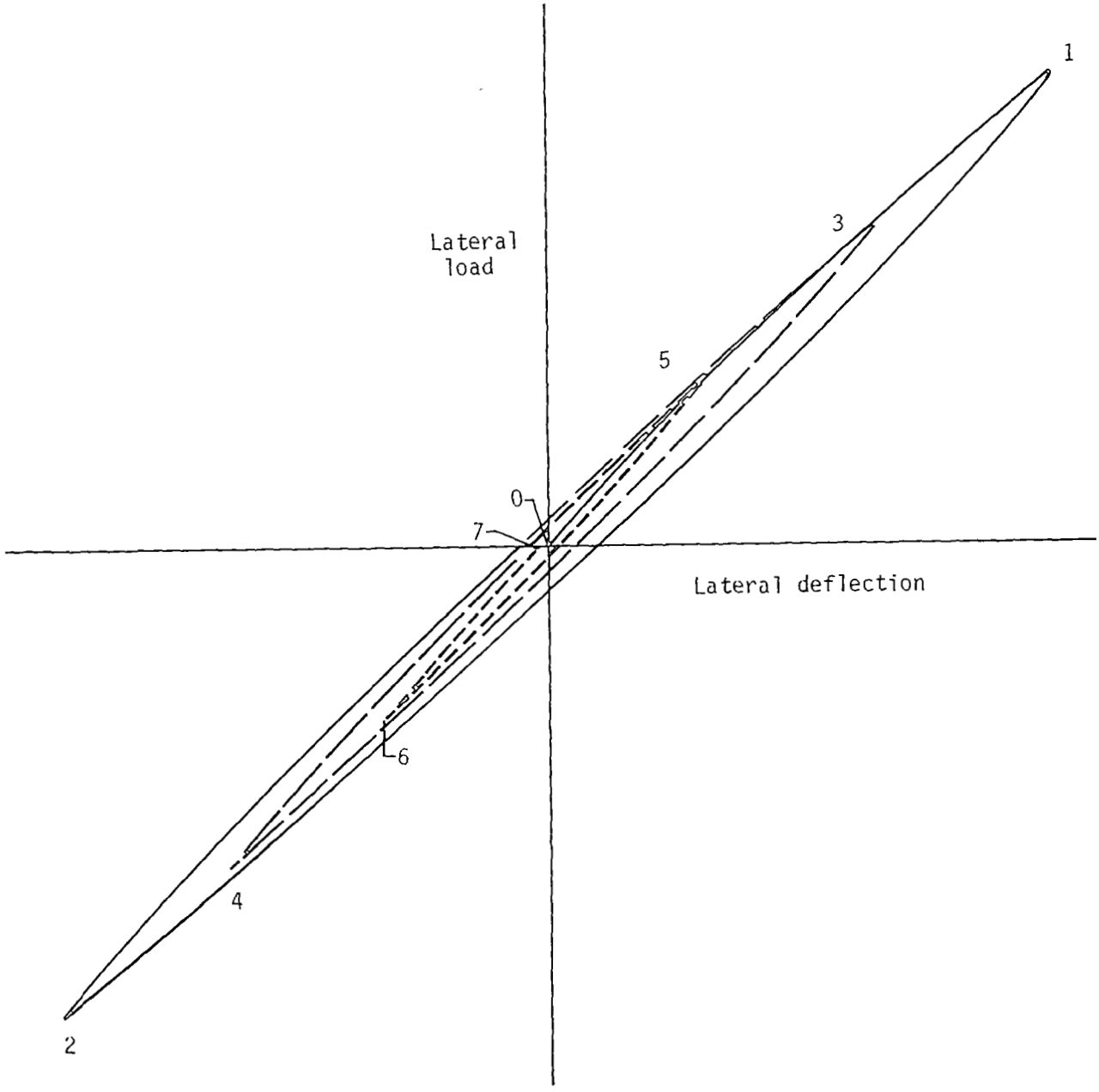

(a) Decreasing cycles.

Figure 21.- Lateral load-deflection curves developed during various cyclic loading conditions (49 × 17 tire). $F_z \approx 200$ kN (45 kips).

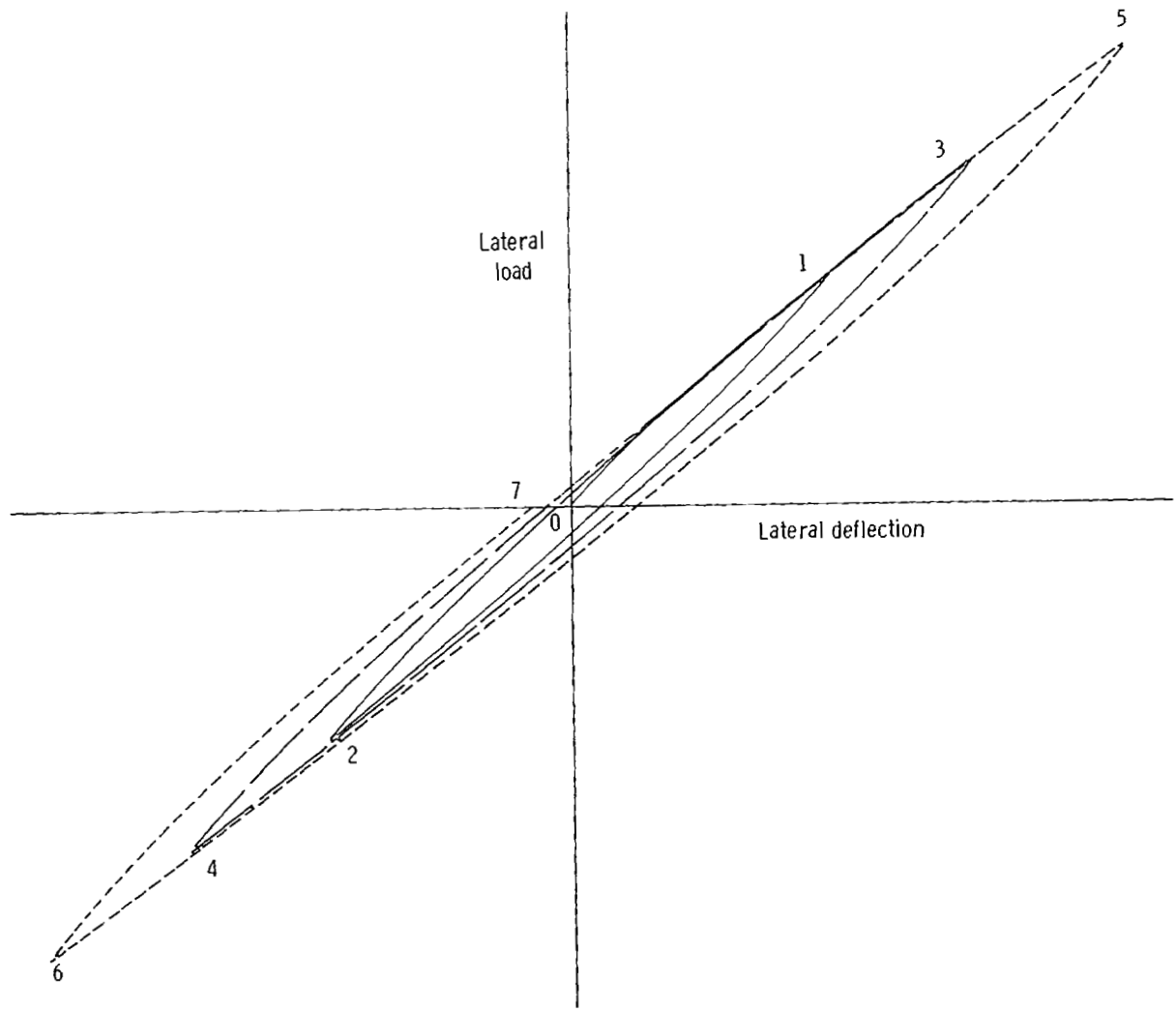

(b) Increasing cycles.

Figure 21.- Continued.

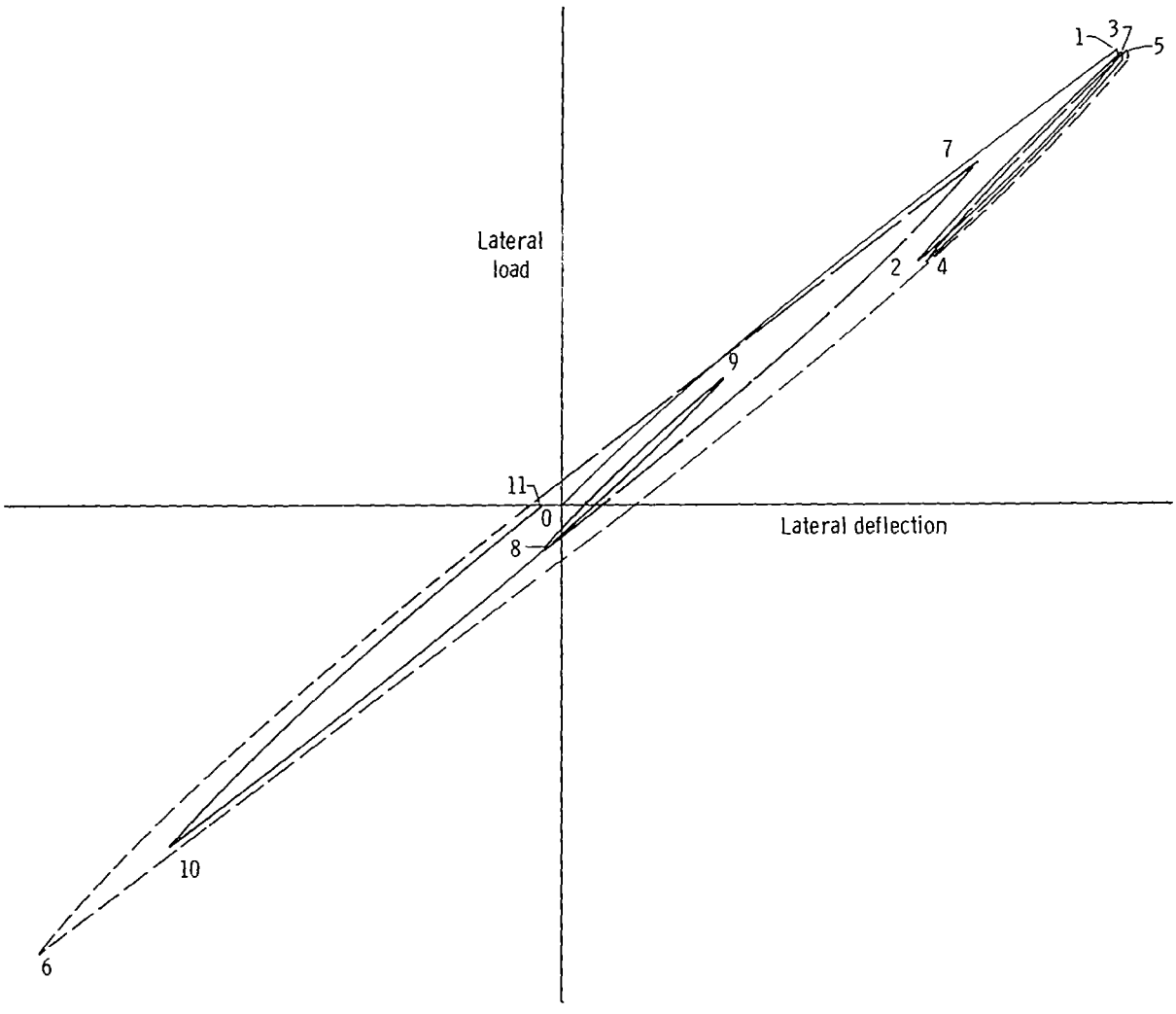

(c) Random cycles.

Figure 21.- Concluded.

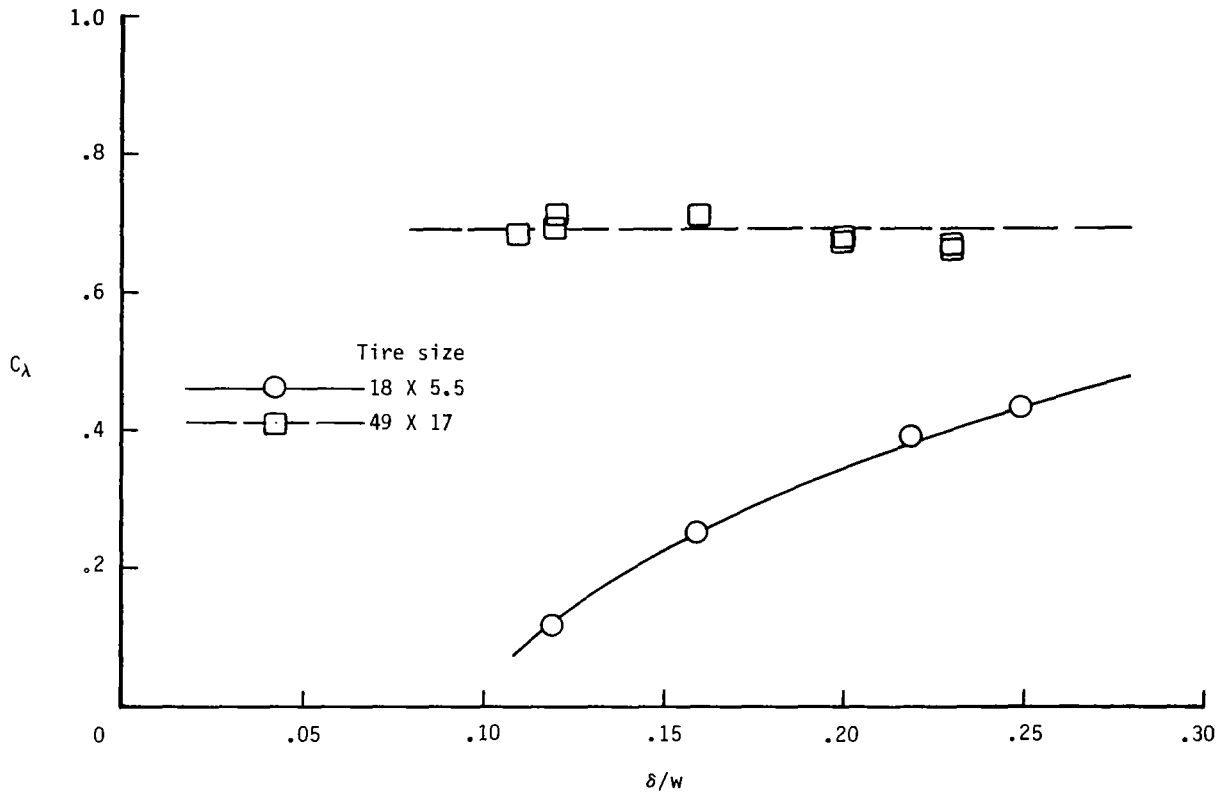

Figure 22.- Variation of tire lateral center-of-pressure coefficient with vertical deflection.

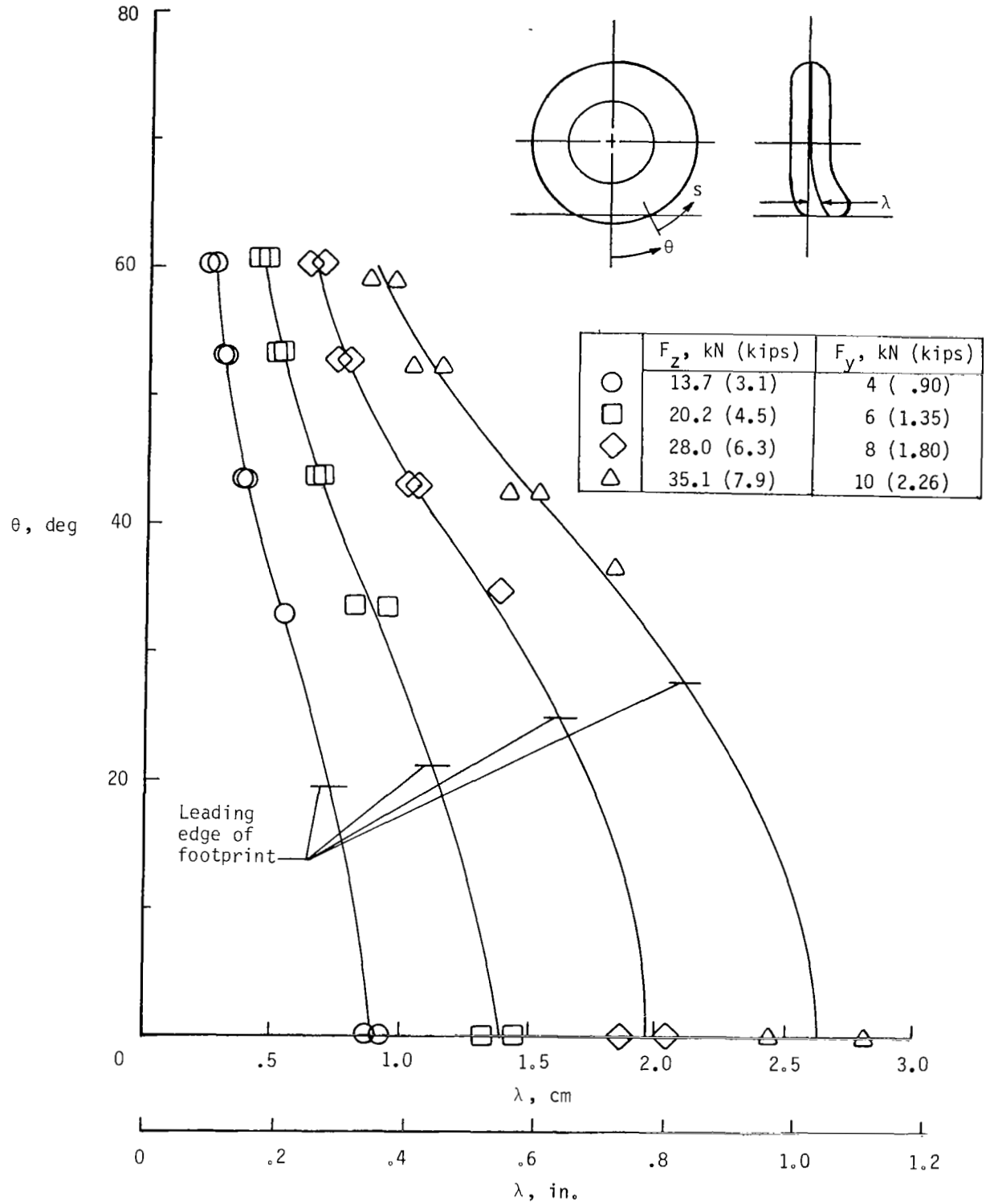

(a) 18 × 5.5 tire.

Figure 23.- Lateral deformation of tire tread periphery under combined vertical and lateral loadings. Table deflection is at $\theta = 0$.

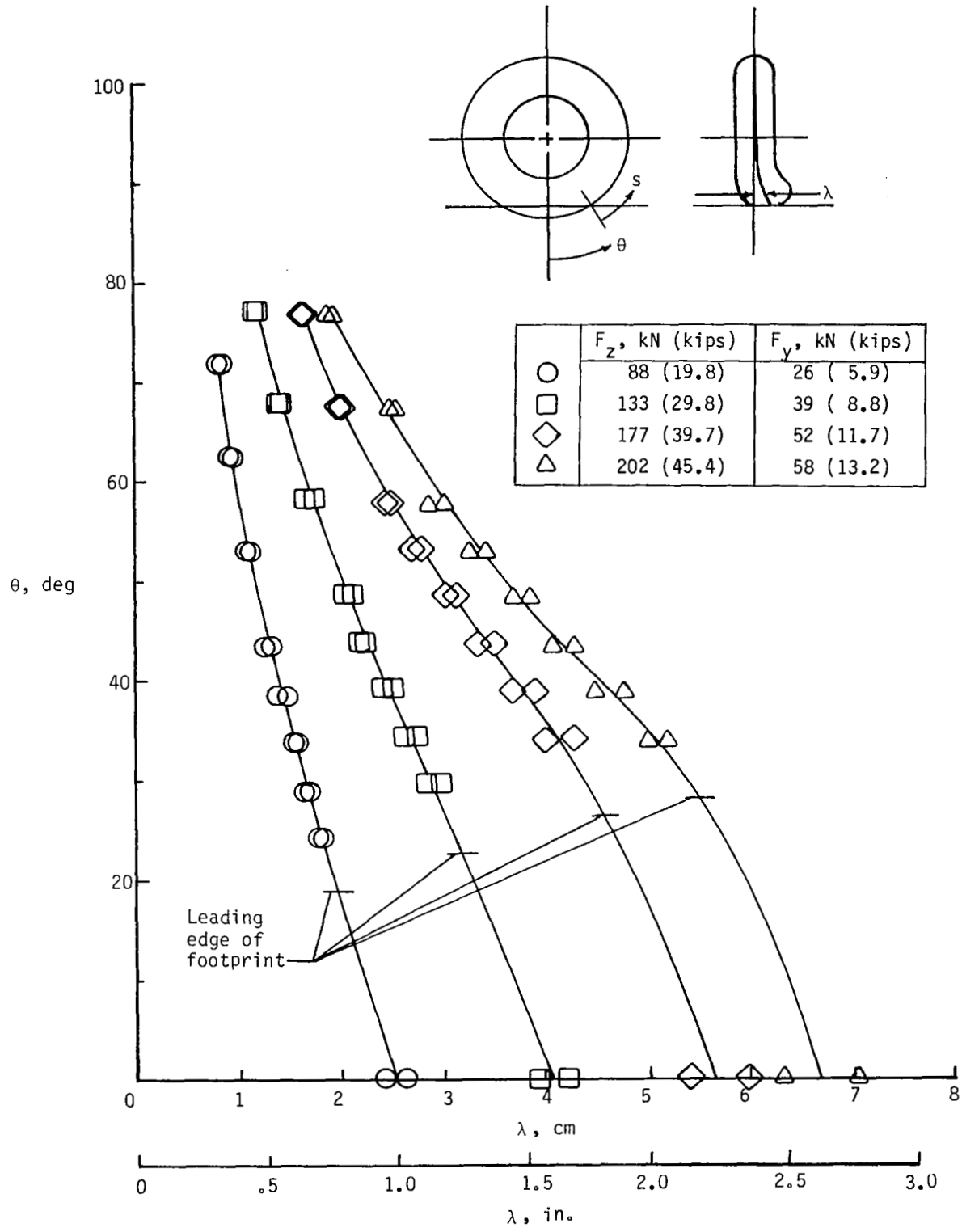

(b) 49 × 17 tire.

Figure 23.- Concluded.

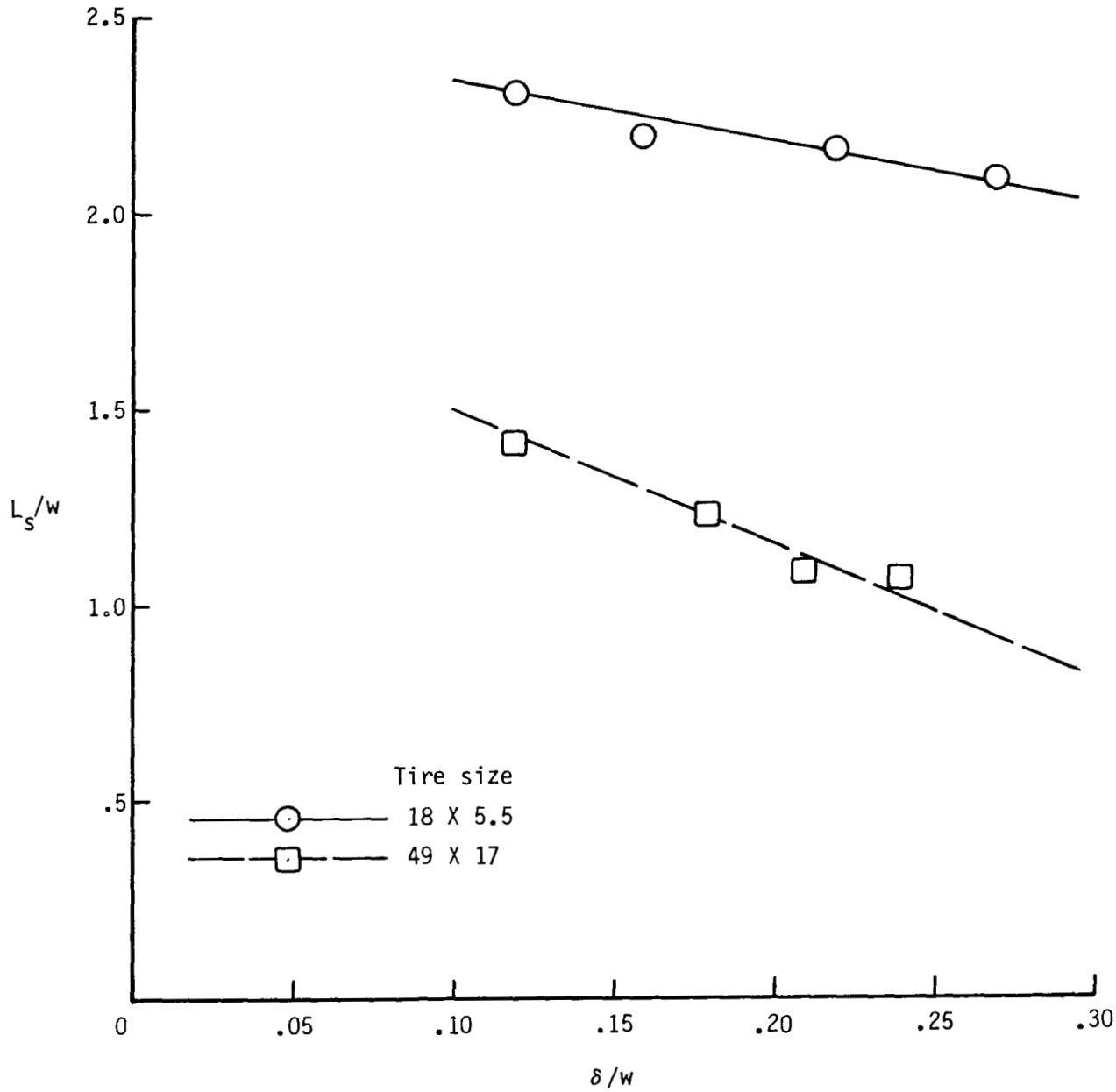

Figure 24.- Variation of tire static relaxation length with vertical deflection.

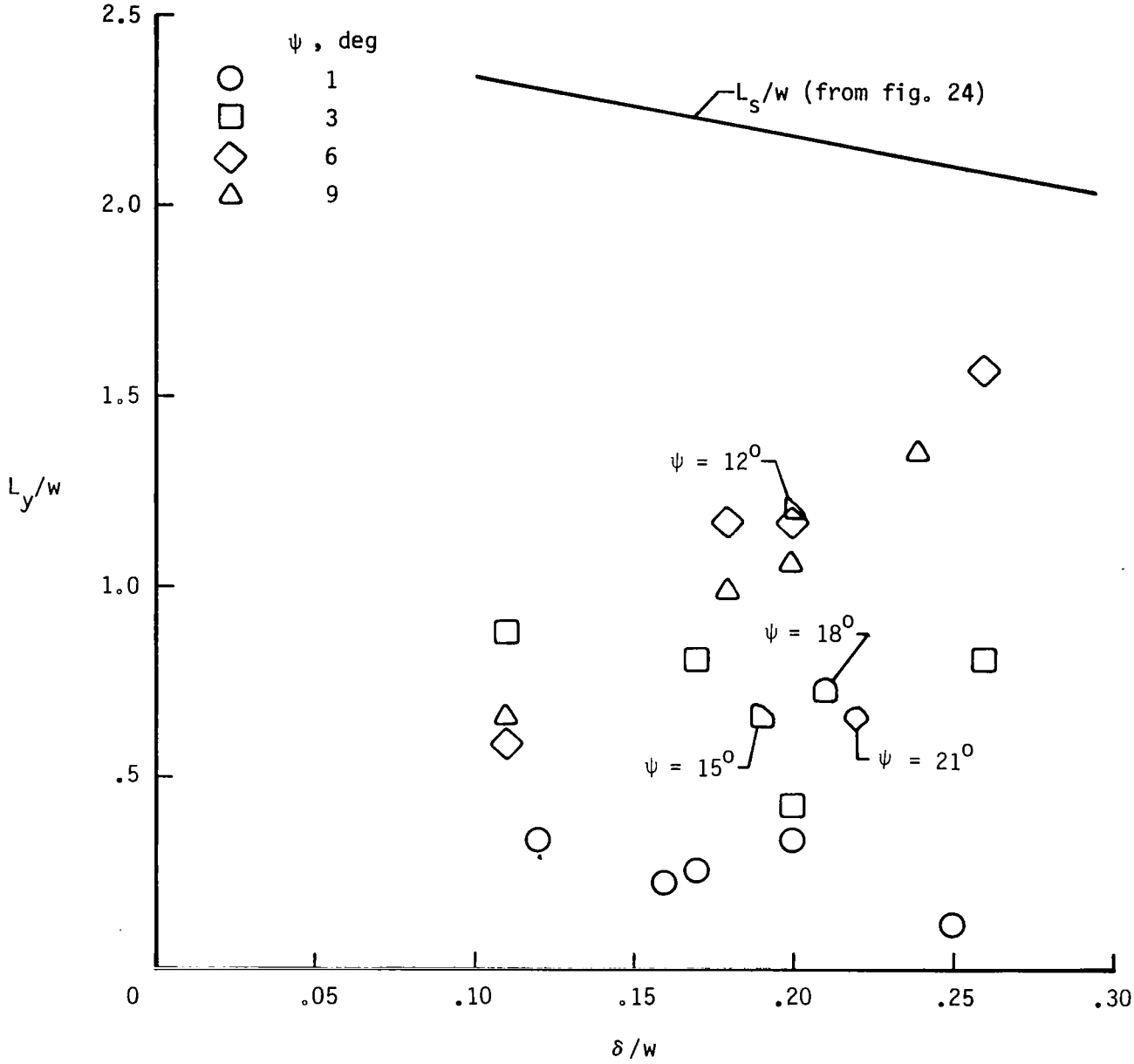

(a) 18 × 5.5 tire.

Figure 25.- Variation of tire yawed-rolling relaxation length with vertical deflection for varying yaw angles.

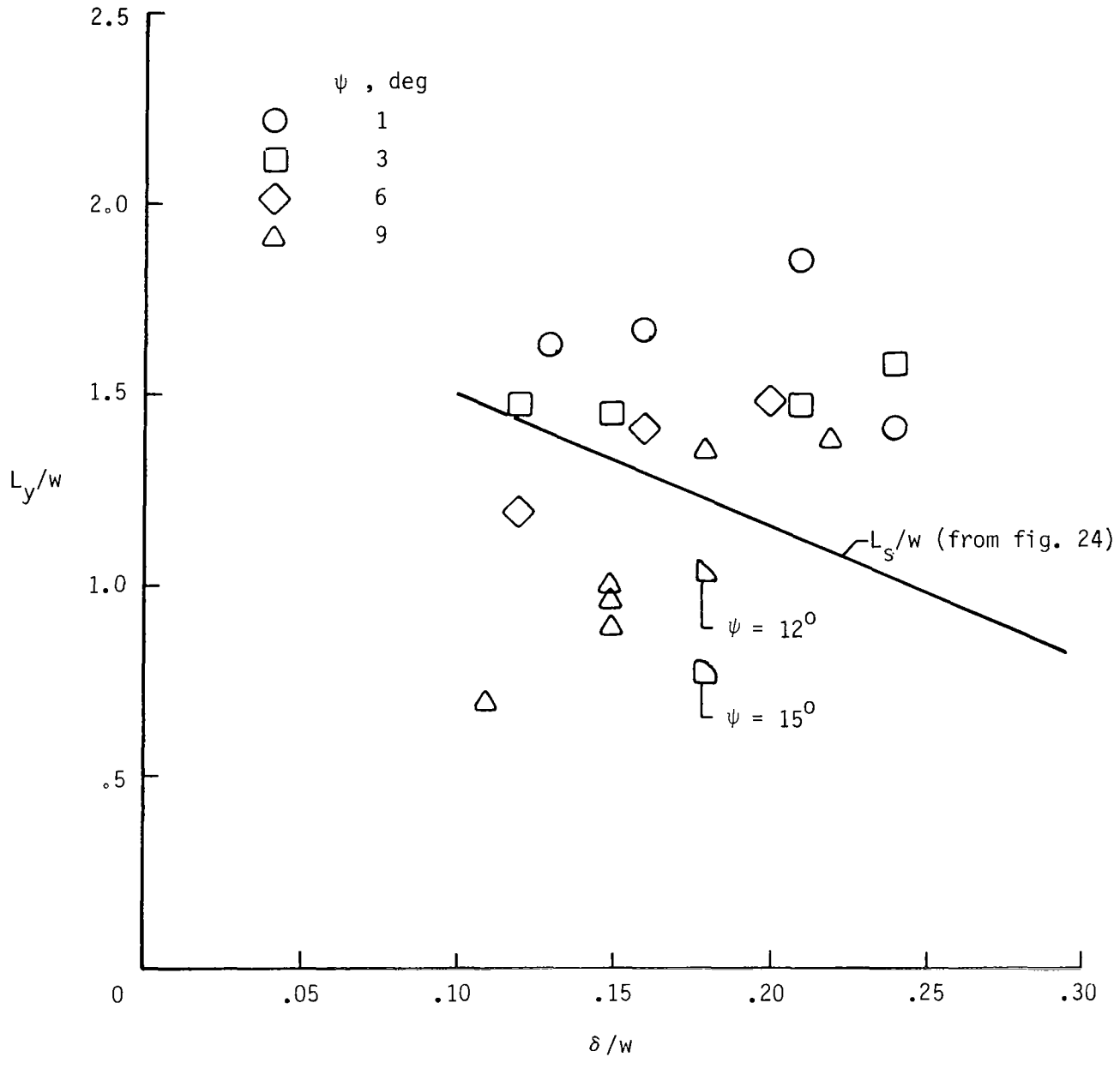

(b) 49 × 17 tire.

Figure 25.- Concluded.

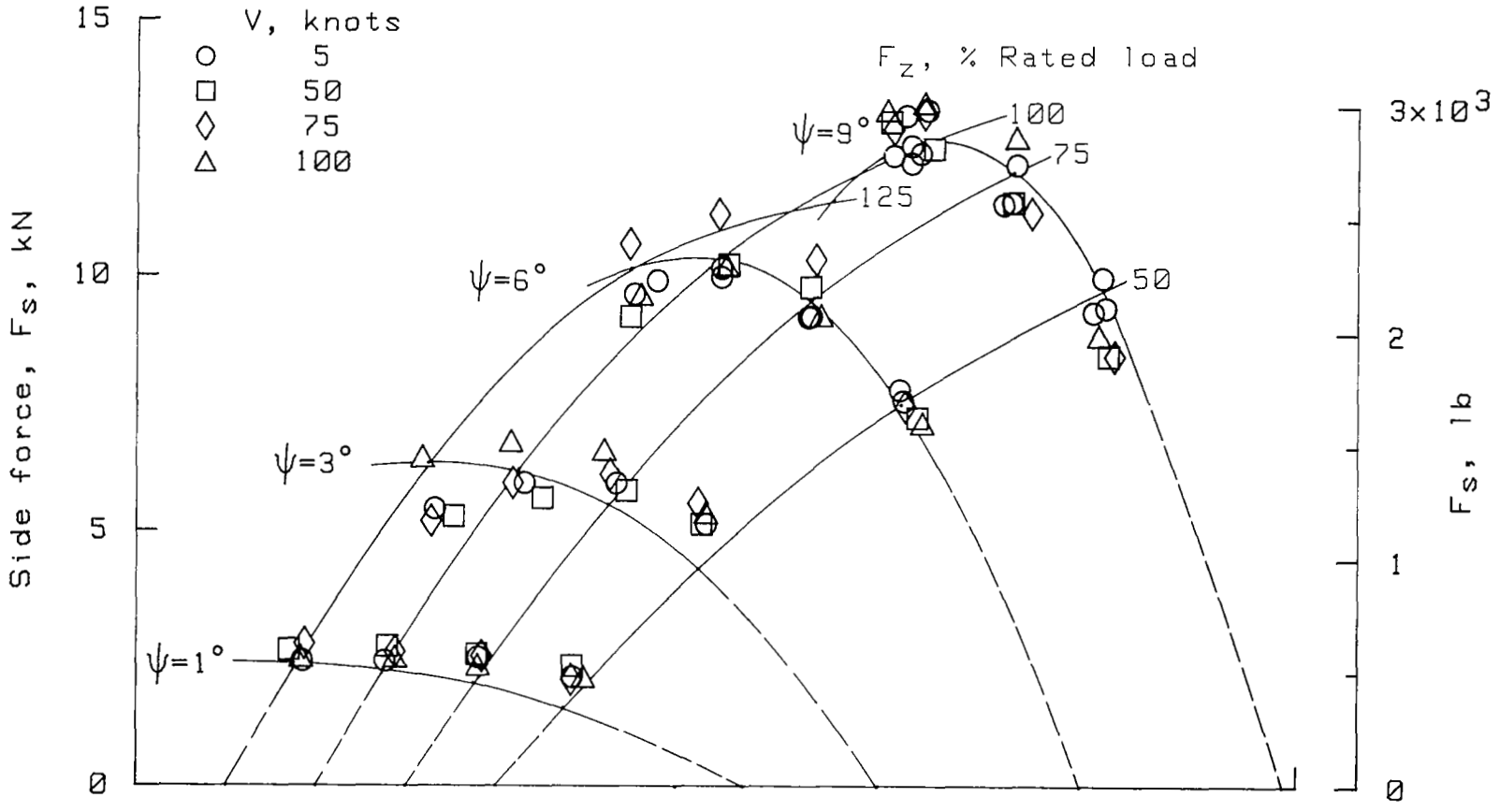

(a) 18 × 5.5 tire. Rated load = 27.6 kN (6.2 kips).

Figure 26.- Variation of tire side force with vertical load and yaw angle over a range of ground speed.

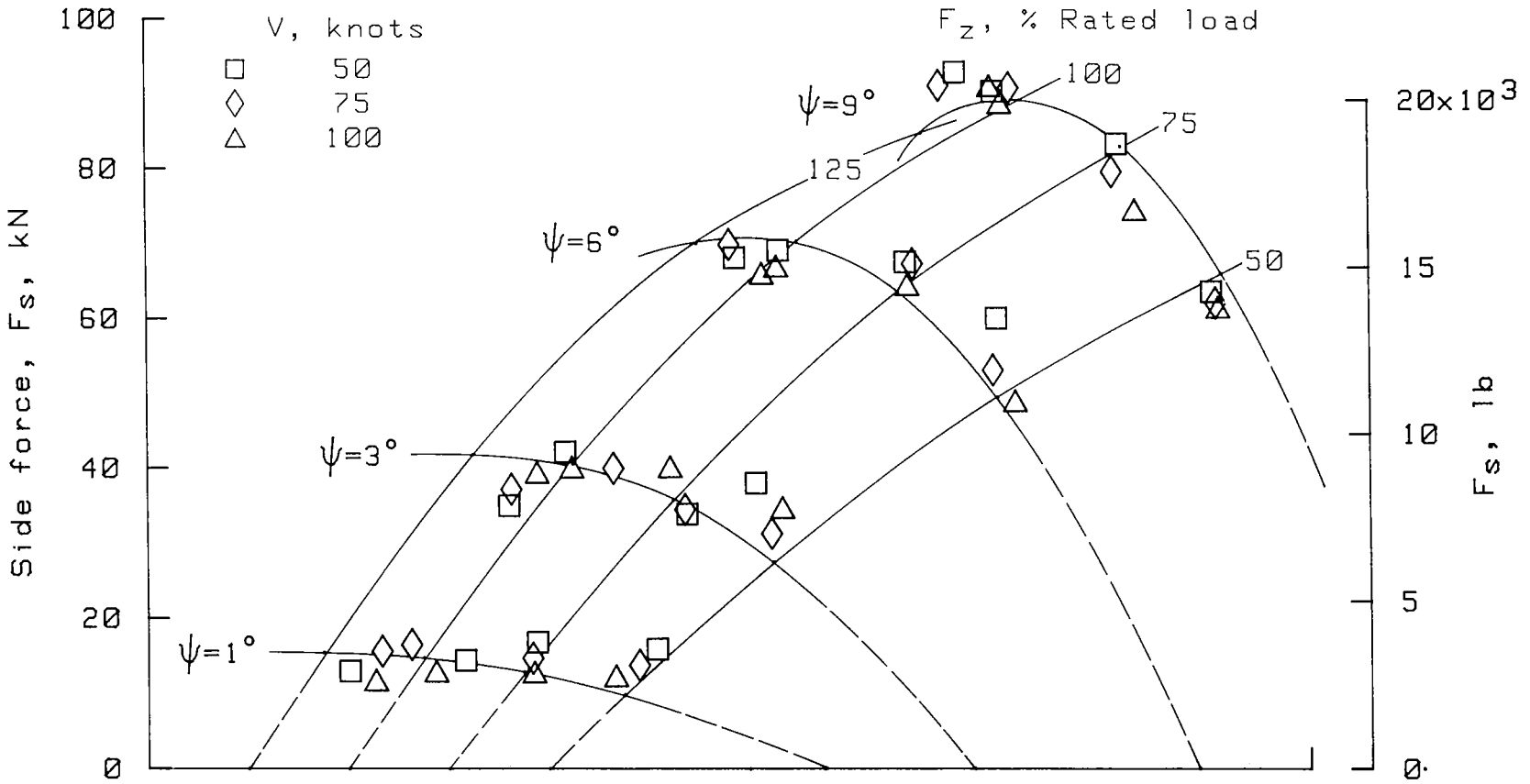

(b) 49 × 17 tire. Rated load = 76.1 kN (39.6 kips).

Figure 26.- Concluded.

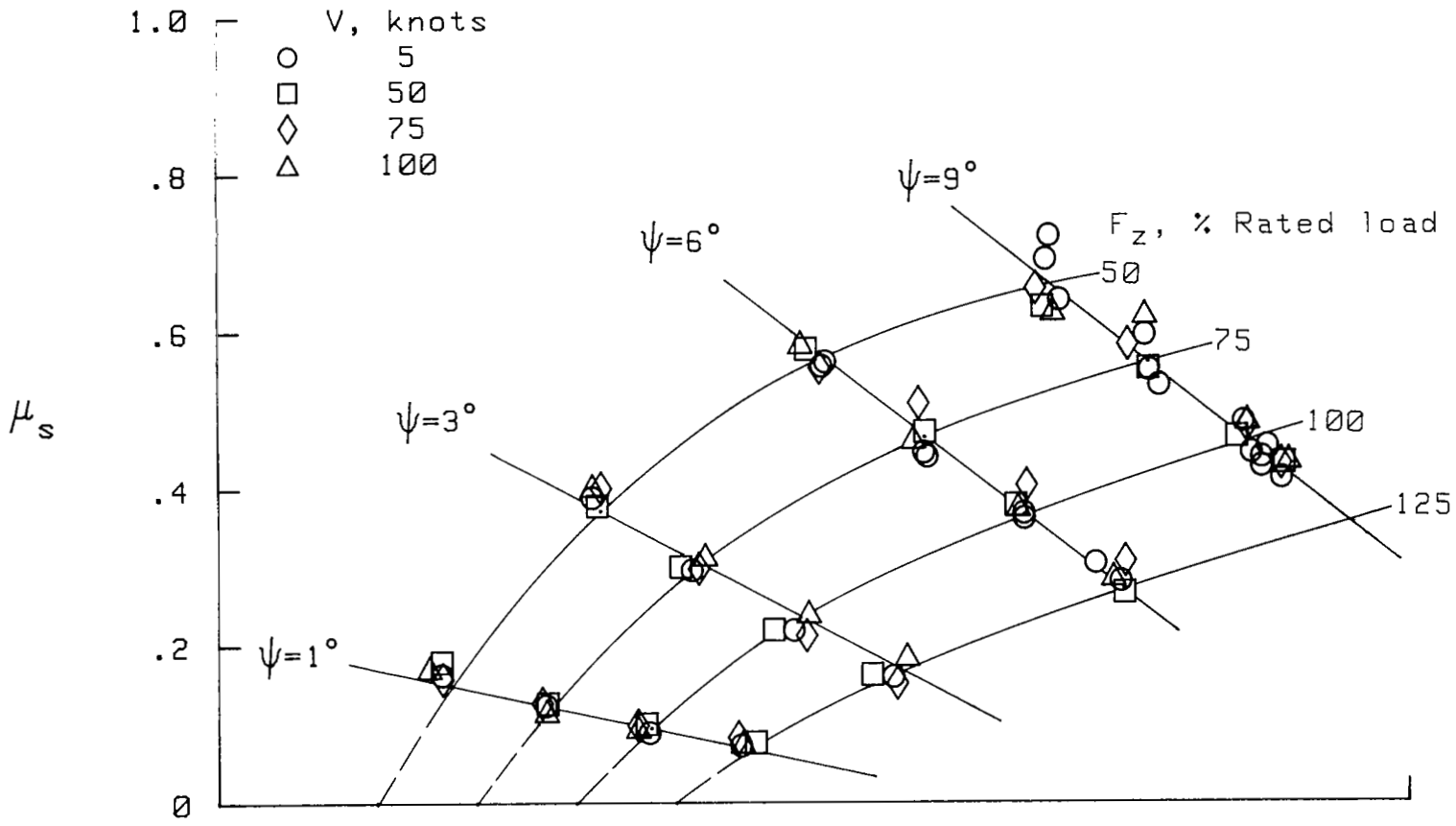

(a) 18 × 5.5 tire. Rated load = 27.6 kN (6.2 kips).

Figure 27.- Variation of tire side-force friction coefficient with vertical load and yaw angle over a range of ground speed.

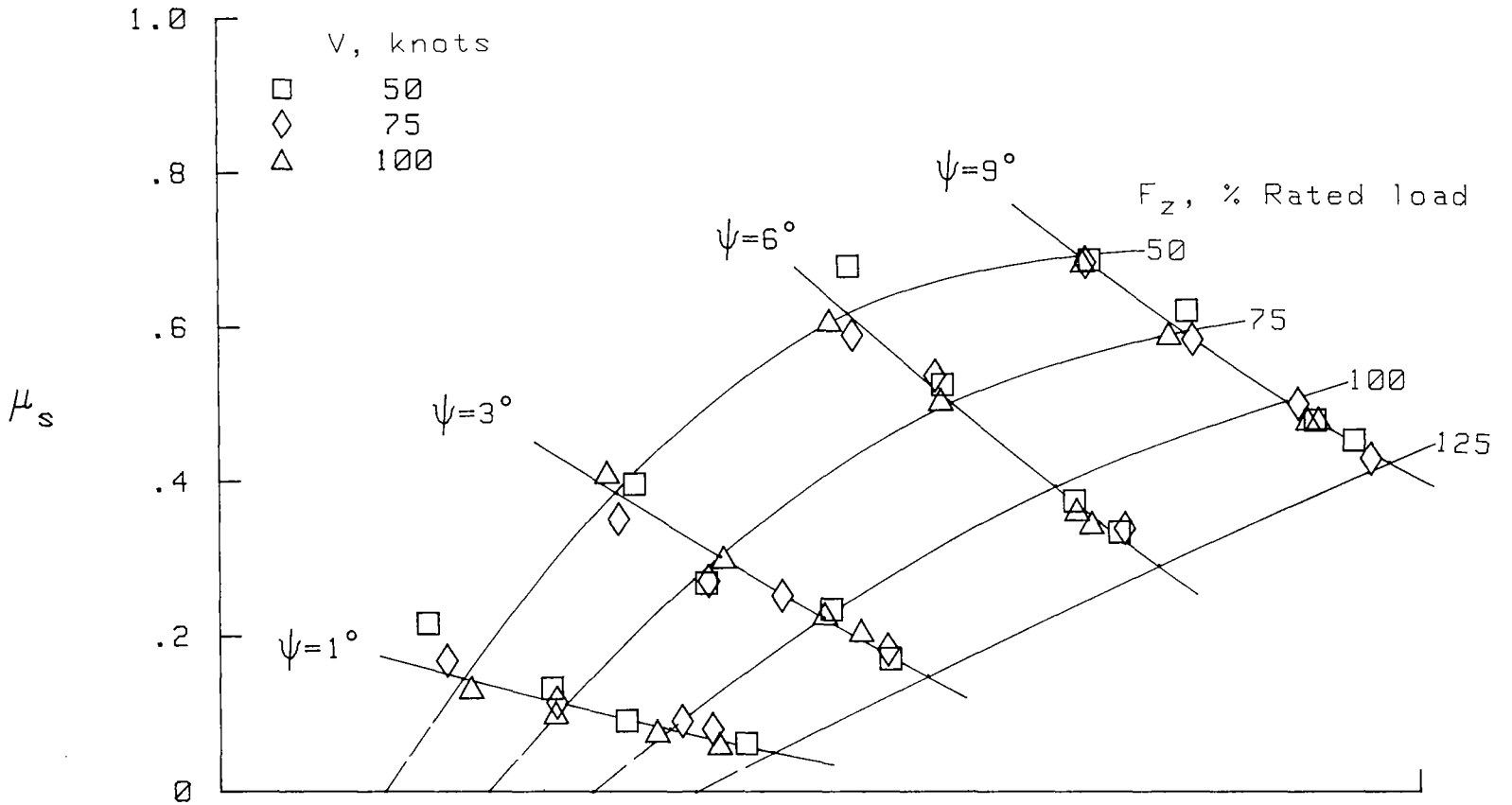

(b) 49 × 17 tire. Rated load = 176.1 kN (39.6 kips).

Figure 27.- Concluded.

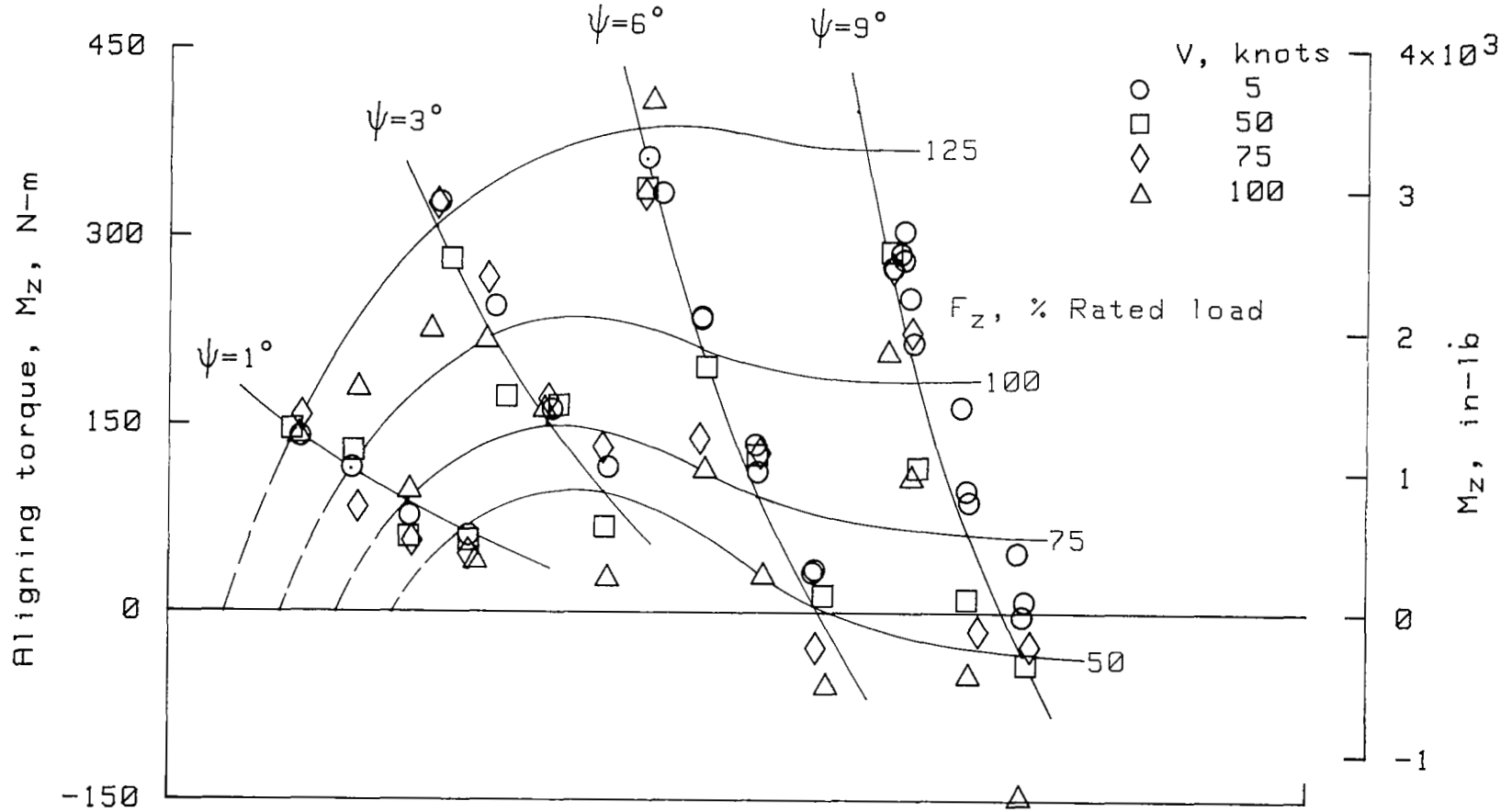

(a) 18 × 5.5 tire. Rated load = 27.6 kN (6.2 kips).

Figure 28.- Variation of tire aligning torque with vertical load and yaw angle over a range of ground speed.

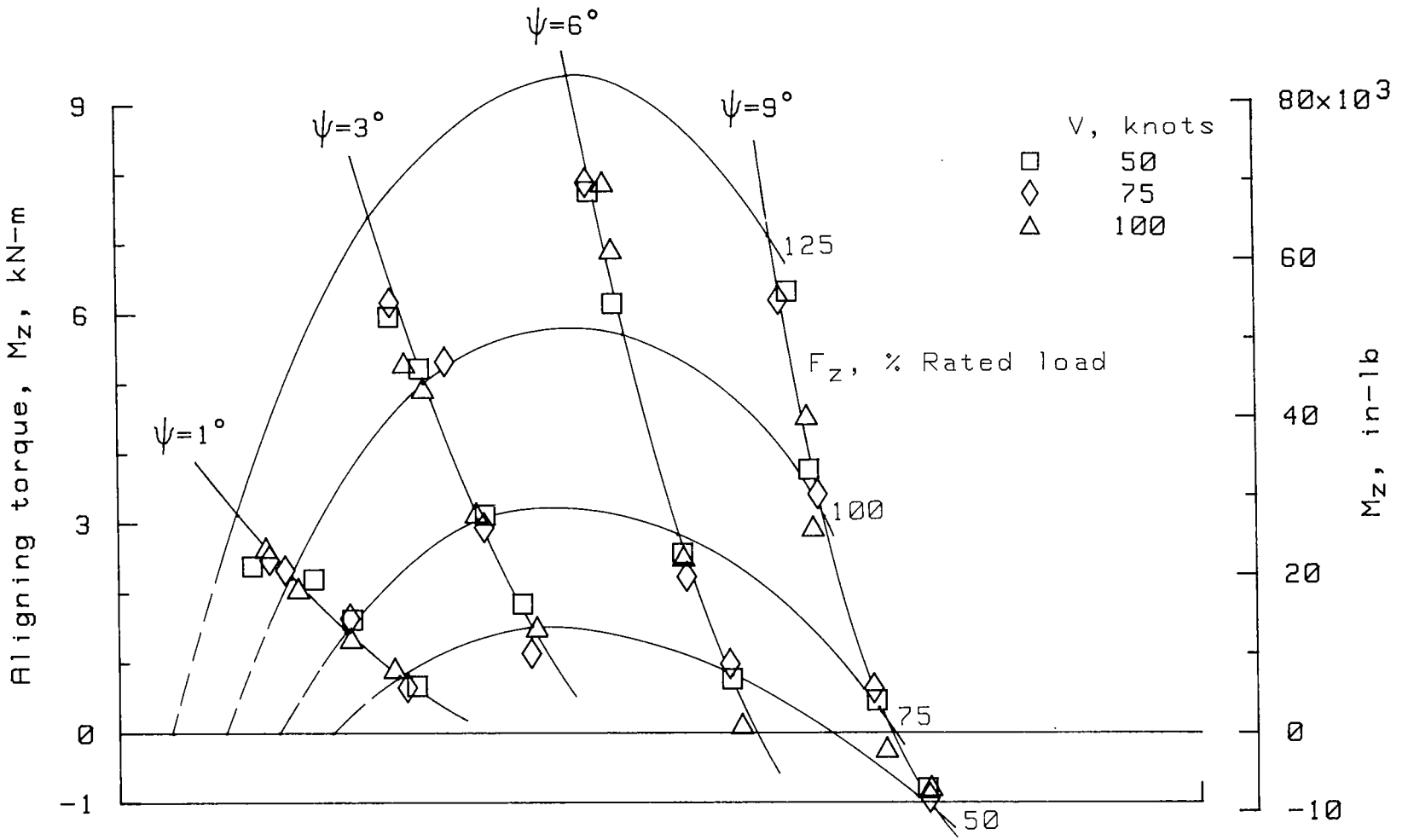

(b) 49 × 17 tire. Rated load = 176.1 (39.6 kips).

Figure 28.- Concluded.

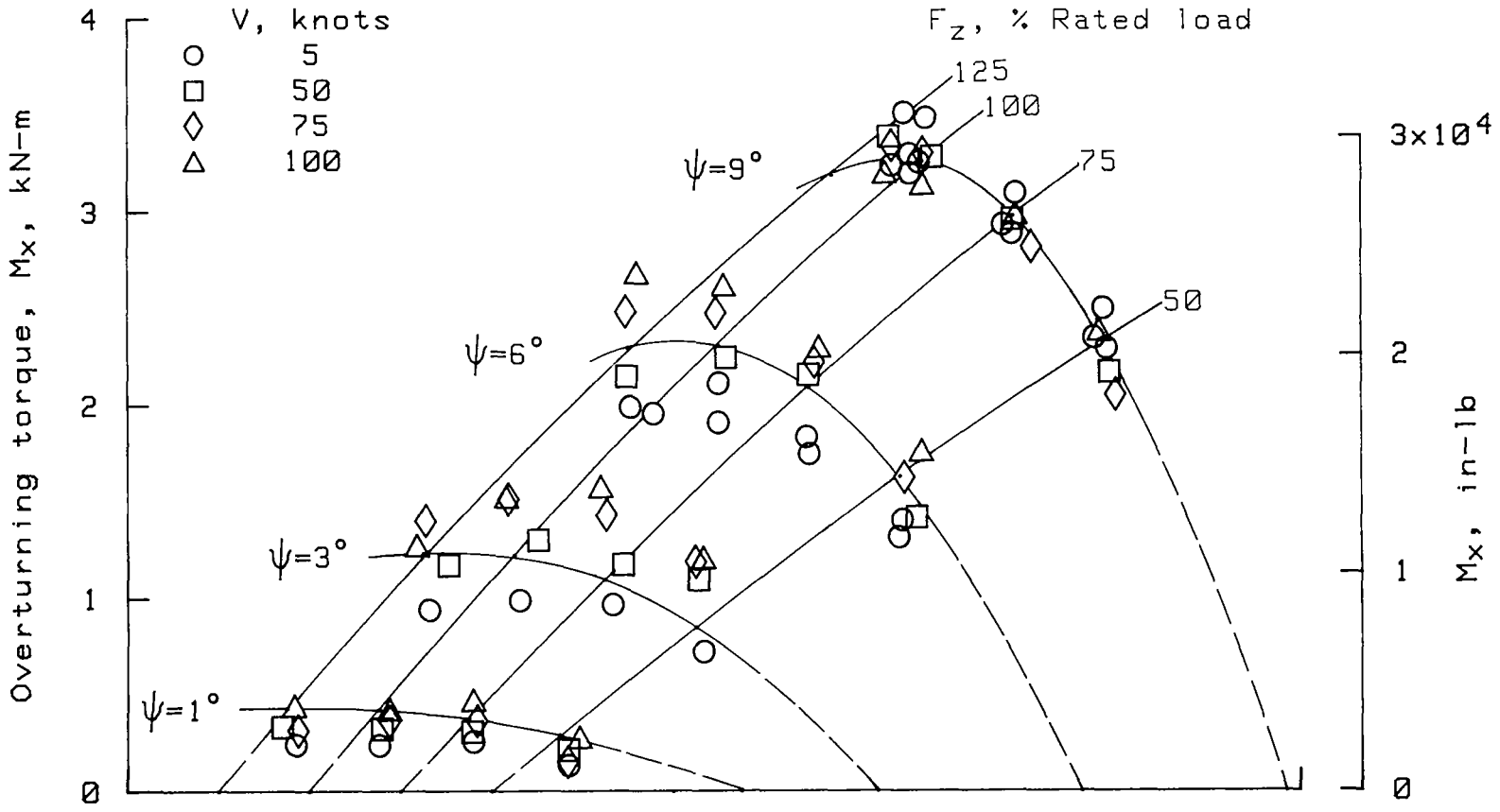

(a) 18 × 5.5 tire. Rated load = 27.6 kN (6.2 kips).

Figure 29.- Variation of tire overturning torque with vertical load and yaw angle over a range of ground speed.

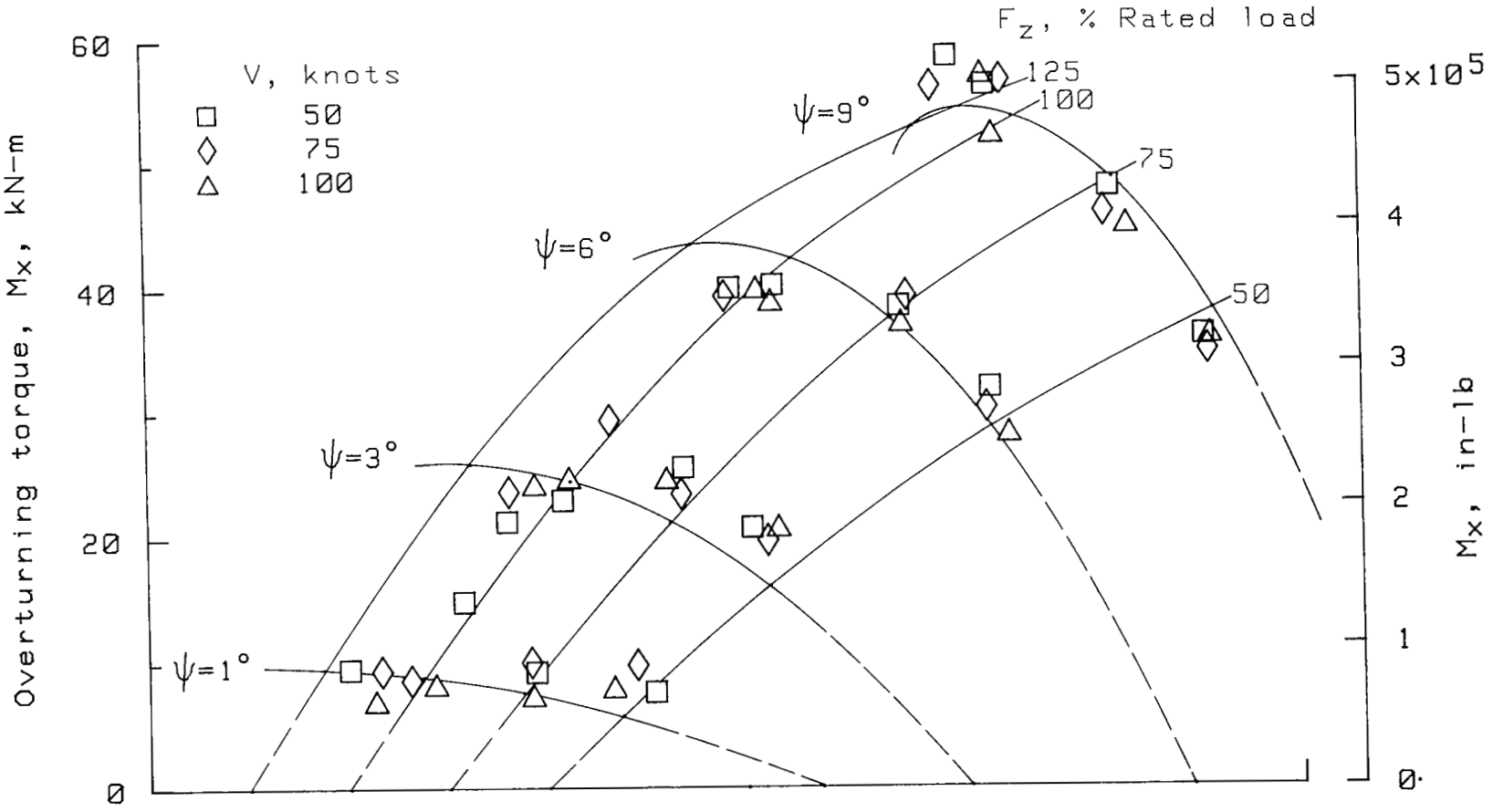

(b) 49 × 17 tire. Rated load = 176.1 kN (39.6 kips).

Figure 29.- Concluded.

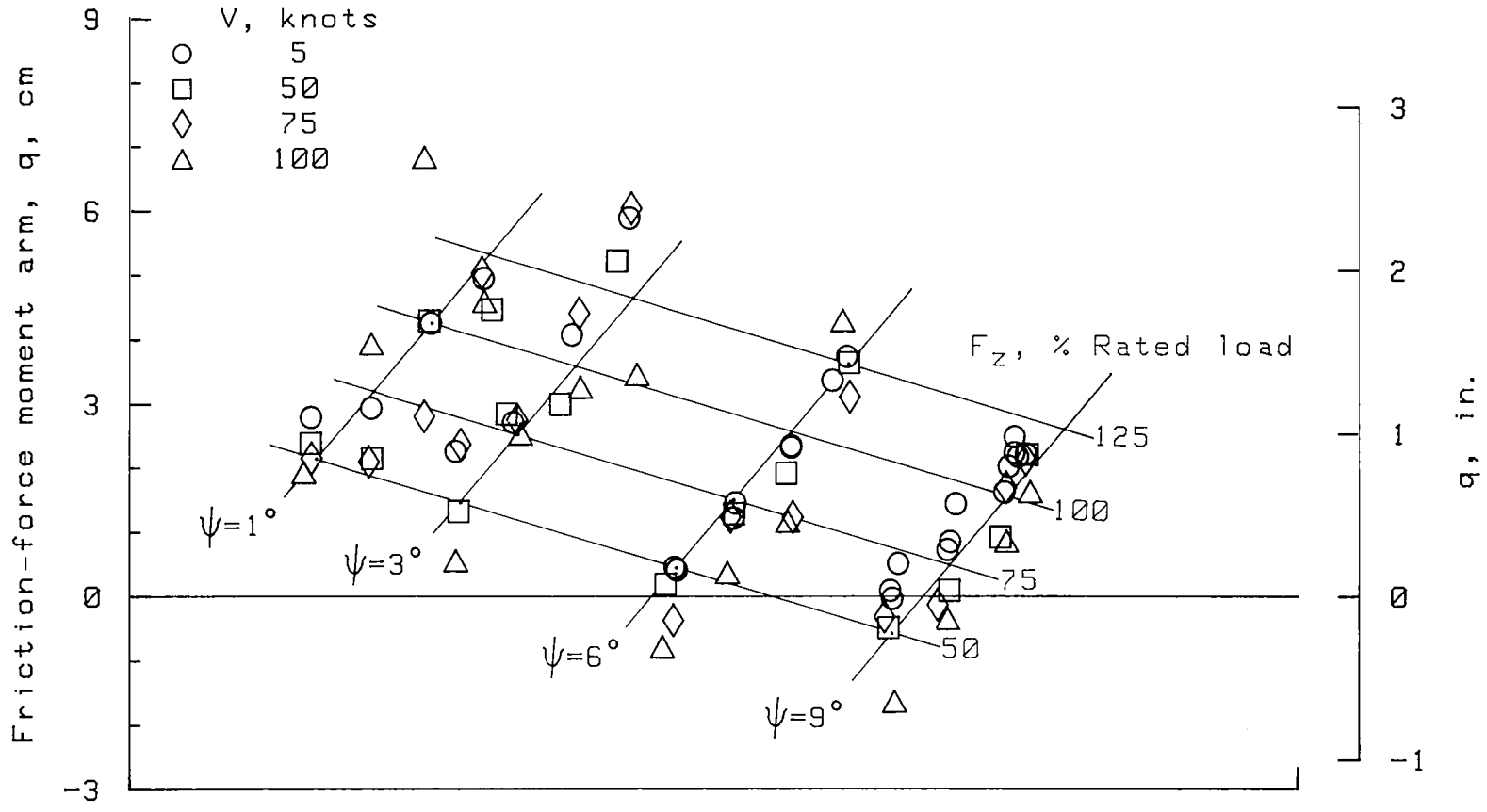

(a) 18 × 5.5 tire. Rated load = 27.6 kN (6.2 kips).

Figure 30.- Variation of tire friction-force moment arm with vertical load and yaw angle over a range of ground speed.

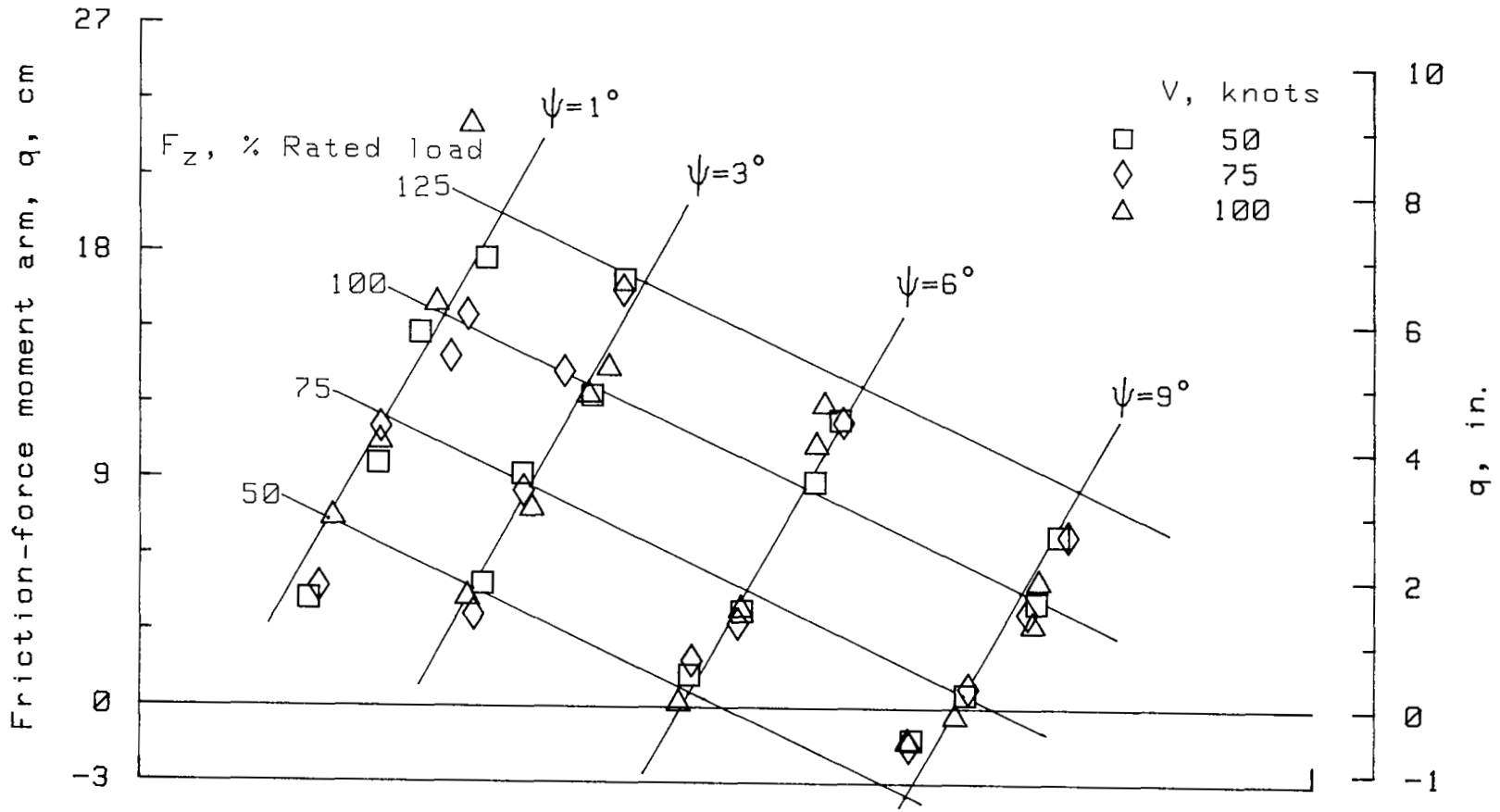

(b) 49 × 17 tire. Rated load = 176.1 kN (39.6 kips).

Figure 30.- Concluded.

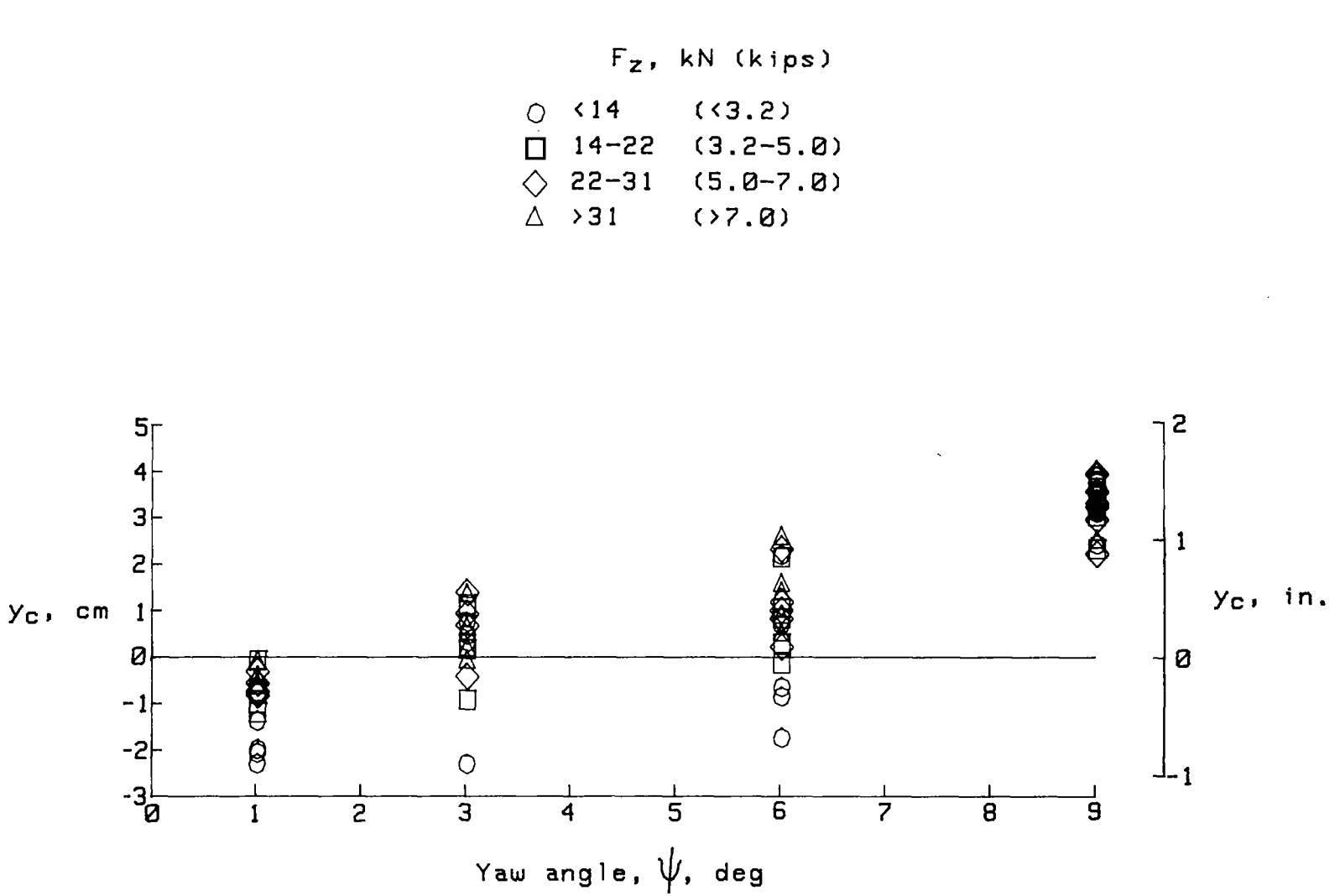

(a) 18 × 5.5 tire.

Figure 31.- Variation of tire lateral center-of-pressure shift with yaw angle for various vertical loads.

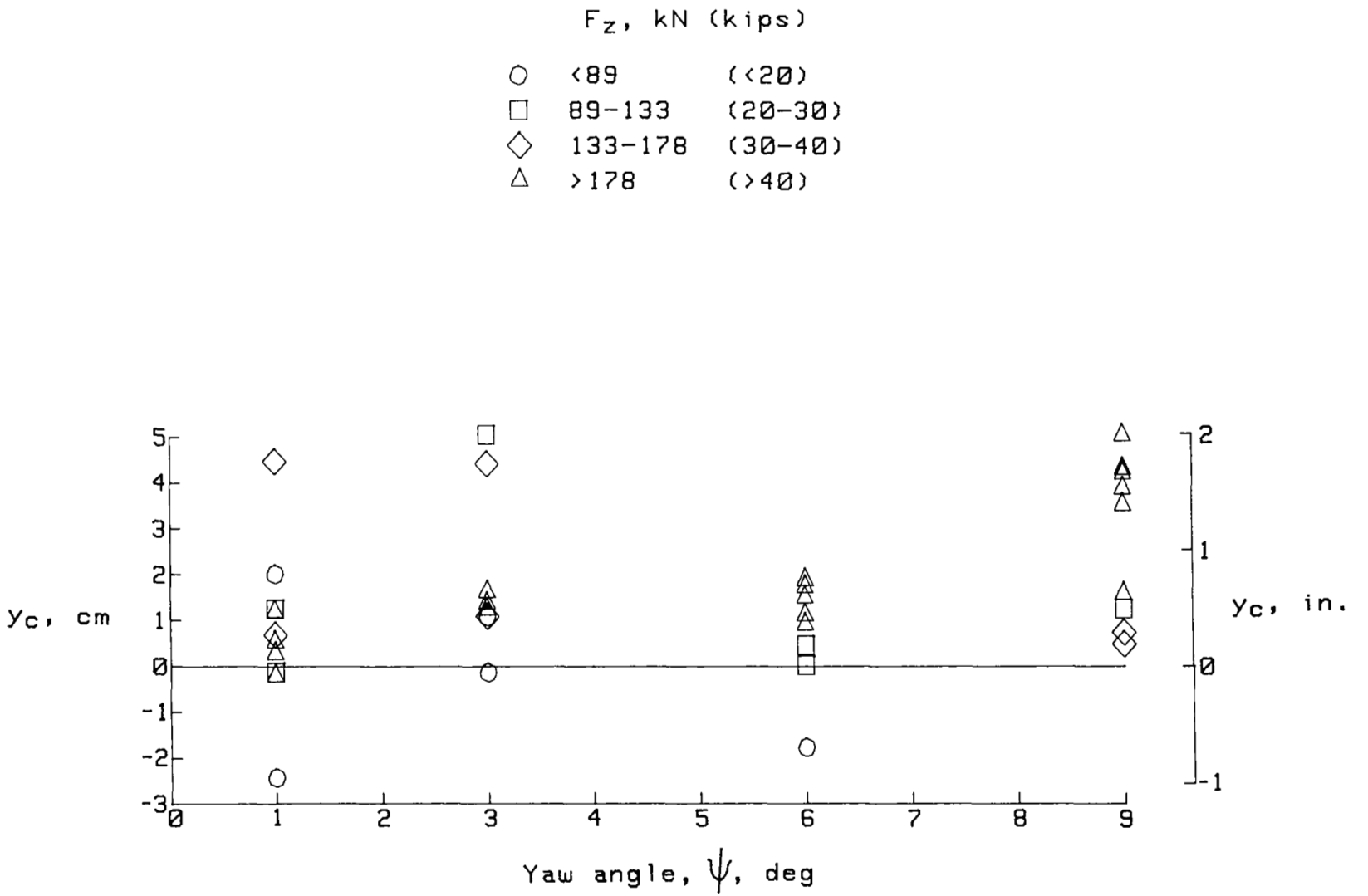

(b) 49 × 17 tire.

Figure 31.- Concluded.

1. Report No.	2. Government Accession No.	3. Recipient's Catalog No.
NASA TP-1863		

4. Title and Subtitle	5. Report Date
STATIC AND YAWED-ROLLING MECHANICAL PROPERTIES OF TWO TYPE VII AIRCRAFT TIRES	May 1981
	6. Performing Organization Code 505-44-33-01

7. Author(s)	8. Performing Organization Report No.
John A. Tanner, Sandy M. Stubbs, and John L. McCarty	L-14125
	10. Work Unit No.

9. Performing Organization Name and Address	11. Contract or Grant No.
NASA Langley Research Center Hampton, VA 23665	

12. Sponsoring Agency Name and Address	13. Type of Report and Period Covered
National Aeronautics and Space Administration Washington, DC 20546	Technical Paper
	14. Sponsoring Agency Code

15. Supplementary Notes

16. Abstract

Selected mechanical properties of 18 × 5.5 and 49 × 17 size, type VII aircraft tires were experimentally evaluated in response to a request by the Society of Automotive Engineers, Inc. The tires were subjected to pure vertical loads and to combined vertical and lateral loads under both static and rolling conditions. Parameters for the static tests consisted of tire load in the vertical and lateral directions, and parameters for the rolling tests included tire vertical load, yaw angle, and ground speed. Effects of each of these parameters on the measured tire characteristics are discussed and, where possible, compared with previous work. Results indicate that dynamic tire properties under investigation were generally insensitive to speed variations and therefore tend to support the conclusion that many tire dynamic characteristics can be obtained from static and low-speed rolling tests. Furthermore, many of the tire mechanical properties are in good agreement with empirical predictions based on earlier research. Sufficient differences appear to exist in some properties to warrant additional research before extending the current empirical prediction procedures to include all new tire designs.

17. Key Words (Suggested by Author(s))	18. Distribution Statement
Aircraft tires Tire mechanical properties High-speed cornering Hysteresis	Unclassified - Unlimited Subject Category 39

19. Security Classif. (of this report)	20. Security Classif. (of this page)	21. No. of Pages	22. Price
Unclassified	Unclassified	78	A05

For sale by the National Technical Information Service, Springfield, Virginia 22161

NASA-Langley, 1981